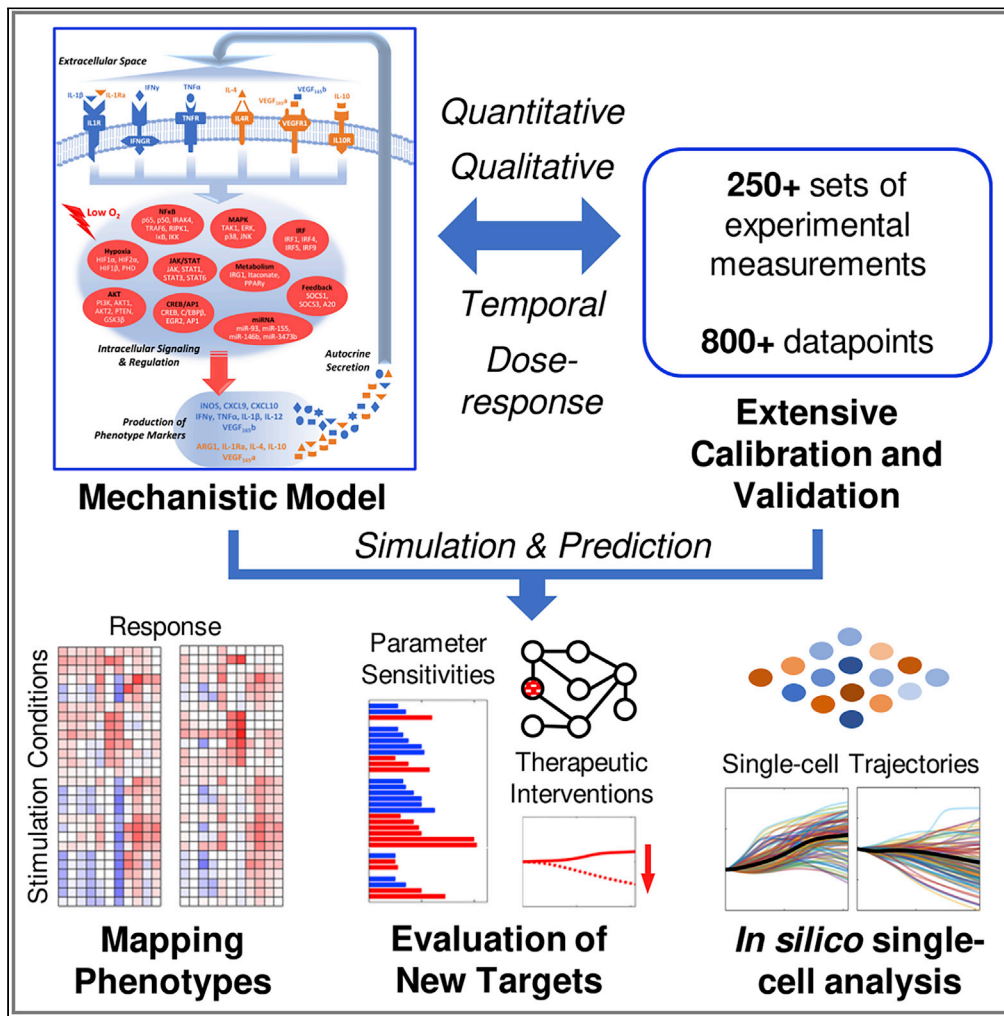## Article

A data-driven computational model enables integrative and mechanistic characterization of dynamic macrophage polarization

Chen Zhao,
Thalyta X.
Medeiros, Richard
J. Sové, Brian H.
Annex,
Aleksander S.
Popel

czhao22@jhmi.edu

HIGHLIGHTS

A large-scale, mechanistic computational model of macrophage polarization

Model enables quantitative, temporal, dose-dependent, and single-cell simulations

Unprecedented predictive resolution empowered by extensive model calibration

Model analyses provide new directions for therapeutic macrophage repolarization

Article

A data-driven computational model enables integrative and mechanistic characterization of dynamic macrophage polarization

Chen Zhao,[1,3,*] Thalyta X. Medeiros,[2] Richard J. Sové,[1] Brian H. Annex,[2] and Aleksander S. Popel[1]

SUMMARY

Macrophages are highly plastic immune cells that dynamically integrate microenvironmental signals to shape their own functional phenotypes, a process known as polarization. Here we develop a large-scale mechanistic computational model that for the first time enables a systems-level characterization, from quantitative, temporal, dose-dependent, and single-cell perspectives, of macrophage polarization driven by a complex multi-pathway signaling network. The model was extensively calibrated and validated against literature and focused on in-house experimental data. Using the model, we generated dynamic phenotype maps in response to numerous combinations of polarizing signals; we also probed into an *in silico* population of model-based macrophages to examine the impact of polarization continuum at the single-cell level. Additionally, we analyzed the model under an *in vitro* condition of peripheral arterial disease to evaluate strategies that can potentially induce therapeutic macrophage repolarization. Our model is a key step toward the future development of a network-centric, comprehensive "virtual macrophage" simulation platform.

INTRODUCTION

Macrophages are considered a critical component of immune homeostasis and a multifaceted mediator of innate and adaptive immunity. Extensive evidence has shown that these myeloid lineage cells can be dynamically educated by diverse signals in the tissue microenvironment to broadly regulate a variety of cell- and tissue-level processes such as antigen presentation, foam cell formation, inflammation, angiogenesis, tissue remodeling, allergy, infection, and tumorigenesis, in addition to their well-established role as a class of professional phagocytes (Sica and Mantovani, 2012; Mosser and Edwards, 2008). In 2000, the conceptual framework of M1-M2 macrophage polarization was first introduced by Mills et al. to describe the differential phenotypic activation of iNOS (inducible nitric oxide synthase) and arginase pathways observed in strain-selected macrophages in response to certain stimuli *in vitro*, mirroring the classical T helper type-1/type-2 dichotomy (Mills et al., 2000). Over the years, accumulating evidence especially a number of single-cell profiling studies have suggested that the M1 (or canonically activated) and M2 (or alternatively activated) macrophages rather represent two extremes in the entire spectrum of macrophage polarization and activation, and that *in vivo* macrophage phenotypes in health and disease tend to be more continuous and less exclusive: the M1 (and M1-like) macrophages are generally associated with microbicidal, pro-inflammatory, and tumoricidal activities, whereas the M2 (and M2-like) macrophages are shown to possess reparative, immune-suppressive, and angiogenic functions (Xue et al., 2014; Sica and Mantovani, 2012; Mosser and Edwards, 2008; Li et al., 2019; Muñoz-Rojas et al., 2020). Therefore, given the high plasticity and context-dependent functions of macrophages as well as their significant presence and infiltration in pathological tissues observed clinically in many major human diseases, therapeutic strategies that are designed to alter the pathology-driven macrophage polarization have been widely explored and tested in cancer (Cassetta and Pollard, 2018), cardiovascular (Barrett, 2020; Peet et al., 2020; Lindsey et al., 2016) and metabolic diseases (Kazankov et al., 2019), central nervous system disorders (Mammana et al., 2018), and autoimmune diseases (Ma et al., 2019).

From a systems-level standpoint, the M1-M2 macrophage polarization spectrum can be interpreted as the dynamic outcome of a complex network composed of a multitude of driving signaling pathways and intracellular regulatory mechanisms. For example, M1 (and M1-like) polarization can be induced, through

[1]Department of Biomedical Engineering, Johns Hopkins University School of Medicine, 720 Rutland Avenue, 613 Traylor Bldg, Baltimore, MD 21205, USA

[2]Department of Medicine, Medical College of Georgia at Augusta University, Augusta, GA 30912, USA

[3]Lead Contact

*Correspondence: czhao22@jhmi.edu

https://doi.org/10.1016/j.isci.2021.102112

respective receptors, by bacterial infection and bacterial products (e.g., lipopolysaccharides); a number of endogenous pro-inflammatory cytokines and growth factors such as IFN-γ (interferon gamma), TNFα (tumor necrosis factor alpha), IL-1β (interleukin-1 beta), GM-CSF (granulocyte-macrophage colony-stimulating factor); and also endogenous danger and stress signals such as HMGB1 (high-mobility group box 1) and HSPs (heat shock proteins) (Atri et al., 2018; Martinez and Gordon, 2014). Likewise, another diverse set of biomolecules including but not limited to IL-4/10/13, transforming growth factor β, VEGF (vascular endothelial growth factor), and prostaglandin E2 are shown to drive M2 (and M2-like) polarization (Wang et al., 2014; Wheeler et al., 2018; Luan et al., 2015). Downstream of these M1-M2 driving factors are highly interactive signal transduction cascades connecting to numerous modules of transcription (e.g., by nuclear factor kappa B [NF-κB], interferon regulatory factors [IRFs]) and post-transcriptional regulation (e.g., by microRNAs), and these modules are known to work in time-dependent, cooperative, or antagonistic fashions to dynamically control the expression of an array of M1 and M2 phenotype readouts (Tugal et al., 2013; Lawrence and Natoli, 2011; Li et al., 2018). Common M1 readouts include high production and secretion of various pro-inflammatory cytokines (e.g., TNFα, IL-1β, IL-12) and chemokines (e.g., C-X-C motif chemokine ligands [CXCLs]), high levels of synthesized reactive oxygen and nitrogen species, increased phagocytosis, and antigen presentation. M2 macrophages are often characterized by significant production of anti-inflammatory cytokines (e.g., IL-10), low secretion of pro-inflammatory cytokines, increased expression of arginase (ARG) proteins, and induction of various cell-surface receptors and markers (e.g., mannose receptor) (Wang et al., 2014; Martinez and Gordon, 2014). In agreement with the systems-level, network-centric view of macrophage polarization, increasing evidence has suggested that under many circumstances the directional changes of isolated M1-M2 readouts may not be definitive or mutually exclusive in terms of understanding macrophage functional phenotypes. For example, a number of canonical M1 stimuli can also induce delayed but significant production of certain M2 markers (e.g., IL-10) in vitro (Chang et al., 2007; Hu et al., 2006). In addition, it has been observed that individual tumor-associated macrophages in many cancer types can express both M1 and M2 markers at the same time, possibly owing to the diverse signals in the tumor microenvironment in vivo (Reinartz et al., 2014; Helm et al., 2014; Pettersen et al., 2011; Gionfriddo et al., 2020); unique macrophage subpopulations with unconventional marker expression profiles (e.g., distinguishable from M1 or M2) have also been discovered in many disease areas (Tatano et al., 2014; Colin et al., 2014; Chavez-Galan et al., 2015). Therefore, to better integrate the decades of experimental knowledge obtained from traditional "one stimulus/one pathway/one marker" approaches, the systems-level modeling approach that mechanistically incorporates aspects of multi-pathway signal transduction and cross talk, multi-modal modulation of a panel of M1-M2 markers, as well as temporal autocrine/paracrine and feedback regulation is emerging as a new frontier in the investigation of the macrophage polarization spectrum in health and disease.

Following this idea, several systems-level computational models with distinctive features have been formulated to investigate this complex polarization process at the cell level. Palma et al. and Ramirez et al. both used a semi-mechanistic approach based on Boolean gene regulatory networks to identify macrophage activation patterns (Ramirez et al., 2019; Palma et al., 2018). Two more models by Rex et al. and Liu et al. both employed logic-based modeling and ordinary differential equations complemented by calibration against selected experimental datasets of M1-M2 marker profiles to simulate macrophage marker expression signatures in response to exogenous stimuli (Rex et al., 2016; Liu et al., 2019). In comparison, here we have developed and analyzed a multi-pathway computational model formulated based on mass-action and Hill-type kinetics to more accurately characterize the biology and mechanistic regulation in macrophage signaling and polarization. To that end, we have incorporated over 200 sets of quantitative experimental measurements, including over 800 data points obtained from the literature and in-house experiments, into the model calibration and validation steps (achieving a much higher level of predictive capacity and comprehensiveness than any prior macrophage modeling studies have done). To the best of our knowledge, our model is the first large-scale mathematical model that can predictively simulate, from temporal, dose-dependent, quantitative, and single-cell perspectives, both the expression of a panel of macrophage phenotype markers and the dynamic activities of essential transcription factors, intermediate regulators, and signaling hubs, driven by a complex network consisting of seven high-importance macrophage pathways spanning the M1-M2 spectrum. Using this model, we generated comprehensive phenotype maps detailing how the M1-M2 paradigm would respond to single and combinatorial polarizing signals; we also created a population of "in silico macrophages" through re-parameterization and probed into their dynamic responses to mechanistically examine the diversity and continuity of macrophage polarization at the single-cell level. Furthermore, we analyzed the model under a specific in vitro condition that is used
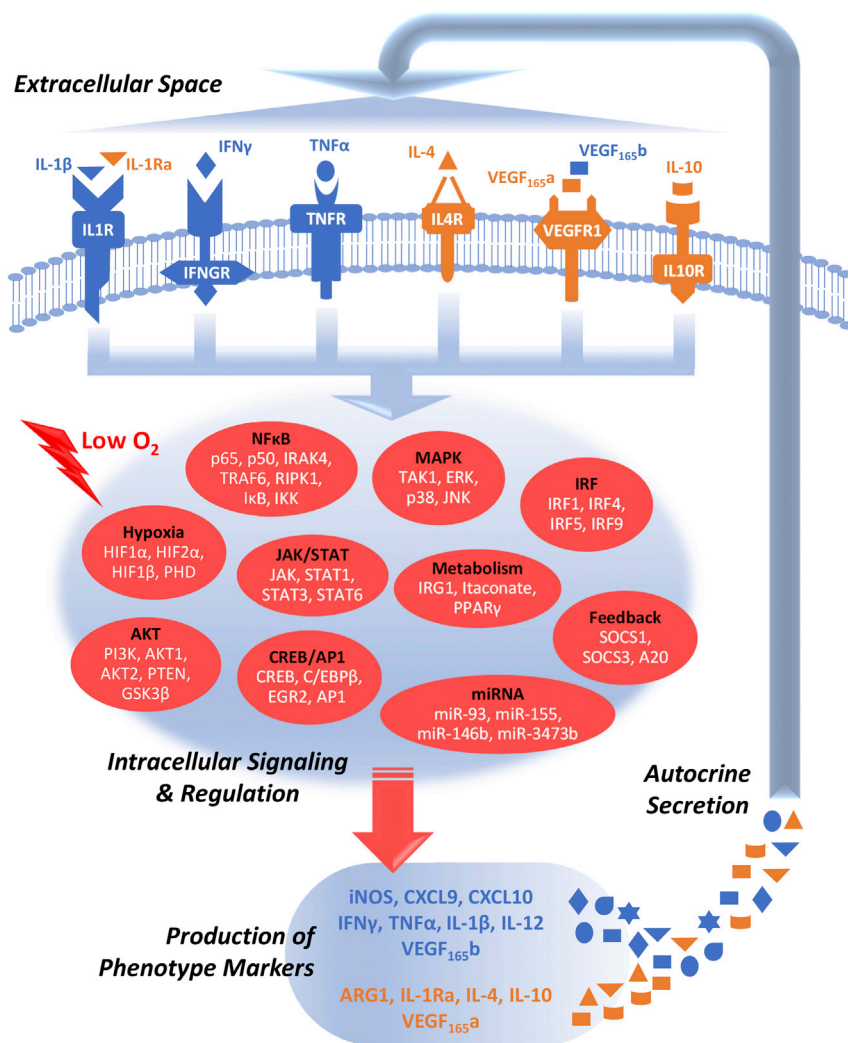
Figure 1. An overview diagram of the mechanistic computational model

The model system we developed is composed of seven essential pathways (six receptor-mediated pathways plus an oxygen-sensing pathway) with profound influences on macrophage activation and M1-M2 polarization in health and disease. When this system is perturbed by external driving signals (e.g., cytokine stimuli, hypoxia), the polarizing effects are integratively computed through a complex wired network of intracellular signaling and regulation (highlighted as different modules in red) that then leads to the production and secretion of various M1-M2 markers (blue, M1-associated; orange, M2-associated). Some of these markers themselves are cytokines that drive macrophage polarization and thus can initiate multiple rounds of signaling on macrophages in an autocrine/paracrine manner to produce a highly diverse spectrum of phenotypes. A more detailed model diagram is shown in Figure S16 in Supplemental Information.

to mimic PAD (peripheral arterial disease) to screen for potential strategies that can induce therapeutic macrophage repolarization (Ganta et al., 2017). Our mechanistic model presented here serves as an important proof-of-concept advancement toward a more comprehensive, kinetics modeling-based realization of an executable network-centric "virtual macrophage" (Wentker et al., 2017).

RESULTS

Overview of model scope and formulation

A total of seven driving pathways were included in this model (Figure 1) based on a manual curation of the macrophage literature: five pathways are relatively well-established M1 (IFNγ, TNFα, IL-1β) and M2 (IL-4, IL-10) stimuli, and the remaining two pathways (hypoxia, VEGF) were selected given their significance in PAD,

which is our primary disease area of interest, as both factors are known to be critical drivers and regulators of PAD pathophysiology (Martinez and Gordon, 2014; Ouma et al., 2012). The general mechanistic framework of this model, which uses mass-action and Hill-type kinetics to capture biochemical details in pathway signal transduction, follows the same literature-based, data-driven model formulation logic as described in a previous modeling study from our group, and from there the IL-4/IFNγ/hypoxia pathways were further enriched with new signaling mechanisms and then implemented in a similar manner as reported before (Zhao et al., 2019). For the IL-10 pathway, a previous model by Braun et al. (2013) was taken as a basis from which we further added corresponding mechanisms to describe the activation of PI3K/AKT (phosphoinositide 3-kinase/protein kinase B) and ERK (extracellular signal-regulated kinase) by IL-10 and also the inhibitory effect of SOCS1 (suppressor of cytokine signaling 1) on IL-10/STAT3 (signal transducer and activator of transcription 3) signaling (Xiao et al., 2019; Zhu et al., 2015; Niemand et al., 2003). The VEGF pathway in the model focuses on the interactions between two functionally distinct VEGF isoforms (165a and 165b) and VEGFR1, which is the major VEGF receptor expressed on macrophages and that VEGFR1 can signal through various modules including PI3K/AKT, STAT3, and ERK to regulate downstream targets (Weddell et al., 2018; Ganta et al., 2019; Boscolo et al., 2011). For TNFα and IL-1β pathways, both stimuli, through different intermediates, can induce the MAPK (mitogen-activated protein kinase) cascades including phosphorylation of p38, ERK, and JNK (c-Jun N-terminal kinase); turn on transcription factors such as CREB (cAMP response element-binding protein), C/EBPβ (CCAAT/enhancer-binding protein beta), and AP-1 (activator protein 1); and drive the canonical activation of NF-κB (Hu et al., 2005; Ermolaeva et al., 2008); here the mechanistic pathway structures were adapted from the toll-like receptor map and also structures proposed by several published models of NF-κB signaling (Werner et al., 2008; Caldwell et al., 2014; Salim et al., 2016; Oda and Kitano, 2006). In addition to the pathway modules, a number of inter-pathway cross talk and feedback mechanisms (e.g., through SOCSs, microRNAs [miRNAs]) were modeled explicitly, and further downstream are the signaling network-mediated differential regulation of a diverse M1-M2 marker panel, while autocrine/paracrine regulation was incorporated for the 6 ligand/receptor pathways (covering 8 secreted M1-M2 cytokine markers). More mechanistic details of model formulation are described in Transparent Methods and Tables S1 and S2 (full description of all model mechanisms, reactions, species, initial conditions, and parameters).

Model calibration and validation against experimental data

Details of calibration (Figures 2 and 3, and S2–S5) and validation (Figure 4) results are presented and discussed in the following sections and in Supplemental Information. Overall, this model contains 67 "unique" species (e.g., functionally unique proteins, mRNAs, miRNAs, and non-gene compounds) and their quantitative initial conditions (in terms of absolute copy numbers), which together represent the resting states of unpolarized macrophages were calibrated against respective quantitative measurements the in literature (see Transparent Methods and Table S2 for more details regarding the initial condition calibration procedure). From there, different stimulation conditions were converted to quantitative inputs into the model to generate a large number of simulations, which were simultaneously calibrated, using a global optimization approach, against extensive experimental data from both literature and in-house experiments (including over 200 sets of time course, single time point, and dose-response measurements). Our final model was then validated against an independent set of data (not included in calibration) that reflects the dynamic regulation of key signaling axes in the model. A comparison between our model and previous studies that modeled macrophage polarization is shown in Figure S1.

Calibration of multi-pathway signal transduction

The signal transduction of IL-1β initiates from receptor-ligand binding and travels downstream through the IRAK/TRAF6 (interleukin 1 receptor associated kinase/TNFR-associated factor 6) axis (Figures S2B–S2D) to activate IKK (IκB kinase, Figure S2E), which results in IκB (inhibitor of κB) degradation and subsequent nuclear translocation of NF-κB complex (Figures 2A and S2F). IL-1β also activates the PI3K/AKT axis (Figure S2G) and MAPKs (Figures S2H–S2J), in addition to several other aforementioned transcription factors. Compared with IL-1β, TNFα signaling, through an axis controlled by RIP1 (receptor interacting protein 1, Figure S2O), activates a similar group of effector molecules (cascades of NF-κB [Figures 2B and S2Q and S2T], MAPKs [Figures 2C and S2U–S2W], AP-1 [Figure 2D], CREB [Figures S3A and S3B], C/EBPβ [Figure S3C]). Both IL-1β and TNFα can induce the expression of various negative feedback regulators, such as A20 (Figures 2E and S3D, also known as TNFAIP3 [TNFα-induced protein 3]), SOCS3 (Figures 2F and 2G), and SOCS1 (Figures S2K and S3E). Furthermore, they also upregulate miR-155 (Figures S3F–S3H), a canonical M1-inducible miRNA, and downregulate miR-93 (Figures S2L and S3K), which targets IRAK4
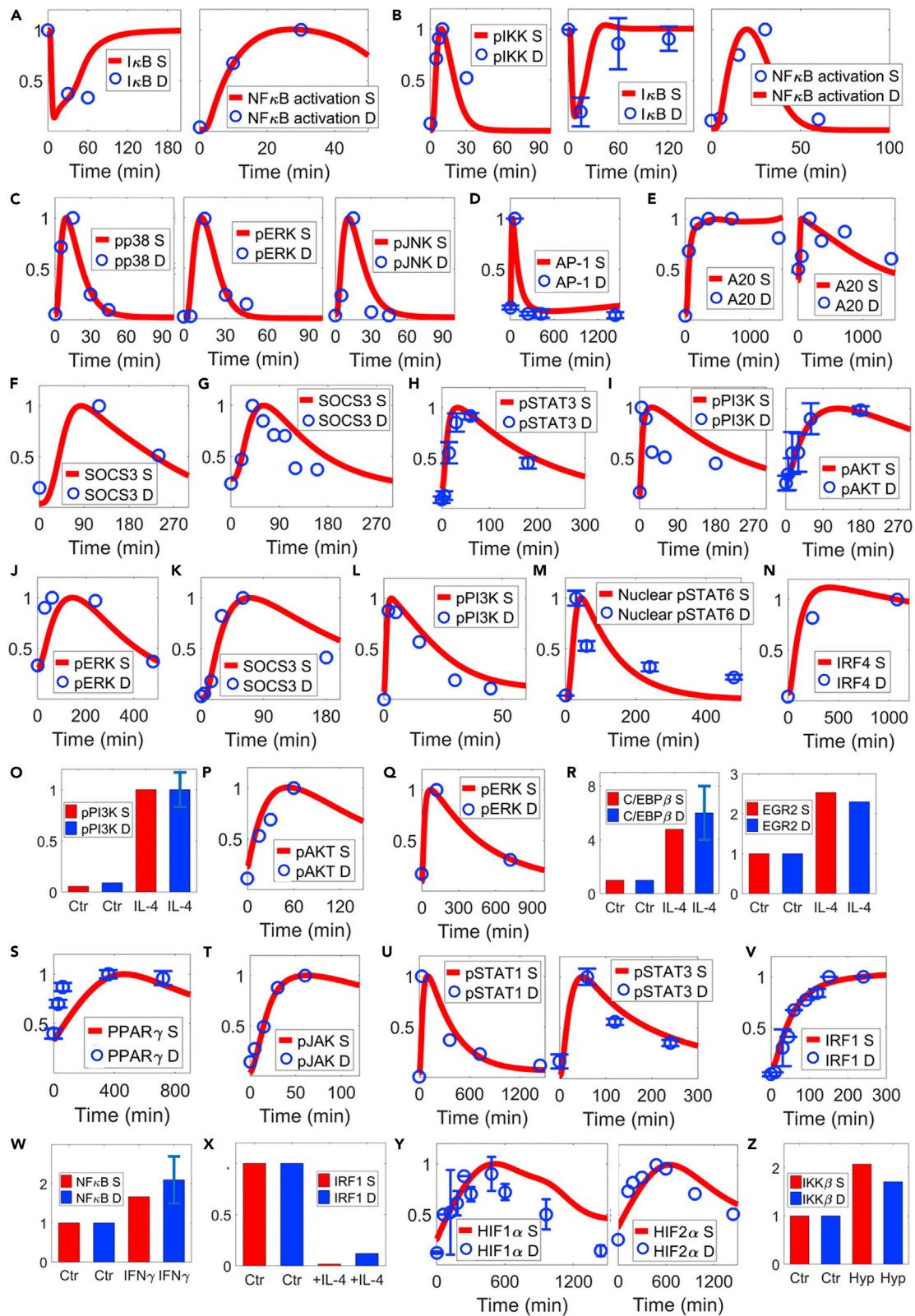
Figure 2. Model calibration of macrophage pathway signal transduction (part 1); parts 2–4 are shown in Figures S2–S4

Model simulations and corresponding experimental data obtained from macrophages are shown together (references are listed in the order of the data mentioned).

(A) IκB expression (Suzuki et al., 2002) and NF-κB activation (Hu et al., 2005) in response to IL-1β.

(B–D) (B) TNFα can induce activation of IKK/IκB/NF-κB axis (Zhang et al., 2016; Etemadi et al., 2015; Lo et al., 2011), (C) MAPKs (Ermolaeva et al., 2008), and (D) AP-1 (Yarilina et al., 2011).

(E–G) (E) Both IL-1β (left) and TNFα (right) can induce A20 (Hu et al., 2014); (F and G) both IL-1β and TNFα can induce SOCS3 (Wong et al., 2006; Ehlting et al., 2007).

(H–J) IL-10 activates STAT3, PI3K/AKT (Zhu et al., 2015), and ERK (Xiao et al., 2019).

(K) IL-10 also upregulates SOCS3 (Zhu et al., 2015).

(L) VEGF induces PI3K activation (Weddell et al., 2018).

(M–S) (M) IL-4 induces STAT6 activation (Sheldon et al., 2013), (N) IRF4 expression (El Chartouni et al., 2010), (O and P) PI3K/AKT (O'connor et al., 2007; Covarrubias et al., 2016), and (Q) ERK activation (Wang et al., 2010); (R) IL-4 also upregulates C/EBPβ, EGR2 (Veremeyko et al., 2018), and (S) PPARγ (Yao et al., 2016) expression.

(T–W) (T) IFNγ activates JAK (Blanchette et al., 2003) and downstream (U) STAT1 (Majoros et al., 2016) and STAT3 (original data, see Figure S9B) and induces (V) IRF1 expression (Ramsauer et al., 2007) and (W) NF-κB activation (Vila-Del Sol et al., 2007).

(X) IFNγ-induced IRF1 expression can be repressed by IL-4 pretreatment (Coccia et al., 2000).

(Y) Hypoxia stabilizes cellular HIF1α and HIF2α (Ortiz-Masia et al., 2014; Frede et al., 2006) and (Z) enhances IKKβ expression (Fang et al., 2009). (A–Z) All values are for protein levels and normalized (y axes are relative expression levels). For normalization of results (simulation and data in A–Z): IκB in (A and B, R, W, and Z) normalized to the respective t = 0 (Ctr) values; (N, T, V), NF-κB in (A), and AKT in (I and P) normalized to their respective values at the last experimental time points; (O) normalized to the values at 15 min of IL-4 treatment; (X) normalized to the Ctr (IFNγ-treated) condition; all others normalized to their respective maximum values. S, simulation; D, experimental data; Hyp, hypoxia; Ctr, control/untreated condition (except in X as described above).

(Figure S3L), IRF9 (Figure S4Y), and VEGF (Figure S5Y) in the model. For the M2 side, IL-10 is known to induce phosphorylation and activation of STAT3 (Figures 2H and S3M–S3O), PI3K/AKT (Figure 2I), and ERK (Figure 2J). SOCS3, a negative regulator of JAK (Janus kinase)/STAT signaling, is also inducible by IL-10 (Figure 2K). As an M2 stimulus, IL-10 represses miR-155 (Figure S3P) and induces miR-146b (Figure S3Q), which can target STAT1 (Figure S3R) to limit pro-inflammatory signaling. IL-10 also directly interacts with the IL-4 pathway by upregulating the production of IL-4 receptors (Figure S3S). Another novel M2 axis included in the model is the VEGF/R1 pathway; upon binding with the pro-angiogenic VEGF isoform (e.g., VEGF$_{165}$a), VEGFR1 can initiate receptor phosphorylation (Figure S3U) and downstream signal activation (Figures 2L and S3V).

The pathway structures of IL-4/IFNγ/hypoxia were initially taken from our previous model and then further enriched with additional mechanistic details of pathway feedback and cross talk (Zhao et al., 2019). Ligation of IL-4 receptors will lead to subsequent activation of STAT6 (Figures 2M and S3X), IRF4 (Figures 2N and S4A), PI3K/AKT (Figures 2O–2P, and S4B), and ERK (Figure 2Q) and induce the expression of EGR2 (early growth response 2) and C/EBPβ (Figures 2R and S4F) as well as PPARγ (peroxisome proliferator activated receptor gamma), which is a signature gene in macrophage lipid metabolism (Figures 2S and S4C). For the IFNγ pathway, in addition to the canonical JAK/STAT1/IRF1 axis (Figures 2T–2V, S4J, and S4M and S4N), we further modeled the effect of IFNγ-induced activation of STAT3 (Figures 2U and S4K) and its functional antagonism against STAT1, as well as the direct and indirect effects of IFNγ on IL-1β signaling (Figures 2W and S4L). In terms of cross talk, both IL-4 and IFNγ can selectively induce SOCS proteins (Figures S4D and S4O) and miRNAs (Figures S4E and S4P–S4Q) to influence other pathway modules, and IL-4 represses IFNγ-induced IRF1 expression (Figure 2X). The hypoxia pathway centers on the oxygen-dependent stabilization of HIF1α (hypoxia-inducible factor 1 alpha) and HIF2α (Figures 2Y and S4R–S4U); the impact of hypoxia on IRF1 activation (Figure S4V), IKK expression (Figures 2Z and S4W), and miR-93 and its downstream target regulation (Figures S4X and S4Y) were also included. Besides, the cellular abundance of HIF1/2α can be controlled by signaling activities downstream of IL-4 and IFNγ in a mutually antagonistic manner (Figures S4G and S4I).

Besides the intracellular signal transductions, each cytokine-activated pathway in our model has a corresponding module that is calibrated to mechanistically describe the dynamic events of ligand-receptor binding, receptor activation and internalization, recycling, and degradation (e.g., IL-1β [Figure S2A], TNFα [Figures S2M and S2N], VEGF [Figure S3T], IL-4 [Figure S3W], IFNγ [Figure S4H]).

Calibration of M1-M2 marker regulation

The three pro-inflammatory drivers in the model, IL-1β, TNFα, and IFNγ, are known to induce macrophage expression and secretion of an array of typical M1 markers: themselves such as IL-1β and TNFα (Figures 3A,
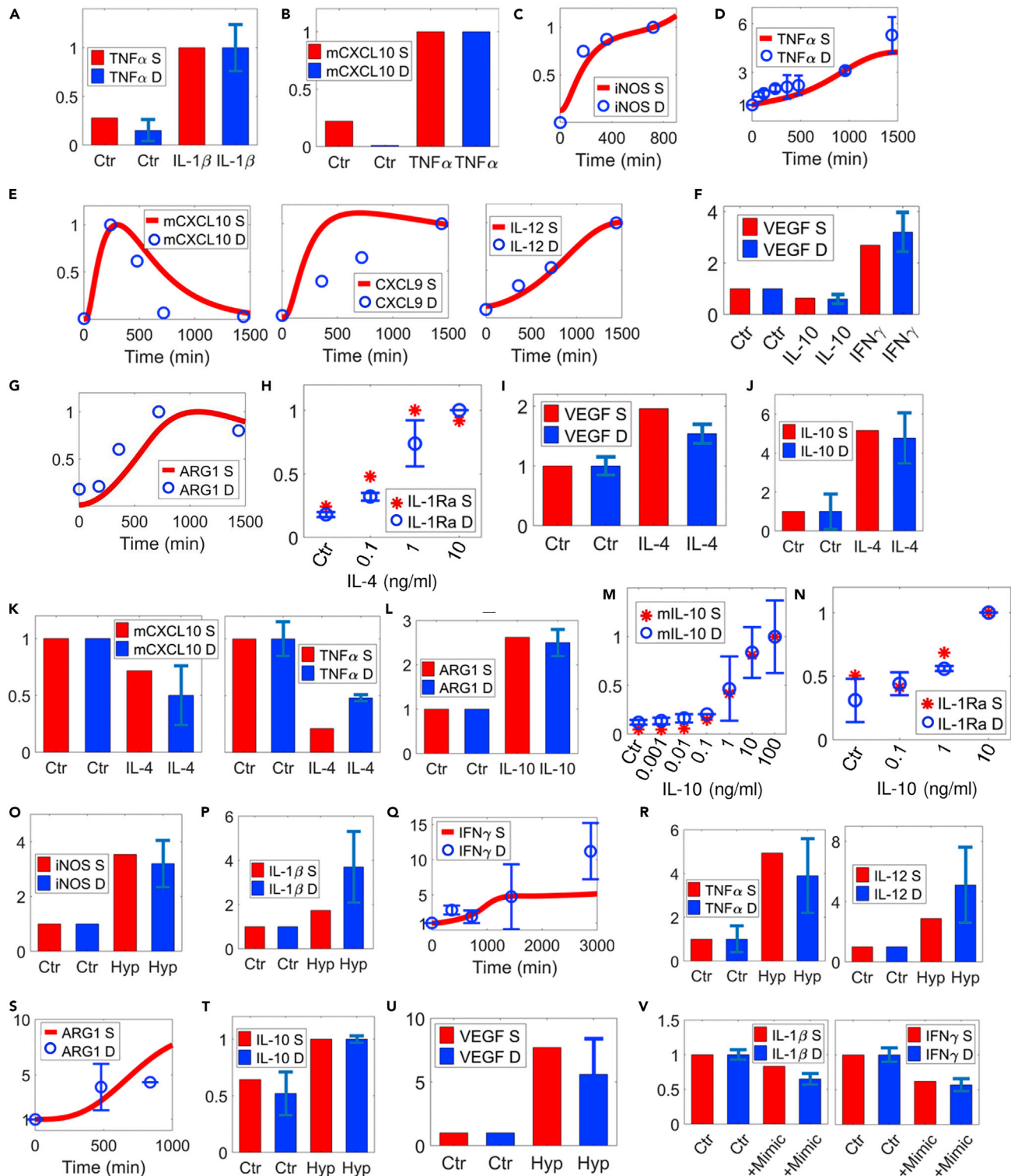
Figure 3. Model calibration of macrophage phenotype marker regulation (part 1); part 2 is shown in Figure S5.
Model simulations and corresponding macrophage experimental data are shown together (references are listed in the order of the data mentioned).
(A) IL-1β induces TNFα secretion (Sato et al., 2012).
(B) TNFα induces CXCL10 (mRNA) expression (Rauch et al., 2015).

Figure 3. *Continued*

(C–E) (C) IFNγ induces iNOS expression (Lin et al., 2008), (D) TNFα secretion (Vila-Del Sol et al., 2008; Vila-Del Sol et al., 2007), (E) CXCL10 (mRNA) (Rauch et al., 2015), and secretion of CXCL9 and IL-12 (Su et al., 2015).

(F) IFNγ also promotes VEGF secretion, whereas IL-10 represses it (Wu et al., 2010).

(G–J) (G) IL-4 induces the expression of ARG1 (Schleicher et al., 2016) and production of (H) IL-1Ra (dose response) (Joyce et al., 1996) and (I and J) VEGF and IL-10 (Lee et al., 2017).

(K) IL-4 also inhibits CXCL10 (mRNA) (Piccolo et al., 2017) and TNFα production (Lee et al., 2017).

(L–R) (L–N) IL-10 induces ARG1 expression (Nakamura et al., 2015) and production of itself (mRNA, dose response) (Staples et al., 2007) and IL-1Ra (dose response) (Joyce et al., 1996). Hypoxia upregulates the production and secretion of multiple M1 markers including (O) iNOS (Gao et al., 2017), (P) IL-1β (Fang et al., 2009), (Q) IFNγ (Carta et al., 2001; Acosta-Iborra et al., 2009), and (R) TNFα (Hempel et al., 1996) and IL-12 (Acosta-Iborra et al., 2009).

(S–U) Hypoxia also promotes M2 markers including (S) ARG1 (Takeda et al., 2010; Gao et al., 2017), (T) IL-10 (Dace et al., 2008), and (U) VEGF (Ramanathan et al., 2003).

(V) Overexpression of miR-93 (through miR mimics) decreases hypoxia-induced IL-1β and IFNγ secretion (Ganta et al., 2017). (A–V) All values are normalized (y axes are relative expression levels) and are for proteins unless noted otherwise. For normalization of results (simulation and data in A–V): (D, F, I–L, O–S, U) normalized to their respective t = 0 (Ctr) values; (V) normalized to the Ctr (hypoxia) condition; (A, B, and T) normalized to their respective values at 24 h of IL-1β/TNFα/hypoxia treatments; (C) CXCL9 and IL-12 in (E) normalized to their respective values at the last experimental time points; all others normalized to their respective maximum values. S, simulation; D, experimental data; Hyp, hypoxia; Ctr, control/untreated condition (except in V as described above).

3D, S5A–S5C, and S5I), other pro-inflammatory chemokines and cytokines such as CXCL9-10 and IL-12 (Figures 3B, 3E, and S5J), canonical M1 intracellular marker iNOS (Figures 3C and S5F–S5H), and also M1-associated metabolite such as itaconate (Figure S5K). In parallel with their pro-inflammatory functions, these M1 drivers can also induce the expression of certain anti-inflammatory and pro-angiogenic molecules such as IL-1Ra (IL-1 receptor antagonist, Figure S5D) and VEGF (Figures 3F and S5E), as a potential mechanism to limit excessive inflammation. On the other side, anti-inflammatory drivers such as IL-4 and IL-10 can produce strong M2 responses including upregulation of the canonical M2 intracellular marker ARG1 (Figures 3G and S5L–S5N) and secretion of anti-inflammatory factors such as IL-10 (Figures 3J, 3M, and S5Q) and IL-1Ra (Figures 3H, 3N, S5P, and S5S). In addition, IL-4 and IL-10 can differentially regulate VEGF production (Figures 3F, 3I, and S5O) and downregulate the production and secretion of multiple M1 cytokines (Figures 3K and S5O) and iNOS (Figure S5R). Hypoxia, through HIFs and other transcriptional and post-transcriptional regulators, induces both M1 markers such as iNOS (Figure 3O), IL-1β (Figure 3P), IFNγ (Figure 3Q), TNFα, and IL-12 (Figure 3R) and M2 markers such as ARG1 (Figure 3S) and IL-10 (Figures 3T and S5W), in addition to VEGF (Figures 3U and S5T–S5U), which is a master pro-angiogenic factor downstream of HIFs. An example of hypoxia-mediated post-transcriptional regulation of macrophage polarization is through miR-93, which is downregulated by hypoxia in macrophages (Figure S4X), whereas its overexpression can indirectly suppress the macrophage production of pro-inflammatory cytokines such as IL-1β, IFNγ, and TNFα (Figures 3V and S5X). In addition to these quantitative data, we also incorporated a number of qualitative experimental observations relating to specific signaling/marker regulation within our multi-pathway model scope to further constrain our model behaviors (presented in Figure S6).

Quantitative model validation

For model validation, a separate quantitative dataset (not included in calibration) was compiled using the criterion as described in Transparent methods. Modular comparisons between experimental results (e.g., macrophages treated with high concentrations of stimuli *in vitro*) and corresponding model simulations suggested that our model can correctly predict, from quantitative and temporal aspects, the activation of essential signal transduction cascades and marker expression for the individual pathways modeled (Figures 4A–4E, 4G, 4H, 4M–4P, and 4S–4T). Moreover, the potential of model applications and analyses beyond isolated *in vitro* conditions was again demonstrated by the validation against numerous experimental dose-response curves (Figures 4F, 4I, 4Q, 4R, and 4U) as well as data of combination treatments (Figures 4J–4L) within our model scope.

Generation and interpretation of dynamic macrophage polarization maps

Using our mechanistic model, we have constructed detailed activation maps (for all single and pairwise stimuli described by our model) to comprehensively characterize the dynamic activities of macrophage intracellular signal transduction and the resulting regulation of phenotype markers under typical *in vitro* conditions (e.g., cytokine concentrations in the ng/mL range). Comparisons between the relative fold changes of different markers at early (4 h), delayed (24 h), and late (48 h) time points (Figure 5A) revealed that the strength of the polarization response is highly time dependent at the level of individual markers, although such M1-M2 markers do respond accordingly to the canonical M1-M2 drivers during the
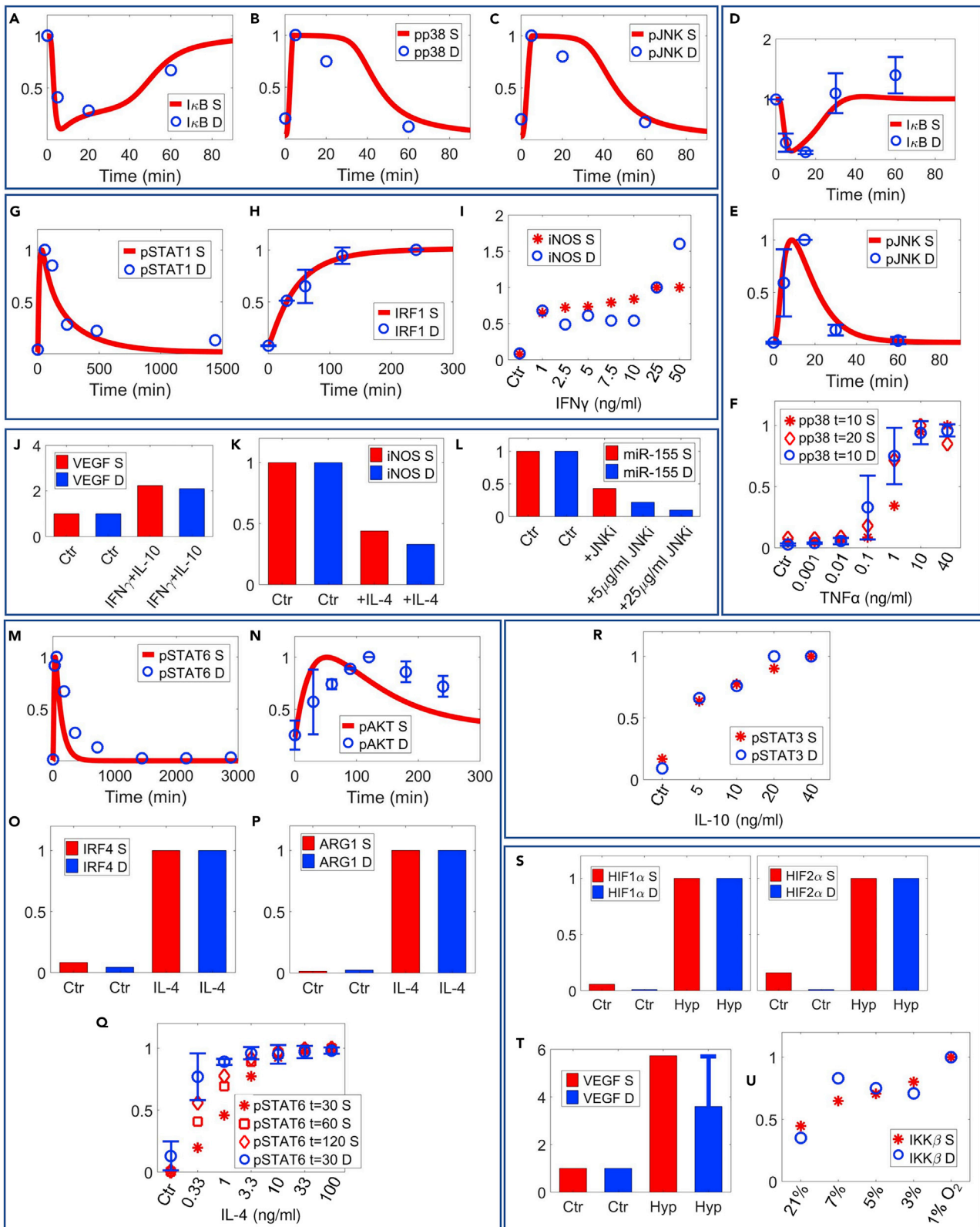
Figure 4. Model validation of essential pathway and marker signatures against untrained experimental data

Model simulations and corresponding macrophage experimental data (not included in calibration) are shown together (references are listed in the order of the data mentioned).

(A–C) IL-1β induces transient IκB degradation and activation of p38 and JNK (Hu et al., 2005).

(D–F) TNFα also induces IκB degradation and JNK activation (Pobezinskaya et al., 2008), and dose-dependent activation of p38 (Winston et al., 1997).

(G–I) IFNγ activates STAT1/IRF1 axis (Piccolo et al., 2017) and dose-dependently induces iNOS expression (Vila-Del Sol et al., 2007).

(J) Simultaneous treatment of IFNγ and IL-10 moderately upregulates VEGF secretion (Wu et al., 2010).

(K) IL-4 pretreatment decreases IFNγ-induced iNOS (Coccia et al., 2000).

(L) Inhibition of JNK decreases TNFα-induced upregulation of miR-155 (O'connell et al., 2007).

(M–P) IL-4 induces time course activation of STAT6 (Zhu et al., 2014) and AKT (Mccormick et al., 2016) and downstream expression of IRF4 and ARG1 (Binder et al., 2013).

(Q and R) (Q) Dose response of IL-4-mediated STAT6 activation (Heller et al., 2008); (R) dose response of IL-10-mediated STAT3 activation (Naiyer et al., 2013).

(S–U) Hypoxia stabilizes HIF1α/HIF2α and induces VEGF secretion (Fang et al., 2009); hypoxia also dose-dependently induces IKKβ expression (Cummins et al., 2006). (A–U) All values are normalized (y axes are relative expression levels) and are for proteins unless noted otherwise. For normalization of results (simulation and data in A–U): (A, D, J, and T) normalized to their respective t = 0 (Ctr) values; (K) normalized to the Ctr (IFNγ-treated) condition; (L) normalized to the Ctr (TNFα-treated) condition; (O and P) normalized to their respective values at 24 h of IL-4 treatment; (S) normalized to the respective values at 18 h of hypoxia; (H) normalized to the values at the last experimental time point; (I) normalized to the values at 25 ng/mL of IFNγ; all others normalized to their respective maximum values. S, simulation; D, experimental data; Hyp, hypoxia; Ctr, control/untreated condition (except in K and L as described above).

simulated time span; at the level of transcription factor activations, the time dependence is, as expected, much stronger as shown in Figure S8A. In addition, our simulations in Figure 5A suggest that the expression of M1-M2 markers are often not mutually exclusive even under single stimuli conditions (e.g., TNFα, hypoxia, IL-1β), and for stimulus combinations the resulting response landscape would very likely differ from the simple qualitative addition of the effects from individual pathways (e.g., IL-1β+IL-10, IFNγ + IL-10). We also calculated the M1/M2 scores (metrics used to estimate the relative dominance of M1 versus M2 response, see Transparent methods for detailed definition) for all single and pairwise stimulus conditions at the three time points evaluated in the activation map. Analyses of time course trajectories (Figure 5B) further indicate that the polarization process can be non-monotonic as seen from examples of self-promoting (a strong overall phenotype response that is augmenting over time, e.g., by IL-4, IL-4+IL-10), self-limiting (a strong response followed by gradual decay or stabilization, e.g., by IFNγ, IFNγ+TNFα), and self-repolarizing (one phenotype response in the beginning and later significantly shifts toward the opposite phenotype, e.g., by IFNγ+IL-4, IL-1β+IL-10). The same analyses were also performed for cytokine stimuli at 100-fold lower concentrations (in the high pg/mL range) to simulate the potential influence of upregulated cytokines *in vivo* on macrophage polarization (Stenken and Poschenrieder, 2015). Our modeling results suggest that for most cases, even modest upregulation of cytokines *in vivo* can still induce differential regulation of transcriptional activities (Figure S8B) in macrophages (although different from their respective *in vitro* patterns) and elicit detectable responses of M1-M2 markers over time (Figure S7), whereas the intensities of the *in vivo* phenotype responses (Figure 5C) are generally much weaker than those under *in vitro* conditions (Figure 5B). These findings again reinforce the argument that macrophage polarization in health and disease should be integratively evaluated as a multi-pathway, multi-marker, and time-dependent response, and that system-level modeling is an effective tool to enable quantitative and mechanistic understanding of the full picture of this response, especially in settings of pathophysiological tissue microenvironments, which are complex and multifactorial by nature.

Model-based sensitivity analyses suggest potential strategies to induce therapeutic macrophage polarization in PAD

We then analyzed the model under a simulated experimental condition of PAD, which is a highly prevalent cardiovascular disease characterized by reduced lower limb blood flow and ischemia, for which therapeutic macrophage polarization has been recently proposed as an emerging route to enhance tissue regeneration and perfusion recovery (Ganta et al., 2017, 2019; Gotze et al., 2020). Hypoxia serum starvation (HSS) is the chosen *in vitro* representation of PAD (Ganta et al., 2017, 2019), and we further simplified it and considered only hypoxia as the essential input for our primary model analyses, because the proliferative effect of serum was so variable and thus was not taken into account during the model formulation. Our model simulations (Figures 6B and S11B) as well as our original experimental data summarized from western blot, qPCR, and flow cytometry analyses (Figures 6C, S9, S10, S14, and S15) together revealed a non-canonical phenotype under HSS that showed selective and time-dependent induction of both M1 and M2 markers. Therefore, to identify potential targets that can effectively reprogram macrophages into less pro-inflammatory and more pro-angiogenic states under HSS, we performed global sensitivity analysis using
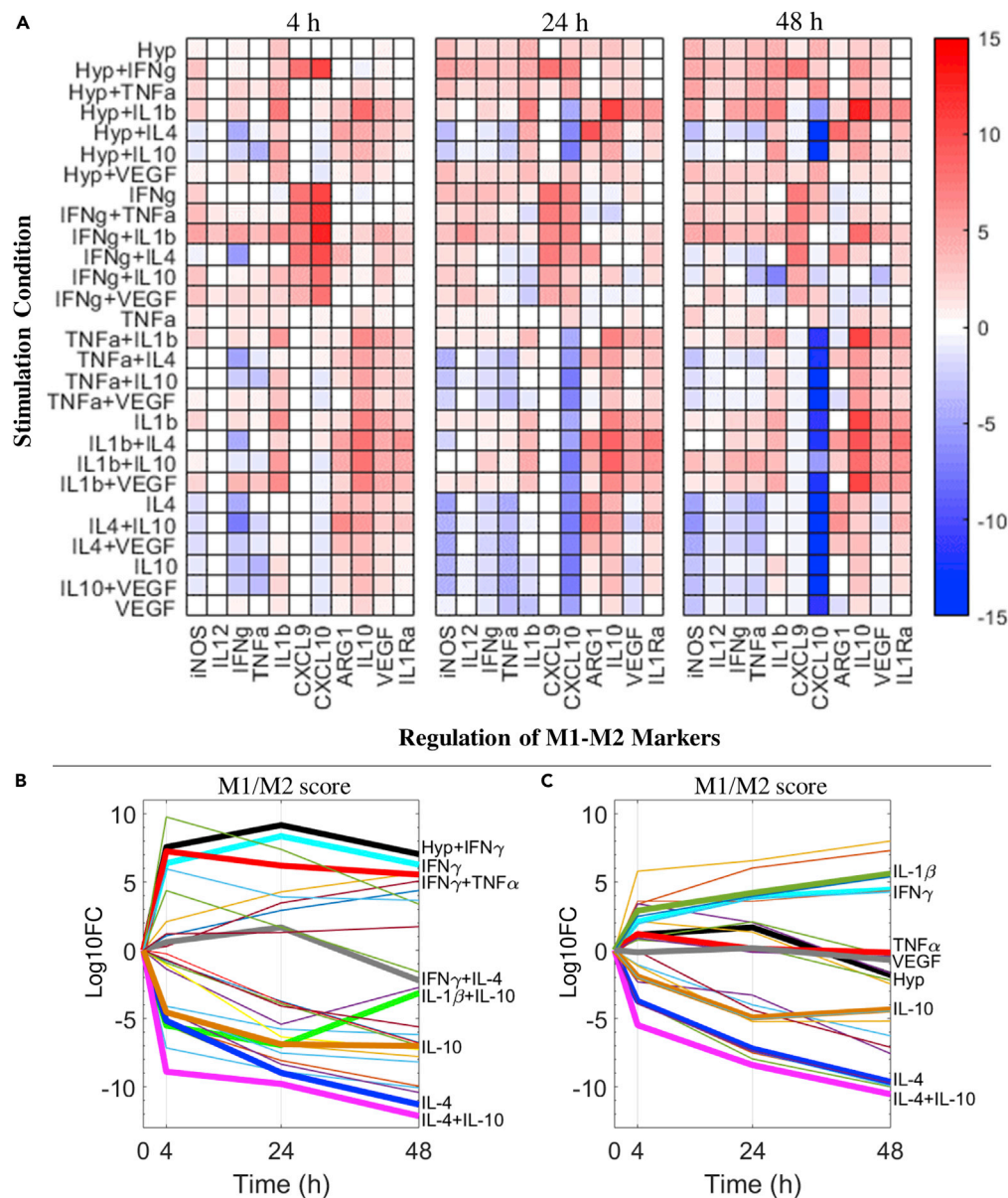
Figure 5. Macrophage polarization map and time course M1-M2 profiles under single and combined stimulation

(A) A model-generated map of M1-M2 marker regulation (at 4, 24, and 48 h of stimulation) by macrophages under different stimulation conditions *in vitro* (7 cases of single stimulus, 21 cases of pairwise combined stimuli). Among the M1-M2 markers described, iNOS, ARG1, IL-12, IL-1Ra, and CXCL9 are protein levels; CXCL10 is mRNA level; and the remaining ones are the respective protein production rates calculated by the model. All results are normalized to the untreated/t = 0 values and then log2 transformed.

(B) Time course trajectories of relative dominance of M1-M2 features (in terms of M1/M2 scores; positive, M1-like; negative, M2-like) in all the *in vitro* stimulation conditions.

(C) Trajectories from the same analyses but under simulated *in vivo* stimulus concentrations. (B and C) All results are normalized to the M1/M2 score calculated at untreated/t = 0 and then log10 transformed. Some of the trajectories are bolded and labeled for better data illustration. Hyp, hypoxia (2% O$_2$).

the PRCC (partial rank correlation coefficient) algorithm to search for model parameters that can most significantly influence the time course macrophage polarization profiles (see Transparent methods for more details) (Marino et al., 2008). From the results in Figure 6A, we see that the most influential parameters can be categorized into seven signaling modules described in our model, and based on that we then
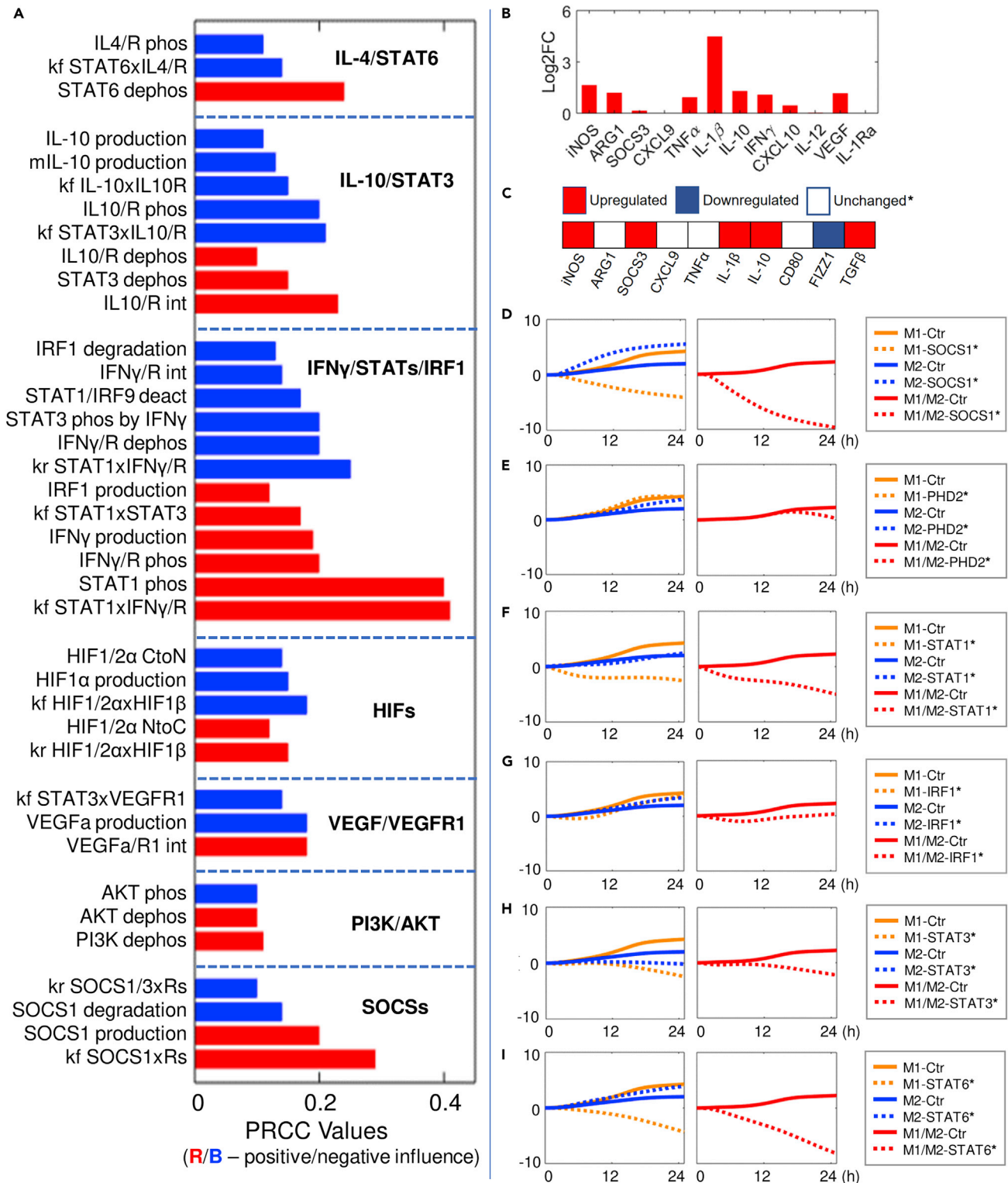
Figure 6. Macrophage response under hypoxia/HSS and evaluation of sensitivity analysis-derived macrophage repolarization strategies

(A) Sensitivity indices (red, positive; blue, negative) of the most influential model parameters (e.g., absolute PRCC values great than 0.1) that control M1 and M2 marker expression (in terms of the 24 h time course integral of M1/M2 score) in hypoxia (2% O_2). The identified parameters are categorized into seven modules, and their functions are briefly described.

Figure 6. Continued

(B) Simulated profile of macrophage M1-M2 marker expression at 8 h under hypoxia/HSS (represented by model as 2% O_2). Expression levels are normalized to the t = 0 (control condition) values and then log2 transformed.

(C) Summary of experimentally measured directional regulation of multiple macrophage M1-M2 markers under HSS based on our original *in vitro* data (experimental results of individual markers are shown in detail in Figures S9 and S10). The category of unchanged also includes markers that are experimentally undetectable.

(D–I) Simulated M1 (orange), M2 (blue) profiles (e.g., M1 and M2 scores) and overall M1/M2 scores (red) over time under hypoxia with various targeted interventions (label as "species*") proposed by the sensitivity analysis. Results are normalized to the respective values at t = 0 and then log10 transformed (y axes). Implementation of targeted interventions: (D) SOCS1 inhibition, 10x k101; (E) PHD2 inhibition, 0.1x kf62; (F) STAT1 inhibition, 0.1x kf3; (G) IRF1 inhibition, 10x k85; (H) STAT3, 0.1x k127; (I) STAT6, 0.1x k26. (A) Details of the listed parameters are described in Table S1 (parameter labels from top to bottom: kf102, k24, k26; k156, k44, kf144, kf145, kf146, kr145, k127, k148; k85, k12, k117, k134, kr2, kr3, k52, kf131, k73, kf2, k4, kf3; kf58, k54, kf60, kr58, kr60; kf207, k72, k201; k138, k140, k137; kr11, k101, k135, kf11).

simulated a number of targeted interventions that are potentially feasible in experiments and assessed the resulting time course M1-M2 profiles. Among the STAT/IRF targets, we see that targeting STAT1 activation (through inhibition of its association with IFNGR, Figure 6F) or STAT6 (through inhibition of its deactivation, Figure 6I) can both lead to potent repolarization toward M2 (anti-inflammatory, pro-angiogenic) phenotypes, whereas the effect of targeting STAT3 (through inhibition of its deactivation, Figure 6H) or IRF1 (through increased degradation, Figure 6G) or inhibiting STAT1 dimerization (Figure S11D) is either less ideal or ineffective. Enhancing HIF1/2α expression (through inhibition of PHD activities, Figure 6E) or AKT activation (Figure S11E) is also suggested to be ineffective overall as both strategies fail to downregulate the pro-inflammatory M1 response, although they are able to enhance the production of anti-inflammatory and pro-angiogenic factors. Interestingly, our simulations showed that inhibition of SOCS1 (through increased degradation, Figure 6D) could also be an effective strategy to drive the M1-to-M2 repolarization under HSS, which is not readily apparent given the negative feedback function of SOCS1 in both canonical M1 (e.g., LPS) and M2 (e.g., IL-4) signaling, but this prediction is in agreement with the finding from a previous study showing that SOCS1 silencing can increase the ratio of anti-inflammatory to pro-inflammatory features in polarized macrophages (Whyte et al., 2011). At the level of cytokines, direct inhibition of endogenous IFNγ production as well as promotion of VEGF (the pro-angiogenic isoform) or IL-10 production are all suggested to effectively induce M1-to-M2 repolarization (Figures S11F–S11H). The predicted effect of targeting IL-10 to improve M2-like macrophage polarization and potentially ischemic tissue perfusion has been recently confirmed in a mouse model of PAD (Gotze et al., 2020).

We also performed the same set of analyses for another potential model representation of HSS (hypoxia plus reduced protein and RNA synthesis, see Transparent Methods for more details) (Zetterberg and Skold, 1969), and the overall results (Figure S11A) were similar to the hypoxia-only representation. In addition to sensitivity analysis, we performed model uncertainty quantification using the bootstrap method (see Transparent methods for more details) with a focus on the identifiability of a set of most influential parameters. The results suggested relatively robust clustering of these parameters against our calibration datasets (Figure S12).

In silico single-cell analysis of model-based virtual macrophages

To further explore the variability in the macrophage polarization spectrum, we generated 100 digital alternative versions of our model (using the method described in Transparent methods), although each alternative version can be considered as an individual macrophage with consistent mechanisms and physiology but different innate biochemical reaction rates compared with the others, to approximate physiological cell-to-cell heterogeneity within a general macrophage population (Altschuler and Wu, 2010). We simulated this virtual macrophage population under hypoxia and observed a widespread spectrum of overall M1-M2 phenotypes, which are not uniform in terms of polarization intensities or directions (Figures 7A–7C), and such diversity likely originated from variabilities in both the intermediate signal transduction cascades (Figures S13A–S13F) and the downstream mechanistic regulation of M1-M2 markers (Figures S13G–S13J) in each individual cell. The impact of such a spectrum-like response is more evident under scenarios of simulated therapeutic interventions: although inhibiting STAT6 or STAT3 deactivation (as discussed in the previous section) under hypoxia can both induce apparent M1-to-M2 repolarization in an average macrophage (e.g., the reference model behavior in bold black lines in Figures 7D and 7E), in the simulated population only a portion of the cells would respond and be repolarized to the M2-like phenotypes upon STAT3 targeting, whereas almost all cells were successfully polarized to the M2-like phenotype transition upon STAT6 targeting (Figures 7D–7F). This simulation-derived phenomenon of partial
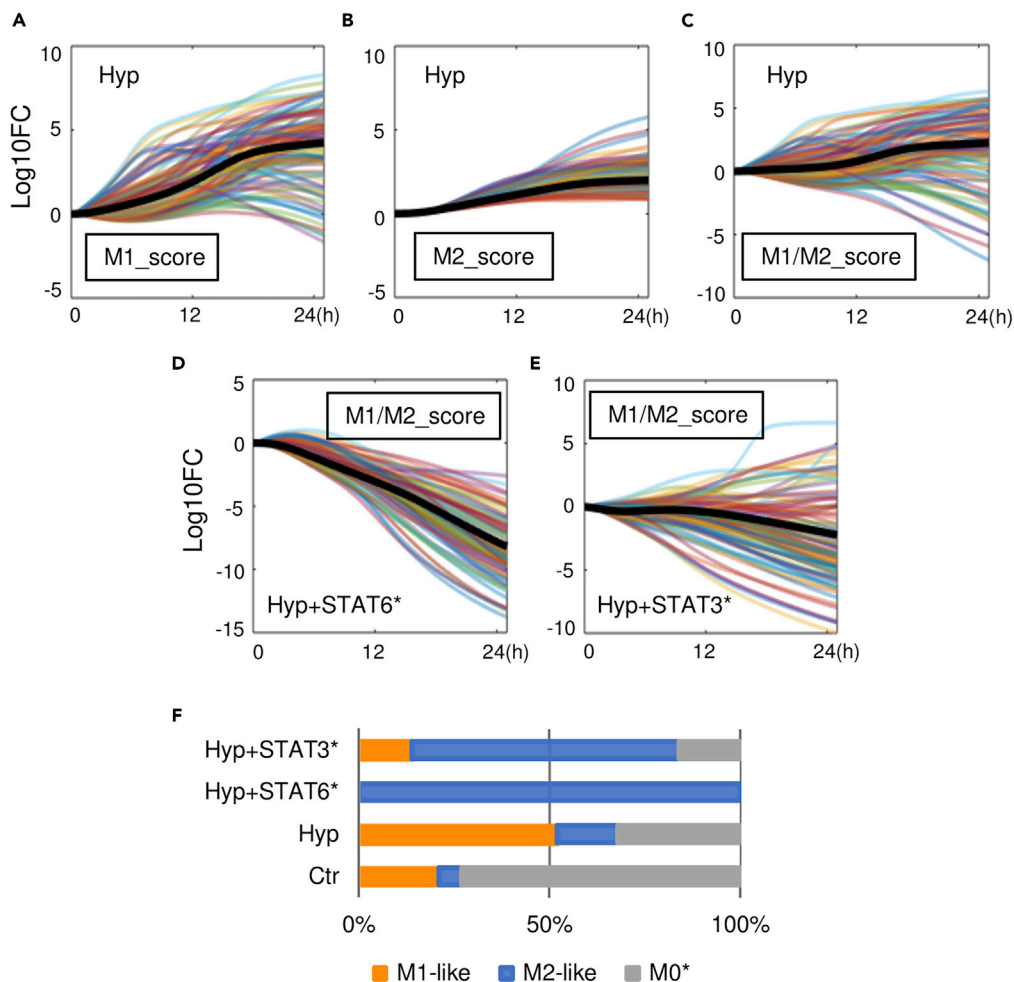
Figure 7. *In silico* single-cell analysis of model-derived virtual macrophage populations

(A–E) Simulated time course responses of 100 model-generated virtual macrophages in terms of (A) relative M1 scores and (B) M2 scores under hypoxia (2% O_2); (C) relative M1/M2 scores under hypoxia, (D) under hypoxia plus intervention targeting STAT6 (dephosphorylation rate x0.1), and (E) under hypoxia plus intervention targeting STAT3 (dephosphorylation rate x0.1). (A–E) Results are normalized to the respective values at t = 0 and then log10 transformed (y axes). Black bolded lines are the trajectories of the reference model.

(F) Percentages of M1-like, M2-like, and insignificantly polarized cells (M0*) under the above simulated conditions evaluated at 24 h (detailed definitions of M1-like, M2-like, and M0* are described in Transparent methods). Ctr, control/ untreated condition; Hyp, hypoxia.

response due to cell-level macrophage heterogeneity could have important implications for therapies that aim to treat diseases by modulating macrophages in the microenvironment (e.g., targeting tumor-associated macrophages to treat cancer), as the remaining macrophages that are unresponsive to targeted therapies may still possess sufficient functions to drive disease progression and hamper the overall treatment efficacies, and this proposed idea is supported by a recent study that examined macrophage-targeted therapies in colon cancer (Zhang et al., 2020). Furthermore, based on the simulation of our virtual macrophage population, we find that a small portion of cells under control condition (no external stimulation) can already exhibit M1-or M2-like phenotypes, whereas most cells are at unpolarized states (Figure 7F), and this phenomenon has also been confirmed *in vitro* by recent single-cell studies (Muñoz-Rojas et al., 2020; Li et al., 2019). In summary, the simulations presented here suggest that our systems-level model can be exploited in highly flexible and efficient ways to enable *in silico* investigation of macrophage polarization from the single-cell perspective, while offering extra mechanistic insights regarding its temporal, dose-dependent, and quantitative features.

DISCUSSION

We have here developed and presented a novel large-scale mechanistic computational model that enables, for the first time, a systems-level description (from quantitative, temporal, dose-dependent, and single-cell perspectives) of macrophage polarization under a complex M1-M2 multi-pathway network. Compared with previous models on this topic (Figure S1), the comprehensive model calibration and validation we implemented using an unprecedentedly large amount of experimental data further allows us to probe into and predictively simulate several essential features that constitute the spectrum-like physiology of macrophage polarization, such as its integrative multi-pathway signal transduction and feedback, multimodal transcriptional and post-transcriptional target regulation, dynamic production of phenotype markers, and fine-tuned self-modulation via autocrine signaling. Although in our analyses we selected an *in vitro* experimental condition of PAD to demonstrate model utility and its potential translational application, the mechanistic setup of our model in terms of the pathways and mechanisms included is equally important for macrophages under general as well as other disease-specific scenarios. Still, the model certainly does not account for the full biology (an innate limitation even for large-scale models), as it is practically infeasible, due to relatively limited experimental data and high computational cost, to detail and calibrate every known pathway and mechanism that regulate macrophage polarization within a single modeling study while maintaining a high degree of model performance accuracy (Frohlich et al., 2018; Bouhaddou et al., 2018; Schmiester et al., 2020). Thus, our current model and its formulation can instead serve as a high-quality mechanistic computational platform that can be accordingly and continuously expanded and enriched with additional pathway details to further investigate macrophage functions in specific disease areas of interest, e.g., TLR pathways in various infectious disease settings (O'neill et al., 2009), CD47/SIRPα axis in macrophage-mediated cancer immunotherapy (Weiskopf, 2017), and cellular metabolic pathways in nonalcoholic fatty liver disease (Oates et al., 2019).

As our model was formulated and calibrated based on a large number of experimental data derived from independent studies using different macrophage cell lines, a major limitation is the unifying assumption we made that these data all come from consistent *in vitro* differentiation and culture conditions before stimulation and that all data were used to model the behavior of an "average" macrophage culture. In fact, technical differences in macrophage culture protocols can notably influence the resulting macrophage behaviors. It has been shown that GM-CSF and M-CSF, two commonly used factors in the experimental differentiation of macrophages from monocytes, can differentially regulate M1-M2 marker expression at baseline and also predispose macrophages to enhanced M1 and M2 responses, respectively, when further challenged by other stimuli (Hamilton et al., 2014; Fleetwood et al., 2007). Different concentrations and durations of PMA (phorbol 12-myristate-13-acetate), which is widely used to condition the human monocytic THP-1 cells, also results in wide variations of downstream protein expression and ultimately nontrivial differences in their polarization responses (Pinto et al., 2020). In addition, innate genetic differences between human and mouse macrophage cell lines (Thomas and Mattila, 2014), between cell lines of human origin (Mendoza-Coronel and Castanon-Arreola, 2016; Shiratori et al., 2017), and between mouse cell lines derived from different strains (Santos et al., 2006) can all lead to differential macrophage phenotype outcomes (e.g., inconsistent marker expression patterns) when these cells are treated with the same stimulation. While this evidence may suggest that the qualitative instead of quantitative aspects of certain model predictions would be more meaningful when tested experimentally across cell lines, our mechanistic model formulation (compared to other logic-based models) can in fact readily incorporate cell line-specific genomic and proteomic data, if available, to simulate the spectrum of response driven by those innate differences (as partially reflected by our *in silico* single-cell analysis). Another limitation resulted from our unifying assumption is that the model does not explicitly consider any potential effects of serum starvation, a commonly used experimental protocol, in its simulations. Although serum composition is poorly defined and also highly variable across studies, which makes it a possible factor that could complicate experimental results and reproducibility, serum depletion/starvation, apart from being a procedure to eliminate that factor, has been also shown to alter basal signaling, transcriptional patterns, and energy metabolism in several cell types, and the combinations of serum starvation with hypoxia or low glucose are considered appropriate *in vitro* models for certain ischemic diseases and tumors (Pirkmajer and Chibalin, 2011; Williams et al., 2016; Zheng et al., 2016; Golpour et al., 2014). As a complete mechanistic description of serum/starvation may be inherently infeasible, future efforts can focus on the most significant serum starvation-induced signaling and metabolic changes in macrophages, using semi-mechanistic or phenomenological methods, to better model its impact when more data becomes available. Another technical limitation is about the uniqueness of model parameterization. Although the large amount of calibration data and initial condition passing

criteria we used have managed to confine the value distribution of the high-sensitivity parameter subset, it is still possible that our full model parameterization is associated with practical unidentifiability to some extent, as the parameter space has not been comprehensively explored here due to the limited degree of freedom allowed in the uncertainty analysis.

The model-based macrophage polarization maps under simulated *in vitro* and *in vivo* conditions revealed a wide space of heterogeneous macrophage functional phenotypes in terms of the dynamic expression and activation (e.g., up/downregulation, expression intensities) of an array of pro- and anti-inflammatory markers as well as transcription factors. This is based on the reasoning that macrophage functions cannot be reliably defined by only one or two phenotype markers, as these individual markers can likely be induced under multiple conditions, and that markers with opposing functions (e.g., M1 versus M2) may also co-express in non-mutually exclusive manners in the polarization spectrum (both observations were reflected in our simulations). Indeed, reliability and reproducibility of these individual markers has been a long-time issue in the field and more experimental studies now have shifted from the single-marker approach (e.g., iNOS versus ARG1, CD86 versus CD163) to the multi-marker approach that encompasses M1-M2 markers of different classes (e.g., cytokine, chemokine, intracellular protein, surface receptor, transcription factor) to better correlate phenotypes with the pleiotropic regulatory functions of macrophages (Murray et al., 2014; Gerrick et al., 2018; Chazaud, 2020; Jayasingam et al., 2019). In addition to the phenotype heterogeneity driven by complex combinations of stimulating signals, our model demonstrated that such heterogeneity could also occur at the single cell-level response even under a uniform polarizing condition. This could be highly relevant for the *in vivo* functional interpretation of macrophages under physiological and pathological settings, as they naturally exist in a continuum of functional states possibly due to the presence of diverse signals that can vary spatiotemporally in the microenvironment as well as normal cell-to-cell variations in gene and protein expression (Martins et al., 2017; Das et al., 2015; Jayasingam et al., 2019). Therefore, it is also of significant research and translational values to integrate mechanistic cell-level macrophage models (like ours) into higher-level tissue and whole-body scales to systematically simulate and investigate molecular-level target regulation, pathway-level signal transduction, and dynamic cell-cell communications that integratively define the underlying biological processes behind the macroscopic macrophage-environment-disease linkages (Martin et al., 2016; Sove et al., 2020; Norton et al., 2019). Interestingly, a recent modeling study by Cess et al. has in fact incorporated a previous cell-level macrophage model developed by us (which was the basis for the model presented here) into their multi-scale system to simulate cell-cell interactions within the tumor microenvironment and has provided mechanistic insights regarding the optimal modalities of macrophage-based immunotherapies against tumors (Cess and Finley, 2020). In summary, the development of our model marks a significant step forward in the data-driven systems biology representation of the "virtual macrophage" concept through which heterogeneous datasets and new discoveries can be continuously and efficiently integrated to enable mechanistic, systems-level investigation of novel emergent properties in macrophage polarization and physiology.

Limitations of the study

Several limitations of the study, including the assumption used in model development that all calibration data were derived from the same culture conditions, the simplification regarding the effects of serum and serum starvation during simulation, uniqueness of model parametrization, and the completeness of model biology, have been discussed in the Discussion section. In addition, it should be noted that although the model can efficiently simulate the dynamic and quantitative aspects of macrophage polarization in terms of the response of individual phenotype markers and a high-level metric (M1/M2 score), there is still a link to be made between the model-generated marker phenotypes and the ultimate functional phenotypes in terms of how macrophages actually regulate other cells in inflammation and angiogenesis. For example, the net regulatory effect of polarized macrophages (driven by a stimulus) on endothelial cell proliferation and tube formation would be a key readout of the macrophage functional phenotype in angiogenesis, although the correlation between this experimental readout and model-simulated marker response still remains to be mechanistically elucidated by future studies through a combination of experimental and computational approaches. For the exploratory *in silico* single-cell analysis that we performed using this model, although we generated a number of virtual single cells based on some mechanistic aspects of cell-to-cell heterogeneity and these cells can together produce a reasonable distribution of response to reflect certain physiological features, future efforts shall further refine the methodology used to formulate model-based single cells so that such virtual cells can be enriched with quantitative inputs from experimentally measured single-cell RNA and protein data, to better enable generation of model predictions with high translational values.

Resource availability

Lead contact

Further information and requests for resources and data should be directed to the Lead Contact, Chen Zhao (czhao22@jhmi.edu).

Materials availability

This study did not generate new unique reagents.

Data and code availability

All relevant data are described within the manuscript and its Supporting Information files. Details of all model reactions, equations, parameters, initial conditions, and data are summarized in Tables S1–S3. The complete model coded in SBML format (.xml file) and executable MATLAB scripts (.m files) that can run the model to generate sample simulations and analysis are provided in the Supplemental Information files.

METHODS

All methods can be found in the accompanying Transparent Methods supplemental file.

SUPPLEMENTAL INFORMATION

Supplemental information can be found online at https://doi.org/10.1016/j.isci.2021.102112.

AUTHOR CONTRIBUTIONS

C.Z., B.H.A., and A.S.P. contributed to the conceptualization of the study. C.Z. designed and implemented the computational model and performed model simulations and analysis. R.J.S. helped with the model uncertainty analysis. C.Z. and T.X.M. designed the *in vitro* experiments, and T.X.M. performed the *in vitro* experiments and collected and analyzed the data. C.Z. wrote the first draft, and all authors contributed to the review and editing of the manuscript.

DECLARATION OF INTERESTS

The authors have declared that no competing interests exist.

REFERENCES

Acosta-Iborra, B., Elorza, A., Olazabal, I.M., Martin-Cofreces, N.B., Martin-Puig, S., Miro, M., Calzada, M.J., Aragones, J., Sanchez-Madrid, F., and Landazuri, M.O. (2009). Macrophage oxygen sensing modulates antigen presentation and phagocytic functions involving IFN-gamma production through the HIF-1 alpha transcription factor. J. Immunol. *182*, 3155–3164.

Altschuler, S.J., and Wu, L.F. (2010). Cellular heterogeneity: do differences make a difference? Cell *141*, 559–563.

Atri, C., Guerfali, F.Z., and Laouini, D. (2018). Role of human macrophage polarization in inflammation during infectious diseases. Int. J. Mol. Sci. *19*, 1801.

Barrett, T.J. (2020). Macrophages in atherosclerosis regression. Arterioscler Thromb. Vasc. Biol. *40*, 20–33.

Binder, F., Hayakawa, M., Choo, M.K., Sano, Y., and Park, J.M. (2013). Interleukin-4-induced beta-catenin regulates the conversion of macrophages to multinucleated giant cells. Mol. Immunol. *54*, 157–163.

Blanchette, J., Jaramillo, M., and Olivier, M. (2003). Signalling events involved in interferon-gamma-inducible macrophage nitric oxide generation. Immunology *108*, 513–522.

Boscolo, E., Mulliken, J.B., and Bischoff, J. (2011). VEGFR-1 mediates endothelial differentiation and formation of blood vessels in a murine model of infantile hemangioma. Am. J. Pathol. *179*, 2266–2277.

Bouhaddou, M., Barrette, A.M., Stern, A.D., Koch, R.J., Distefano, M.S., Riesel, E.A., Santos, L.C., Tan, A.L., Mertz, A.E., and Birtwistle, M.R. (2018). A mechanistic pan-cancer pathway model informed by multi-omics data interprets stochastic cell fate responses to drugs and mitogens. PLoS Comput. Biol. *14*, e1005985.

Braun, D.A., Fribourg, M., and Sealfon, S.C. (2013). Cytokine response is determined by duration of receptor and signal transducers and activators of transcription 3 (STAT3) activation. J. Biol. Chem. *288*, 2986–2993.

Caldwell, A.B., Cheng, Z., Vargas, J.D., Birnbaum, H.A., and Hoffmann, A. (2014). Network dynamics determine the autocrine and paracrine signaling functions of TNF. Genes Dev. *28*, 2120–2133.

Carta, L., Pastorino, S., Melillo, G., Bosco, M.C., Massazza, S., and Varesio, L. (2001). Engineering of macrophages to produce IFN-gamma in response to hypoxia. J. Immunol. *166*, 5374–5380.

Cassetta, L., and Pollard, J.W. (2018). Targeting macrophages: therapeutic approaches in cancer. Nat. Rev. Drug Discov. *17*, 887–904.

Cess, C.G., and Finley, S.D. (2020). Multi-scale modeling of macrophage-T cell interactions within the tumor microenvironment. PLoS Comput. Biol. *16*, e1008519.

Chang, E.Y., Guo, B., Doyle, S.E., and Cheng, G. (2007). Cutting edge: involvement of the type I IFN production and signaling pathway in lipopolysaccharide-induced IL-10 production. J. Immunol. *178*, 6705–6709.

Chavez-Galan, L., Olleros, M.L., Vesin, D., and Garcia, I. (2015). Much more than M1 and M2 macrophages, there are also CD169(+) and TCR(+) macrophages. Front. Immunol. *6*, 263.

Chazaud, B. (2020). Inflammation and skeletal muscle regeneration: leave it to the macrophages! Trends Immunol. *41*, 481–492.

Coccia, E.M., Stellacci, E., Marziali, G., Weiss, G., and Battistini, A. (2000). IFN-gamma and IL-4 differently regulate inducible NO synthase gene expression through IRF-1 modulation. Int. Immunol. *12*, 977–985.

Colin, S., Chinetti-Gbaguidi, G., and Staels, B. (2014). Macrophage phenotypes in atherosclerosis. Immunol. Rev. *262*, 153–166.

Covarrubias, A.J., Aksoylar, H.I., Yu, J., Snyder, N.W., Worth, A.J., Iyer, S.S., Wang, J., Ben-Sahra, I., Byles, V., Polynne-Stapornkul, T., et al. (2016). Akt-mTORC1 signaling regulates Acly to integrate metabolic input to control of macrophage activation. Elife *5*, e11612.

Cummins, E.P., Berra, E., Comerford, K.M., Ginouves, A., Fitzgerald, K.T., Seeballuck, F., Godson, C., Nielsen, J.E., Moynagh, P., Pouyssegur, J., and Taylor, C.T. (2006). Prolyl hydroxylase-1 negatively regulates IkappaB kinase-beta, giving insight into hypoxia-induced NFkappaB activity. Proc. Natl. Acad. Sci. U S A *103*, 18154–18159.

Dace, D.S., Khan, A.A., Kelly, J., and Apte, R.S. (2008). Interleukin-10 promotes pathological angiogenesis by regulating macrophage response to hypoxia during development. PLoS One *3*, e3381.

Das, A., Sinha, M., Datta, S., Abas, M., Chaffee, S., Sen, C.K., and Roy, S. (2015). Monocyte and macrophage plasticity in tissue repair and regeneration. Am. J. Pathol. *185*, 2596–2606.

Ehlting, C., Lai, W.S., Schaper, F., Brenndorfer, E.D., Matthes, R.J., Heinrich, P.C., Ludwig, S., Blackshear, P.J., Gaestel, M., Haussinger, D., and Bode, J.G. (2007). Regulation of suppressor of cytokine signaling 3 (SOCS3) mRNA stability by TNF-alpha involves activation of the MKK6/ p38MAPK/MK2 cascade. J. Immunol. *178*, 2813–2826.

El Chartouni, C., Schwarzfischer, L., and Rehli, M. (2010). Interleukin-4 induced interferon regulatory factor (Irf) 4 participates in the regulation of alternative macrophage priming. Immunobiology *215*, 821–825.

Ermolaeva, M.A., Michallet, M.C., Papadopoulou, N., Utermohlen, O., Kranidioti, K., Kollias, G., Tschopp, J., and Pasparakis, M. (2008). Function of TRADD in tumor necrosis factor receptor 1 signaling and in TRIF-dependent inflammatory responses. Nat. Immunol. *9*, 1037–1046.

Etemadi, N., Chopin, M., Anderton, H., Tanzer, M.C., Rickard, J.A., Abeysekera, W., Hall, C., Spall, S.K., Wang, B., Xiong, Y., et al. (2015). TRAF2 regulates TNF and NF-kappaB signalling to suppress apoptosis and skin inflammation independently of Sphingosine kinase 1. Elife *4*, e10592.

Fang, H.Y., Hughes, R., Murdoch, C., Coffelt, S.B., Biswas, S.K., Harris, A.L., Johnson, R.S., Imityaz, H.Z., Simon, M.C., Fredlund, E., et al. (2009). Hypoxia-inducible factors 1 and 2 are important transcriptional effectors in primary macrophages experiencing hypoxia. Blood *114*, 844–859.

Fleetwood, A.J., Lawrence, T., Hamilton, J.A., and Cook, A.D. (2007). Granulocyte-macrophage colony-stimulating factor (CSF) and macrophage CSF-dependent macrophage phenotypes display differences in cytokine profiles and transcription factor activities: implications for CSF blockade in inflammation. J. Immunol. *178*, 5245–5252.

Frede, S., Stockmann, C., Freitag, P., and Fandrey, J. (2006). Bacterial lipopolysaccharide induces HIF-1 activation in human monocytes via p44/42 MAPK and NF-kappaB. Biochem. J. *396*, 517–527.

Frohlich, F., Kessler, T., Weindl, D., Shadrin, A., Schmiester, L., Hache, H., Muradyan, A., Schutte, M., Lim, J.H., Heinig, M., et al. (2018). Efficient parameter estimation enables the prediction of drug response using a mechanistic pan-cancer pathway model. Cell Syst. *7*, 567–579 e6.

Ganta, V.C., Choi, M., Farber, C.R., and Annex, B.H. (2019). Antiangiogenic VEGF165b regulates macrophage polarization via S100A8/S100A9 in peripheral artery disease. Circulation *139*, 226–242.

Ganta, V.C., Choi, M.H., Kutateladze, A., Fox, T.E., Farber, C.R., and Annex, B.H. (2017). A MicroRNA93-interferon regulatory factor-9-immunoresponsive gene-1-itaconic acid pathway modulates M2-like macrophage polarization to revascularize ischemic muscle. Circulation *135*, 2403–2425.

Gao, S., Li, C., Zhu, Y., Wang, Y., Sui, A., Zhong, Y., Xie, B., and Shen, X. (2017). PEDF mediates pathological neovascularization by regulating macrophage recruitment and polarization in the mouse model of oxygen-induced retinopathy. Sci. Rep. *7*, 42846.

Gerrick, K.Y., Gerrick, E.R., Gupta, A., Wheelan, S.J., Yegnasubramanian, S., and Jaffee, E.M. (2018). Transcriptional profiling identifies novel regulators of macrophage polarization. PLoS One *13*, e0208602.

Gionfriddo, G., Plastina, P., Augimeri, G., Catalano, S., Giordano, C., Barone, I., Morelli, C., Giordano, F., Gelsomino, L., Sisci, D., et al. (2020). Modulating tumor-associated macrophage polarization by synthetic and natural PPARgamma ligands as a potential target in breast cancer. Cells *9*, 174.

Golpour, M., Akhavan Niaki, H., Khorasani, H.R., Hajian, A., Mehrasa, R., and Mostafazadeh, A. (2014). Human fibroblast switches to anaerobic metabolic pathway in response to serum starvation: a mimic of warburg effect. Int. J. Mol. Cell Med. *3*, 74–80.

Gotze, A.M., Schubert, C., Jung, G., Dorr, O., Liebetrau, C., Hamm, C.W., Schmitz-Rixen, T., Troidl, C., and Troidl, K. (2020). IL10 alters peri-collateral macrophage polarization and hind-limb reperfusion in mice after femoral artery ligation. Int. J. Mol. Sci. *21*, 2821.

Hamilton, T.A., Zhao, C., Pavicic, P.G., Jr., and Datta, S. (2014). Myeloid colony-stimulating factors as regulators of macrophage polarization. Front. Immunol. *5*, 554.

Heller, N.M., Qi, X., Junttila, I.S., Shirey, K.A., Vogel, S.N., Paul, W.E., and Keegan, A.D. (2008). Type I IL-4Rs selectively activate IRS-2 to induce target gene expression in macrophages. Sci. Signal. *1*, ra17.

Helm, O., Held-Feindt, J., Grage-Griebenow, E., Reiling, N., Ungefroren, H., Vogel, I., Kruger, U., Becker, T., Ebsen, M., Rocken, C., et al. (2014). Tumor-associated macrophages exhibit pro- and anti-inflammatory properties by which they impact on pancreatic tumorigenesis. Int. J. Cancer *135*, 843–861.

Hempel, S.L., Monick, M.M., and Hunninghake, G.W. (1996). Effect of hypoxia on release of IL-1 and TNF by human alveolar macrophages. Am. J. Respir. Cell Mol. Biol. *14*, 170–176.

Hu, J., Wang, G., Liu, X., Zhou, L., Jiang, M., and Yang, L. (2014). A20 is critical for the induction of Pam3CSK4-tolerance in monocytic THP-1 cells. PLoS One *9*, e87528.

Hu, X., Ho, H.H., Lou, O., Hidaka, C., and Ivashkiv, L.B. (2005). Homeostatic role of interferons conferred by inhibition of IL-1-mediated inflammation and tissue destruction. J. Immunol. *175*, 131–138.

Hu, X., Paik, P.K., Chen, J., Yarilina, A., Kockeritz, L., Lu, T.T., Woodgett, J.R., and Ivashkiv, L.B. (2006). IFN-gamma suppresses IL-10 production and synergizes with TLR2 by regulating GSK3 and CREB/AP-1 proteins. Immunity *24*, 563–574.

Jayasingam, S.D., Citartan, M., Thang, T.H., Mat Zin, A.A., Ang, K.C., and Ch'ng, E.S. (2019). Evaluating the polarization of tumor-associated

macrophages into M1 and M2 phenotypes in human cancer tissue: technicalities and challenges in routine clinical practice. Front. Oncol. 9, 1512.

Joyce, D.A., Steer, J.H., and Kloda, A. (1996). Dexamethasone antagonizes IL-4 and IL-10-induced release of IL-1RA by monocytes but augments IL-4-, IL-10-, and TGF-beta-induced suppression of TNF-alpha release. J. Interferon Cytokine Res. 16, 511–517.

Kazankov, K., Jorgensen, S.M.D., Thomsen, K.L., Moller, H.J., Vilstrup, H., George, J., Schuppan, D., and Gronbaek, H. (2019). The role of macrophages in nonalcoholic fatty liver disease and nonalcoholic steatohepatitis. Nat. Rev. Gastroenterol. Hepatol. 16, 145–159.

Lawrence, T., and Natoli, G. (2011). Transcriptional regulation of macrophage polarization: enabling diversity with identity. Nat. Rev. Immunol. 11, 750–761.

Lee, C., Bae, S.S., Joo, H., and Bae, H. (2017). Melittin suppresses tumor progression by regulating tumor-associated macrophages in a Lewis lung carcinoma mouse model. Oncotarget 8, 54951–54965.

Li, C., Menoret, A., Farragher, C., Ouyang, Z., Bonin, C., Holvoet, P., Vella, A.T., and Zhou, B. (2019). Single cell transcriptomics based-MacSpectrum reveals novel macrophage activation signatures in diseases. JCI Insight 5, e126453.

Li, H., Jiang, T., Li, M.Q., Zheng, X.L., and Zhao, G.J. (2018). Transcriptional regulation of macrophages polarization by MicroRNAs. Front. Immunol. 9, 1175.

Lin, C.F., Tsai, C.C., Huang, W.C., Wang, C.Y., Tseng, H.C., Wang, Y., Kai, J.I., Wang, S.W., and Cheng, Y.L. (2008). IFN-gamma synergizes with LPS to induce nitric oxide biosynthesis through glycogen synthase kinase-3-inhibited IL-10. J. Cell Biochem. 105, 746–755.

Lindsey, M.L., Saucerman, J.J., and Deleon-Pennell, K.Y. (2016). Knowledge gaps to understanding cardiac macrophage polarization following myocardial infarction. Biochim. Biophys. Acta 1862, 2288–2292.

Liu, X., Zhang, J., Zeigler, A.C., Nelson, A.R., Lindsey, M.L., and Saucerman, J.J. (2019). Network Analysis Reveals a Distinct axis of Macrophage Activation in Response to Conflicting Inflammatory Cues (bioRxiv), p. 844464.

Lo, S.Z., Steer, J.H., and Joyce, D.A. (2011). Tumor necrosis factor-alpha promotes survival in methotrexate-exposed macrophages by an NF-kappaB-dependent pathway. Arthritis Res. Ther. 13, R24.

Luan, B., Yoon, Y.S., Le Lay, J., Kaestner, K.H., Hedrick, S., and Montminy, M. (2015). CREB pathway links PGE2 signaling with macrophage polarization. Proc. Natl. Acad. Sci. U S A 112, 15642–15647.

Ma, W.T., Gao, F., Gu, K., and Chen, D.K. (2019). The role of monocytes and macrophages in autoimmune diseases: a comprehensive review. Front. Immunol. 10, 1140.

Majoros, A., Platanitis, E., Szappanos, D., Cheon, H., Vogl, C., Shukla, P., Stark, G.R., Sexl, V., Schreiber, R., Schindler, C., et al. (2016). Response to interferons and antibacterial innate immunity in the absence of tyrosine-phosphorylated STAT1. EMBO Rep. 17, 367–382.

Mammana, S., Fagone, P., Cavalli, E., Basile, M.S., Petralia, M.C., Nicoletti, F., Bramanti, P., and Mazzon, E. (2018). The role of macrophages in neuroinflammatory and neurodegenerative pathways of alzheimer's disease, amyotrophic lateral sclerosis, and multiple sclerosis: pathogenetic cellular effectors and potential therapeutic targets. Int. J. Mol. Sci. 19, 831.

Marino, S., Hogue, I.B., Ray, C.J., and Kirschner, D.E. (2008). A methodology for performing global uncertainty and sensitivity analysis in systems biology. J. Theor. Biol. 254, 178–196.

Martin, K.S., Virgilio, K.M., Peirce, S.M., and Blemker, S.S. (2016). Computational modeling of muscle regeneration and adaptation to advance muscle tissue regeneration strategies. Cells Tissues Organs 202, 250–266.

Martinez, F.O., and Gordon, S. (2014). The M1 and M2 paradigm of macrophage activation: time for reassessment. F1000Prime Rep. 6, 13.

Martins, A.J., Narayanan, M., Prustel, T., Fixsen, B., Park, K., Gottschalk, R.A., Lu, Y., Andrews-Pfannkoch, C., Lau, W.W., Wendelsdorf, K.V., and Tsang, J.S. (2017). Environment tunes propagation of cell-to-cell variation in the human macrophage gene network. Cell Syst. 4, 379–392 e12.

Mccormick, S.M., Gowda, N., Fang, J.X., and Heller, N.M. (2016). Suppressor of cytokine signaling (SOCS)1 regulates interleukin-4 (IL-4)-activated insulin receptor substrate (IRS)-2 tyrosine phosphorylation in monocytes and macrophages via the proteasome. J. Biol. Chem. 291, 20574–20587.

Mendoza-Coronel, E., and Castanon-Arreola, M. (2016). Comparative evaluation of in vitro human macrophage models for mycobacterial infection study. Pathog. Dis. 74, ftw052.

Mills, C.D., Kincaid, K., Alt, J.M., Heilman, M.J., and Hill, A.M. (2000). M-1/M-2 macrophages and the Th1/Th2 paradigm. J. Immunol. 164, 6166–6173.

Mosser, D.M., and Edwards, J.P. (2008). Exploring the full spectrum of macrophage activation. Nat. Rev. Immunol. 8, 958–969.

Muñoz-Rojas, A.R., Kelsey, I., Pappalardo, J., and Miller-Jensen, K. (2020). Co-stimulation with opposing macrophage polarization cues leads to orthogonal secretion programs in individual cells. bioRxiv 2020, 04.04.025536.

Murray, P.J., Allen, J.E., Biswas, S.K., Fisher, E.A., Gilroy, D.W., Goerdt, S., Gordon, S., Hamilton, J.A., Ivashkiv, L.B., Lawrence, T., et al. (2014). Macrophage activation and polarization: nomenclature and experimental guidelines. Immunity 41, 14–20.

Naiyer, M.M., Saha, S., Hemke, V., Roy, S., Singh, S., Musti, K.V., and Saha, B. (2013). Identification and characterization of a human IL-10 receptor antagonist. Hum. Immunol. 74, 28–31.

Nakamura, R., Sene, A., Santeford, A., Gdoura, A., Kubota, S., Zapata, N., and Apte, R.S. (2015). IL10-driven STAT3 signalling in senescent macrophages promotes pathological eye angiogenesis. Nat. Commun. 6, 7847.

Niemand, C., Nimmesgern, A., Haan, S., Fischer, P., Schaper, F., Rossaint, R., Heinrich, P.C., and Muller-Newen, G. (2003). Activation of STAT3 by IL-6 and IL-10 in primary human macrophages is differentially modulated by suppressor of cytokine signaling 3. J. Immunol. 170, 3263–3272.

Norton, K.A., Gong, C., Jamalian, S., and Popel, A.S. (2019). Multiscale Agent-based and hybrid modeling of the tumor immune microenvironment. Processes (Basel) 7, 37.

O'connell, R.M., Taganov, K.D., Boldin, M.P., Cheng, G., and Baltimore, D. (2007). MicroRNA-155 is induced during the macrophage inflammatory response. Proc. Natl. Acad. Sci. U S A 104, 1604–1609.

O'connor, J.C., Sherry, C.L., Guest, C.B., and Freund, G.G. (2007). Type 2 diabetes impairs insulin receptor substrate-2-mediated phosphatidylinositol 3-kinase activity in primary macrophages to induce a state of cytokine resistance to IL-4 in association with overexpression of suppressor of cytokine signaling-3. J. Immunol. 178, 6886–6893.

O'neill, L.A., Bryant, C.E., and Doyle, S.L. (2009). Therapeutic targeting of Toll-like receptors for infectious and inflammatory diseases and cancer. Pharmacol. Rev. 61, 177–197.

Oates, J.R., Mckell, M.C., Moreno-Fernandez, M.E., Damen, M., Deepe, G.S., Jr., Qualls, J.E., and Divanovic, S. (2019). Macrophage function in the pathogenesis of non-alcoholic fatty liver disease: the Mac Attack. Front. Immunol. 10, 2893.

Oda, K., and Kitano, H. (2006). A comprehensive map of the toll-like receptor signaling network. Mol. Syst. Biol. 2, 2006 0015.

Ortiz-Masia, D., Cosin-Roger, J., Calatayud, S., Hernandez, C., Alos, R., Hinojosa, J., Apostolova, N., Alvarez, A., and Barrachina, M.D. (2014). Hypoxic macrophages impair autophagy in epithelial cells through Wnt1: relevance in IBD. Mucosal Immunol. 7, 929–938.

Ouma, G.O., Jonas, R.A., Usman, M.H., and Mohler, E.R., 3rd (2012). Targets and delivery methods for therapeutic angiogenesis in peripheral artery disease. Vasc. Med. 17, 174–192.

Palma, A., Jarrah, A.S., Tieri, P., Cesareni, G., and Castiglione, F. (2018). Gene regulatory network modeling of macrophage differentiation corroborates the continuum hypothesis of polarization states. Front. Physiol. 9, 1659.

Peet, C., Ivetic, A., Bromage, D.I., and Shah, A.M. (2020). Cardiac monocytes and macrophages after myocardial infarction. Cardiovasc. Res. 116, 1101–1112.

Pettersen, J.S., Fuentes-Duculan, J., Suarez-Farinas, M., Pierson, K.C., Pitts-Kiefer, A., Fan, L., Belkin, D.A., Wang, C.Q., Bhuvanendran, S., Johnson-Huang, L.M., et al. (2011). Tumor-associated macrophages in the cutaneous SCC microenvironment are heterogeneously activated. J. Invest. Dermatol. 131, 1322–1330.

Piccolo, V., Curina, A., Genua, M., Ghisletti, S., Simonatto, M., Sabo, A., Amati, B., Ostuni, R., and Natoli, G. (2017). Opposing macrophage polarization programs show extensive epigenomic and transcriptional cross-talk. Nat. Immunol. 18, 530–540.

Pinto, S.M., Kim, H., Subbannayya, Y., Giambelluca, M., Bösl, K., and Kandasamy, R.K. (2020). Dose-dependent phorbol 12-myristate-13-acetate-mediated monocyte-to-macrophage differentiation induces unique proteomic signatures in THP-1 cells. bioRxiv 2020, 02.27.968016.

Pirkmajer, S., and Chibalin, A.V. (2011). Serum starvation: caveat emptor. Am. J. Physiol. Cell Physiol. 301, C272–C279.

Pobezinskaya, Y.L., Kim, Y.S., Choksi, S., Morgan, M.J., Li, T., Liu, C., and Liu, Z. (2008). The function of TRADD in signaling through tumor necrosis factor receptor 1 and TRIF-dependent Toll-like receptors. Nat. Immunol. 9, 1047–1054.

Ramanathan, M., Giladi, A., and Leibovich, S.J. (2003). Regulation of vascular endothelial growth factor gene expression in murine macrophages by nitric oxide and hypoxia. Exp. Biol. Med. (Maywood) 228, 697–705.

Ramirez, R., Herrera, A.M., Ramirez, J., Qian, C., Melton, D.W., Shireman, P.K., and Jin, Y.F. (2019). Deriving a Boolean dynamics to reveal macrophage activation with in vitro temporal cytokine expression profiles. BMC Bioinformatics 20, 725.

Ramsauer, K., Farlik, M., Zupkovitz, G., Seiser, C., Kroger, A., Hauser, H., and Decker, T. (2007). Distinct modes of action applied by transcription factors STAT1 and IRF1 to initiate transcription of the IFN-gamma-inducible gbp2 gene. Proc. Natl. Acad. Sci. U S A 104, 2849–2854.

Rauch, I., Rosebrock, F., Hainzl, E., Heider, S., Majoros, A., Wienerroither, S., Strobl, B., Stockinger, S., Kenner, L., Muller, M., and Decker, T. (2015). Noncanonical effects of IRF9 in intestinal inflammation: more than type I and type III interferons. Mol. Cell Biol. 35, 2332–2343.

Reinartz, S., Schumann, T., Finkernagel, F., Wortmann, A., Jansen, J.M., Meissner, W., Krause, M., Schworer, A.M., Wagner, U., Muller-Brusselbach, S., and Muller, R. (2014). Mixed-polarization phenotype of ascites-associated macrophages in human ovarian carcinoma: correlation of CD163 expression, cytokine levels and early relapse. Int. J. Cancer 134, 32–42.

Rex, J., Albrecht, U., Ehlting, C., Thomas, M., Zanger, U.M., Sawodny, O., Haussinger, D., Ederer, M., Feuer, R., and Bode, J.G. (2016). Model-based characterization of inflammatory gene expression patterns of activated macrophages. PLoS Comput. Biol. 12, e1005018.

Salim, T., Sershen, C.L., and May, E.E. (2016). Investigating the role of TNF-alpha and IFN-gamma activation on the dynamics of iNOS gene expression in LPS stimulated macrophages. PLoS One 11, e0153289.

Santos, J.L., Andrade, A.A., Dias, A.A., Bonjardim, C.A., Reis, L.F., Teixeira, S.M., and Horta, M.F. (2006). Differential sensitivity of C57BL/6 (M-1) and BALB/c (M-2) macrophages to the stimuli of IFN-gamma/LPS for the production of NO: correlation with iNOS mRNA and protein expression. J. Interferon Cytokine Res. 26, 682–688.

Sato, A., Ohtaki, H., Tsumuraya, T., Song, D., Ohara, K., Asano, M., Iwakura, Y., Atsumi, T., and Shioda, S. (2012). Interleukin-1 participates in the classical and alternative activation of microglia/macrophages after spinal cord injury. J. Neuroinflammation 9, 65.

Schleicher, U., Paduch, K., Debus, A., Obermeyer, S., Konig, T., Kling, J.C., Ribechini, E., Dudziak, D., Mougiakakos, D., Murray, P.J., et al. (2016). TNF-mediated restriction of arginase 1 expression in myeloid cells triggers type 2 NO synthase activity at the site of infection. Cell Rep. 15, 1062–1075.

Schmiester, L., Schalte, Y., Frohlich, F., Hasenauer, J., and Weindl, D. (2020). Efficient parameterization of large-scale dynamic models based on relative measurements. Bioinformatics 36, 594–602.

Sheldon, K.E., Shandilya, H., Kepka-Lenhart, D., Poljakovic, M., Ghosh, A., and Morris, S.M., Jr. (2013). Shaping the murine macrophage phenotype: IL-4 and cyclic AMP synergistically activate the arginase I promoter. J. Immunol. 191, 2290–2298.

Shiratori, H., Feinweber, C., Luckhardt, S., Linke, B., Resch, E., Geisslinger, G., Weigert, A., and Parnham, M.J. (2017). THP-1 and human peripheral blood mononuclear cell-derived macrophages differ in their capacity to polarize in vitro. Mol. Immunol. 88, 58–68.

Sica, A., and Mantovani, A. (2012). Macrophage plasticity and polarization: in vivo veritas. J. Clin. Invest. 122, 787–795.

Sove, R.J., Jafarnejad, M., Zhao, C., Wang, H., Ma, H., and Popel, A.S. (2020). QSP-IO: a quantitative systems pharmacology toolbox for mechanistic multi-scale modeling for immuno-oncology applications. CPT Pharmacometrics Syst. Pharmacol. 9, 484–497.

Staples, K.J., Smallie, T., Williams, L.M., Foey, A., Burke, B., Foxwell, B.M., and Ziegler-Heitbrock, L. (2007). IL-10 induces IL-10 in primary human monocyte-derived macrophages via the transcription factor Stat3. J. Immunol. 178, 4779–4785.

Stenken, J.A., and Poschenrieder, A.J. (2015). Bioanalytical chemistry of cytokines–a review. Anal Chim. Acta 853, 95–115.

Su, Z., Yang, R., Zhang, W., Xu, L., Zhong, Y., Yin, Y., Cen, J., Dewitt, J.P., and Wei, Q. (2015). The synergistic interaction between the calcineurin B subunit and IFN-gamma enhances macrophage antitumor activity. Cell Death Dis. 6, e1740.

Suzuki, N., Suzuki, S., Duncan, G.S., Millar, D.G., Wada, T., Mirtsos, C., Takada, H., Wakeham, A., Itie, A., Li, S., et al. (2002). Severe impairment of interleukin-1 and Toll-like receptor signalling in mice lacking IRAK-4. Nature 416, 750–756.

Takeda, N., O'dea, E.L., Doedens, A., Kim, J.W., Weidemann, A., Stockmann, C., Asagiri, M., Simon, M.C., Hoffmann, A., and Johnson, R.S. (2010). Differential activation and antagonistic function of HIF-{alpha} isoforms in macrophages are essential for NO homeostasis. Genes Dev. 24, 491–501.

Tatano, Y., Shimizu, T., and Tomioka, H. (2014). Unique macrophages different from M1/M2 macrophages inhibit T cell mitogenesis while upregulating Th17 polarization. Sci. Rep. 4, 4146.

Thomas, A.C., and Mattila, J.T. (2014). Of mice and men": arginine metabolism in macrophages. Front. Immunol. 5, 479.

Tugal, D., Liao, X., and Jain, M.K. (2013). Transcriptional control of macrophage polarization. Arterioscler Thromb. Vasc. Biol. 33, 1135–1144.

Veremeyko, T., Yung, A.W.Y., Anthony, D.C., Strekalova, T., and Ponomarev, E.D. (2018). Early growth response gene-2 is essential for M1 and M2 macrophage activation and plasticity by modulation of the transcription factor CEBPbeta. Front. Immunol. 9, 2515.

Vila-Del Sol, V., Diaz-Munoz, M.D., and Fresno, M. (2007). Requirement of tumor necrosis factor alpha and nuclear factor-kappaB in the induction by IFN-gamma of inducible nitric oxide synthase in macrophages. J. Leukoc. Biol. 81, 272–283.

Vila-Del Sol, V., Punzon, C., and Fresno, M. (2008). IFN-gamma-induced TNF-alpha expression is regulated by interferon regulatory factors 1 and 8 in mouse macrophages. J. Immunol. 181, 4461–4470.

Wang, N., Liang, H., and Zen, K. (2014). Molecular mechanisms that influence the macrophage m1-m2 polarization balance. Front. Immunol. 5, 614.

Wang, W., Wang, J., Dong, S.F., Liu, C.H., Italiani, P., Sun, S.H., Xu, J., Boraschi, D., Ma, S.P., and Qu, D. (2010). Immunomodulatory activity of andrographolide on macrophage activation and specific antibody response. Acta Pharmacol. Sin 31, 191–201.

Weddell, J.C., Chen, S., and Imoukhuede, P.I. (2018). VEGFR1 promotes cell migration and proliferation through PLCgamma and PI3K pathways. NPJ Syst. Biol. Appl. 4, 1.

Weiskopf, K. (2017). Cancer immunotherapy targeting the CD47/SIRPalpha axis. Eur. J. Cancer 76, 100–109.

Wentker, P., Eberhardt, M., Dreyer, F.S., Bertrams, W., Cantone, M., Griss, K., Schmeck, B., and Vera, J. (2017). An interactive macrophage signal transduction map facilitates comparative analyses of high-throughput data. J. Immunol. 198, 2191–2201.

Werner, S.L., Kearns, J.D., Zadorozhnaya, V., Lynch, C., O'dea, E., Boldin, M.P., Ma, A., Baltimore, D., and Hoffmann, A. (2008). Encoding NF-kappaB temporal control in response to TNF: distinct roles for the negative regulators IkappaBalpha and A20. Genes Dev. 22, 2093–2101.

Wheeler, K.C., Jena, M.K., Pradhan, B.S., Nayak, N., Das, S., Hsu, C.D., Wheeler, D.S., Chen, K., and Nayak, N.R. (2018). VEGF may contribute to macrophage recruitment and M2 polarization in the decidua. PLoS One 13, e0191040.

Whyte, C.S., Bishop, E.T., Ruckerl, D., Gaspar-Pereira, S., Barker, R.N., Allen, J.E., Rees, A.J., and Wilson, H.M. (2011). Suppressor of cytokine signaling (SOCS)1 is a key determinant of

differential macrophage activation and function. J. Leukoc. Biol. *90*, 845–854.

Williams, M.R., Cauvi, D.M., Rivera, I., Hawisher, D., and De Maio, A. (2016). Changes in macrophage function modulated by the lipid environment. Innate Immun. *22*, 141–151.

Winston, B.W., Chan, E.D., Johnson, G.L., and Riches, D.W. (1997). Activation of p38mapk, MKK3, and MKK4 by TNF-alpha in mouse bone marrow-derived macrophages. J. Immunol. *159*, 4491–4497.

Wong, P.K., Egan, P.J., Croker, B.A., O'donnell, K., Sims, N.A., Drake, S., Kiu, H., Mcmanus, E.J., Alexander, W.S., Roberts, A.W., and Wicks, I.P. (2006). SOCS-3 negatively regulates innate and adaptive immune mechanisms in acute IL-1-dependent inflammatory arthritis. J. Clin. Invest. *116*, 1571–1581.

Wu, W.K., Llewellyn, O.P., Bates, D.O., Nicholson, L.B., and Dick, A.D. (2010). IL-10 regulation of macrophage VEGF production is dependent on macrophage polarisation and hypoxia. Immunobiology *215*, 796–803.

Xiao, P., Zhang, H., Zhang, Y., Zheng, M., Liu, R., Zhao, Y., Zhang, X., Cheng, H., Cao, Q., and Ke, Y. (2019). Phosphatase Shp2 exacerbates intestinal inflammation by disrupting macrophage

responsiveness to interleukin-10. J. Exp. Med. *216*, 337–349.

Xue, J., Schmidt, S.V., Sander, J., Draffehn, A., Krebs, W., Quester, I., De Nardo, D., Gohel, T.D., Emde, M., Schmidleithner, L., et al. (2014). Transcriptome-based network analysis reveals a spectrum model of human macrophage activation. Immunity *40*, 274–288.

Yao, Y., Wang, Y., Zhang, Z., He, L., Zhu, J., Zhang, M., He, X., Cheng, Z., Ao, Q., Cao, Y., et al. (2016). Chop deficiency protects mice against bleomycin-induced pulmonary fibrosis by attenuating M2 macrophage production. Mol. Ther. *24*, 915–925.

Yarilina, A., Xu, K., Chen, J., and Ivashkiv, L.B. (2011). TNF activates calcium-nuclear factor of activated T cells (NFAT)c1 signaling pathways in human macrophages. Proc. Natl. Acad. Sci. U S A *108*, 1573–1578.

Zetterberg, A., and Skold, O. (1969). The effect of serum starvation on DNA, RNA and protein synthesis during interphase in L-cells. Exp. Cell Res. *57*, 114–118.

Zhang, L., Blackwell, K., Workman, L.M., Gibson-Corley, K.N., Olivier, A.K., Bishop, G.A., and Habelhah, H. (2016). TRAF2 exerts opposing effects on basal and TNFalpha-induced activation of the classic IKK complex in

hematopoietic cells in mice. J. Cell Sci. *129*, 1455–1467.

Zhang, L., Li, Z., Skrzypczynska, K.M., Fang, Q., Zhang, W., O'brien, S.A., He, Y., Wang, L., Zhang, Q., Kim, A., et al. (2020). Single-cell analyses inform mechanisms of myeloid-targeted therapies in colon cancer. Cell *181*, 442–459 e29.

Zhao, C., Mirando, A.C., Sove, R.J., Medeiros, T.X., Annex, B.H., and Popel, A.S. (2019). A mechanistic integrative computational model of macrophage polarization: implications in human pathophysiology. PLoS Comput. Biol. *15*, e1007468.

Zheng, N., Wang, K., He, J., Qiu, Y., Xie, G., Su, M., Jia, W., and Li, H. (2016). Effects of ADMA on gene expression and metabolism in serum-starved LoVo cells. Sci. Rep. *6*, 25892.

Zhu, L., Yang, T., Li, L., Sun, L., Hou, Y., Hu, X., Zhang, L., Tian, H., Zhao, Q., Peng, J., et al. (2014). TSC1 controls macrophage polarization to prevent inflammatory disease. Nat. Commun. *5*, 4696.

Zhu, Y.P., Brown, J.R., Sag, D., Zhang, L., and Suttles, J. (2015). Adenosine 5'-monophosphate-activated protein kinase regulates IL-10-mediated anti-inflammatory signaling pathways in macrophages. J. Immunol. *194*, 584–594.

Supplemental Information

A data-driven computational model enables

integrative and mechanistic characterization

of dynamic macrophage polarization

Chen Zhao, Thalyta X. Medeiros, Richard J. Sové, Brian H. Annex, and Aleksander S. Popel

Items included in this file:

Transparent Methods

Figure S1: Model specifics compared to previous mathematical multi-pathway models of macrophage polarization; related to Figure 1

Figure S2: Additional quantitative model calibration of pathway signal transduction (part 2); related to Figure 2

Figure S3: Additional quantitative model calibration of pathway signal transduction (part 3); related to Figure 2

Figure S4: Additional quantitative model calibration of pathway signal transduction (part 4); related to Figure 2

Figure S5: Additional quantitative model calibration of M1-M2 marker regulation (part 2); related to Figure 3

Figure S6: Constraining the model with additional qualitative experimental data; related to Figure 3

Figure S7: Macrophage polarization map under simulated *in vivo* stimulation conditions; related to Figure 5

Figure S8: Macrophage transcriptional regulation map under simulated *in vitro* and *in vivo* stimulation conditions; related to Figure 5

Figure S9: Experimental analysis of STAT signaling and HSS-induced M1-M2 marker regulation; related to Figures 2 and 6

Figure S10: Flow cytometry analysis of macrophage markers; related to Figure 6

Figure S11: Macrophage response under HSS and *in silico* targeted interventions to promote M2-like phenotypes; related to Figure 6

Figure S12: Parameter estimate distributions after bootstrapping; related to Figure 6

Figure S13: *In silico* analysis of hypoxia-driven transcriptional and marker regulation at the single-cell level; related to Figure 7

Figure S14: Raw data for qPCR analysis; related to Figure 6

Figure S15: Raw data for Western Blot analysis; related to Figures 2 and 6

Figure S16: Detailed model diagram; related to Figure 1

Other supplemental items as individual files:

Table S1 (Excel spreadsheet): Complete list of model reactions and parameter values; related to Figure 1

Table S2 (Excel spreadsheet): Differential equations and initial conditions of all model nodes; related to Figure 1

Table S3 (Excel spreadsheet): All quantitative data used in model calibration and validation; related to Figures 2-4 and S2-S5

Data S1: Model SBML code and sample MATLAB scripts (compiled in a .zip file) for model setup, simulation and analyses; related to Figures 1-7

Transparent Methods

Summary of Model Formulation, Simulation, Calibration and Analysis

Our mechanistic systems-level model was constructed based on ODEs with a total number of 166 model nodes (from the 67 "unique species") and 258 reactions (details regarding all reaction descriptions, equations, parameter values and initial conditions are summarized in Tables S1-S2). The general ideas and methodologies employed during model formulation (e.g. implementation of pathway structures, mechanisms of regulation, external and internal perturbations) follow a similar logic as reported in a previous modeling study from us (Zhao et al., 2019) and are described in more detail in the modular sections below. We used the same unit conversion method as described in (Zhao et al., 2019) to compute the corresponding molecular initial conditions for the model to simulate the different stimulus concentrations used in *in vitro* experiments. All model reactions and data (e.g. reaction rules of modeled species and nodes, parameter values, initial conditions) were compiled in MATLAB SimBiology Toolbox (MathWorks, Natick, MA) and the ode15s solver in MATLAB was used for model simulations. Model calibration was done at two levels: dynamic model behavior and model initial conditions. The rules we used for the initial condition calibration, in order to capture the quantitative states of unpolarized macrophages before any external driving stimuli or internal perturbations were applied, were designed based on the experimental measurements (compiled from literature, in terms of absolute concentrations or copy numbers) of the quantitative levels of the unique species modeled (all rules are summarized in Table S2). Calibration of dynamic model behaviors was implemented using global optimization (*patternsearch* function) in MATLAB. Full details of model calibration (for both dynamic behavior and initial conditions) are described in the "Model Calibration and Validation" section below. ImageJ software (NIH) was used for the blot densitometry analysis and other image measurements during quantification of experimental data. All quantitative data used in model calibration and validation were summarized in Table S3 (in addition to mean values, SEM or SD values are also included in figure displays if available). Model SBML code (in .xml format) and sample MATLAB scripts (.m files) for model simulation and analyses are also provided in Supplemental Information (Data S1 file) to ensure reproducibility

Sensitivity analyses were performed using the PRCC algorithm as described in (Marino et al., 2008) and in the "Model Sensitivity and Uncertainty Analyses" section below. For the primary outputs of interest in sensitivity analysis and in the analyses described in Figs.5-7 (and Figs.S7-8, S11-13), we introduced numerical metrics (M1-, M2- and M1/M2 scores) that consider major M1-M2 markers modeled to quantitatively characterize the relative dominance of M1 or M2 (pro-inflammatory or anti-inflammatory) phenotypes for stimulated macrophages. M1-score is the multiplication of the levels (e.g. protein/mRNA copy numbers) of 7 modeled pro-inflammatory markers iNOS, IL-12, IFNγ, TNFα, IL-1β, CXCL9 and CXCL10, while M2-score is the multiplication of 4 modeled anti-inflammatory markers ARG1, IL-10, IL-1Ra and VEGF (only the pro-angiogenic isoform VEGF165a is considered for M2-score). The overall M1/M2 score is the division of M1-score by M2-score and in the analyses they were further divided by the M1/M2 score under the baseline (control) condition to reflect directional regulation (for better display, the results were then log10 transformed, and more positive/negative would indicate more M1-/M2-like respectively). For the analyses in Figs.5B-C, simulated protein production rates instead of absolute levels of IL-1β, TNFα, IFNγ, IL-10 and VEGF (pro-angiogenic isoform) were used to calculate M1/M2 scores as these markers themselves were also stimuli (whose initial conditions would be manually modified to reflect *in vitro* and *in vivo* stimulation). For the categorization presented in Fig.7F, based on the number of markers we considered for M1 (7) versus M2 (4), we then assumed that log10 transformed relative M1/M2 scores greater than 2 and less than -1 would correspond to M1-like and M2-like respectively, while values in the remaining range (from -1 to 2) correspond to M0*.

Summary of In-house Experimental Data

Our experimental time-course expression data of pSTAT1/STAT1 and pSTAT3/STAT3 were used for model calibration; our experimental data of the response of iNOS, ARG1, CXCL9, TNFα, IL-1β, IL-10, TGFβ, SOCS3, FIZZ1 and CD80 under HSS were summarized in a qualitative manner and then compared with model simulations in Fig.6. The processed (and raw) experimental data for each individual gene/protein measured are shown in Figs.S9, S10, S14 and S15. Detailed experimental protocols are described in the sections below.

Cell Culture

Raw 264.7 murine macrophages were purchased (Millipore Sigma, Sigma-Aldrich, St Louis, MO, Cat # 91062702) and grown in standard Dulbecco's Modified Eagle Medium (DMEM) with 10% FBS (Thermo-Fisher Scientific, Cat # 11965092). Cells were exposed to hypoxia (2% oxygen, BioSpherix, Lacona, NY) with serum starvation (Cell Applications Inc, Cat # 209-250) to simulate ischemia *in vitro* or treated with 50 ng/mL of recombinant IFNγ (Shenandoah Biotechnology Inc., Cat # 200-16) or 10 ng/mL of recombinant IL-4 (Shenandoah Biotechnology Inc., Cat # 200-18) to induce M1 and M2 phenotypes.

RNA Isolation & Quantitative PCR

Total RNA was extracted using PureLink RNA Mini Kit (Ambion by Life Technologies, Cat # 12183025) according to manufacturer's protocol. cDNA was synthesized from 311.2 ng of RNA using SuperScript III first strand synthesis super mix (Thermo Fisher, Cat # 11752-250) according to the manufacturer's protocol. qPCR was performed using the Taqman Gene Expression Mastermix (Applied Biosystems), cDNA, and Taqman assay (Applied Biosystems) probes with FAM labels for murine TNF-α, TGF-β, IL-10, IL-1β, and CXCL9, and VIC labels for murine GAPDH and Rplp0 from Thermo-Fisher Scientific (Cat # Mm00443258_m1, Mm00237725_cn, Mm00039670_cn, Mm00434228_m1, Mm00434946_m1, Mm00186822_cn, Mm00725448_s1). Data were collected and analyzed using the Biorad CFX96 Real Time System with C1000 Touch Thermal Cycler instrument with GAPDH and Rplp0 as internal expression controls.

Western Blotting

Levels of target protein were analyzed by western blotting using antibodies to iNOS (BD Biosciences, Woburn, MA, Cat # 610432) and Arg1, pSTAT1, STAT1, pSTAT3 and STAT3 (Cell Signaling Technology, Danvers, MA, Cat # 93668s, 9167s, 14994s, 9145L, 12640s). Western blots were analyzed by Odyssey Infrared Imaging System (LI-COR Biosciences, NE).

Flow Cytometry

For flow cytometry staining, macrophages were dissociated from T75 flasks using cold PBS and ice for 0.5–1h. Then, about 10^6 cells were placed in individual 5mL round-bottom tubes (Falcon, Cat # 352058), stained with appropriate membrane antibody mixtures (CD80 FITC Biolegend Cat # 104705, F4/80 APC Fire 750 Biolegend Cat # 123151) or permeabilized with BD Cytofix/Cytoperm Fixation and Permeabilization Solution (BD Biosciences, Cat # 554722) and stained for intracellular markers with anti-SOCS3 (Biolegend, Cat # 626602) or anti-FIZZ1 (Novus Biologicals, Cat # NBP229355), washed with BD Perm/Wash buffer (BD Biosciences, Cat # 51-2091KZ) and finally stained with secondary antibodies (Invitrogen, Alexa-Fluor 488 Cat # A11001 and Alexa-Fluor 647 Cat # A21244). Percentages of parent events presenting target proteins were sorted by flow cytometry using BD FACSCanto Flow Cytometer (BD Biosciences, MA).

Statistical Analysis

Statistical analysis was performed with GraphPad Prism software. An unpaired t test was used for comparison between 2 groups, and comparisons in experiments with ≥3 groups were performed with one-way ANOVA. Statistical significance was set at $p < 0.05$.

Additional Details of Model Formulation and Analysis

The 7-pathway model (including 6 receptor-mediated pathways and oxygen-sensing pathway) presented in this paper is a continuation of a 3-pathway model previously developed by our group (Zhao et al., 2019). Therefore, in a similar manner, the major mechanistic regulations and biochemical reactions in the current model were formulated based on findings in the literature (as shown in Figs.1-4 and S2-S6) and also certain assumptions we made. In the below sections, we describe additional details in the formulation and implementation of several model components that were not explicitly discussed in the calibration and validation sections (a complete list of all species and reactions can be found in Tables S1-S2). We also elaborate further on the mathematical methodologies used in the analyses of our simulation results.

Activation/Deactivation Cycle of STATs

The STATs (STAT1, STAT3, STAT6) in our model follow a canonical activation and deactivation process: monomer phosphorylation, dimerization of phosphorylated monomers (reversible), dimer translocation to nucleus, dimer deactivation (e.g. dephosphorylation) in nucleus, dissociation of deactivated dimers into monomers in nucleus, monomer export from nucleus to cytoplasm (in addition, phosphorylated monomers can also be deactivated in cytoplasm) (Mitchell and John, 2005). We also modeled the mutual sequestration between STAT1 and STAT3 that phosphorylated STAT1 and STAT3 monomers can form a heterodimer (reversible), which can then translocate to the nucleus but is nonfunctional (according to our assumption) so the heterodimers would later be deactivated and broken down to STAT1 and STAT3 monomers. Such a mutual sequestration phenomenon has been reported as a potential mechanism to limit the signaling of STAT1 by STAT3 (and vice versa) (Delgoffe and Vignali, 2013; Ho and Ivashkiv, 2006). For the interactions between STAT1 and IRF9, we assumed that activated STAT1/IRF9 complexes in nucleus can be formed in two ways: by the association (reversible) between IRF9 and activated STAT1 dimers in nucleus, and by the same reactions happening in cytoplasm followed by nuclear translocation (Suprunenko and Hofer, 2016). The activated STAT1/IRF9 complexes can also be deactivated and dissociate in the nucleus (assumed to be a one-step process that gives IRF9 proteins and deactivated STAT1 dimers).

Receptor/Ligand Kinetics

All receptors in the model were regulated by constitutive production and degradation, in addition to ligand-mediated internalization and degradation. Bound ligand-receptor complexes that were internalized can enter pre-degradation states (along with the dissociation of other accessory proteins, e.g. JAK, SOCS) and then undergo either degradation of both ligands and receptors, or degradation of ligands only and recycling of the receptors (Casaletto and McClatchey, 2012). Among the 6 receptor-mediated pathways in the model, only IL-4 signaling was shown to require receptor internalization (Kurgonaite et al., 2015; Cendrowski et al., 2016; Wei et al., 2006; Hansen et al., 2013; Blouin and Lamaze, 2013; Green et al., 2017).

JAK proteins (e.g. JAK1, JAK2, JAK3) were shown to be associated with different cytokine receptors in a partially redundant manner, so we made a simplification and merged them together into one JAK species that binds all IL-4/IL-10/IFNγ receptors (O'Shea et al., 2015). In our model, the majority of IL-4, IL-10 and IFNγ receptors were pre-associated with JAK proteins before binding their respective ligands (Marchetti et al., 2006). JAK can also be targeted by SOCS proteins (e.g. SOCS1, SOCS3) for direct degradation (Croker et al., 2008).

In our model, the quantitative copy numbers of ligands in different stimulation conditions were calculated using their respective doses (e.g. in ng/ml) found in literature studies and molecular weights (e.g. in kilodalton) together with the assumption that every 10^6 cells share 1 mL of culture media *in vitro* (Zhao et al., 2019). Hypoxia was simulated as variations in the O_2 initial conditions by assuming that an O_2 concentration of 200 µM (then converted to absolute copy numbers) reflects normoxia (21% O_2) (Tuckerman et al., 2004). Apart from the 6 activating ligands (IL-1β, IL-4, IL-10, IFNγ, TNFα, $VEGF_{165}a$) in the model, the autocrine effect of IL-12 (modeled as one single species instead of a heterodimer) was implicitly captured in terms of its ability to upregulate IFNγ production (Munder et al., 1998). In addition, there were two ligands that potentially act as signal inhibitors in the model. IL-1Ra can bind to IL-1 receptors but cannot induce any downstream signaling or receptor internalization (Dripps et al., 1991). For $VEGF_{165}b$, it was assumed that it binds VEGFR1 and induces receptor internalization, degradation and recycling (similar to $VEGF_{165}a$) (Boucher et al., 2017); however, binding of $VEGF_{165}b$ would not induce any signaling events. We also assumed that only $VEGF_{165}a$ (but not $VEGF_{165}b$) production is directly upregulated by hypoxia through HIFs (Varey et al., 2008). When 'VEGF' is mentioned in the manuscript as a stimulus, it refers to pro-angiogenic isoforms only unless otherwise noted; when 'VEGF' is mentioned in the manuscript as a product, it refers to the sum of both pro-angiogenic and anti-angiogenic isoforms.

AKT Isoforms

In our model, we included two isoforms of AKT, AKT1 and AKT2. Both isoforms can be activated by PI3K and were assumed to regulate downstream targets in a similar manner, except for miR-155 as AKT1 inhibits miR-155 production and AKT2 has the opposite effect (Arranz et

al., 2012). To compare with literature results where only a single AKT species was considered, the sum of activated (e.g. phosphorylated) AKT1 and AKT2 was used.

IRFs

IRF1, a master regulator downstream of the IFNγ/STAT1 axis, was assumed to be the essential effector (instead of STAT1, as suggested by optimization results) for two IFNγ-regulated effects: inhibition of miR-3473b and IL1R production (Wu et al., 2014; Hu et al., 2005). In our model, the expression levels of IRF1, IRF4 and IRF9 can be up- and down-regulated by external stimuli to reflect activation and repression, while the level of IRF5 was assumed to be constant so IRF5 was dynamically regulated between inactive and active states (Ren et al., 2014). The inhibitory effect of IRF4 on IRF5 was modeled as an IRF-4-mediated decrease in the rate of IRF5 activation (Negishi et al., 2005). Another well-studied IRF member, IRF3, was not included here as it is not significantly regulated by any of the model pathways (Endo et al., 2014; Wang et al., 2016).

MAPKs

In our model, the life cycles of three MAPKs (p38, ERK, JNK) followed a simple canonical cascade: activation (e.g. by phosphorylation) in cytoplasm, translocation of activated MAPKs to nucleus, deactivation (e.g. by dephosphorylation) of activated MAPKs in nucleus and export to cytoplasm (merged into a one-step reaction). In addition, activated MAPKs can also be deactivated directly in cytoplasm. We also assumed that their regulatory functions are only determined by the levels of activated MAPKs in nucleus (Plotnikov et al., 2011). One of their major downstream targets in the model, transcription factor AP-1, was simplified as one single species (instead of protein dimers) whose production was jointly regulated by the three MAPKs (Lopez-Bergami et al., 2010). For the activation of ERK in response to IL-4 and IL-10, we semi-mechanistically introduced two species (named INT1/2, refer to Table S1 for more details) to represent the coarse-grained signal transduction processes between respective receptor ligation and downstream ERK activation, and this has significantly improved the model calibration.

Protein Production, Secretion and Degradation

For most species (e.g. those whose mRNAs were not explicitly modeled), protein production (and subsequent secretion, if applicable) is simplified as a one-step process. All species (e.g. mRNA, protein) whose expression can be induced in the model have a corresponding degradation reaction (mostly intracellular). Among all the secreted M1-M2 markers modeled, we assumed that CXCL9, IL-12 and IL-1Ra only undergo extracellular degradation; the other secreted M1-M2 markers only undergo ligand-mediated internalization and subsequent degradation.

Hypoxia Serum Starvation (HSS)

HSS was simplified as hypoxia only (2% O_2) in our primary model analyses in Fig.6. Additional analyses were also performed for an alternative simplified representation which is hypoxia plus 25% reduction in all RNA/protein synthesis rates (denoted as HSS* in Fig.S11) based on findings from (Zetterberg and Skold, 1969).

Model Calibration and Validation

Model calibration was done in a combination of manual tuning and computer optimization. We first searched the literature and were able to derive values (from both experimental data and published models) for a subset of the model parameters; for the remaining ones without literature reference, we put in tentative values to start with. Then we manually tuned the model parameter space until the model simulations achieved good visual agreements with all the corresponding calibration datasets simultaneously (the data are summarized in Figs.2-3 and S2-S5). In the meantime, we ensured that the initial conditions of all "unique" species in the model stayed in quantitative predefined ranges as estimated from literature (Table S2); we also ensured that the time-course levels of all model nodes with initial conditions greater than 20 did not display significant fluctuations (within $\pm15\%$ from the initial condition) over a span of 10000 minutes (~7 days) under the resting (no-treatment) condition, which were meant to indicate that these unpolarized, untreated macrophages in culture have achieved a relative equilibrium.

We then performed preliminary sensitivity analysis using the PRCC algorithm under seven stimulation conditions (e.g. by the 7 stimuli one at a time) and selected the top-ranked free parameters (e.g. those with absolute PRCC indices larger than 0.1) from each run. This gave a total of 80 parameters, which were then input as parameters to be optimized into a global optimization procedure in MATLAB (using *patternsearch* function, with 0.5x-2x as the allowed ranges for parameter value variations) with respect to all the calibration datasets presented in this paper. The objective function to be minimized in optimization is the weighted sum of squared errors (computed from the differences between simulated and experimental values, and normalized by the respective SD/SEM when applicable). For the weighting of the experimental data, individual time-course (and dose response) data series from macrophages was given a weight of 2 (1 for data series from non-macrophages); individual single-timepoint data from macrophages was given a weight of 1 (0.5 for single-timepoint data from non-macrophages). The computer optimization process also checked the initial condition bounds (using a similar method as described in (Zhao et al., 2019) but this time initial conditions were evaluated at 10000, 50000 and 100000 minutes of simulation under no-treatment condition to find any set of values that can satisfy the bounds) and fluctuation bounds at every iteration. The final parameter values generated by MATLAB were then rounded to 5 significant digits.

Overall, there are two main reasons that we chose this two-step approach (manual tuning then computer optimization) over the *patternsearch* only approach for model calibration and optimization. First reason is that the compilation of all calibration data from many disparate sources is a continuous process done over many months, given the large scope of model and the large number of data potentially available in the literature from different sources (instead of in one or two curated databases which there were none). Thus, if we were to do a new round of *patternsearch* every time we found new data, the overall process would be infeasible and would cost significantly more time. Second reason is that our model has a unique feature which is its background nonzero initial condition to represent unpolarized macrophages with autocrine signaling (plus the "fluctuation" constraint as mentioned above), and *patternsearch* only with unselected large starting ranges seems to perform very poorly on this, which may be due to many reasons, e.g. too many long-range autocrine feedbacks in the model that influence the initial conditions, poorly defined starting ranges.

The dataset used in model validation (Fig.4) was compiled in the following ways. If at least two cases (e.g. different stimulation doses) of "A regulates B" have been included in calibration, then a third case of "A regulates B" (e.g. stimulated at higher dose, or dose response curve) will be included in the validation set (single literature sources that contain multiple pieces of qualified data were also preferentially selected). In addition, three scenarios of combination treatment were included in the validation set. All data in the validation set were obtained from macrophage cell lines, while a small portion of data in the calibration set were derived from non-macrophage cell lines.

Generation of in silico Macrophages

We generated 100 digital alternative versions of our model ("*in silico* macrophages") to represent the diversity in the macrophage phenotype response at the single-cell level. This is under the assumption that each individual macrophage can be educated only by the secreted signals produced by itself (e.g. autocrine effect only, no paracrine effect). For these 100 *in silico* macrophages, we used the parameters obtained from model calibration (e.g. the reference model) as the basis and further varied the production/degradation (or activation/deactivation) of 5 selected pathway regulators (RIP1, IRF1, IRF4, TRAF6, SOCS1) and 5 autocrine cytokines (TNFα, IL-1β, IFNγ, IL-10, VEGF$_{165}$a). To do that, we varied the Hill constants or normalization factors (randomly within the range of 0.1x-10x) used in the production/degradation (or activation/deactivation) of these molecules and then computed the new rates so that their overall resting state reaction fluxes are the same as in the reference model. Then these 100 *in silico* macrophages were simulated using the same initial conditions under various stimulation conditions as described in the manuscript main text.

Model Sensitivity and Uncertainty Analyses

Model sensitivity analyses were performed based on the algorithm and code as published in (Marino et al., 2008). For the algorithm settings, we used Latin Hypercube Sampling (LHS), p=0.05 as the cutoff for statistical significance, 5000 iterations for each run, evaluation time integral of t=0 to 24 h, and 0.5x-2x as the allowed ranges for parameter value variations (0.2x-5x

yielded similar results). The M1/M2 score, which is the multiplication (in terms of time integrals of relative fold changes) of 7 M1 markers ([iNOS]*[IL12]*[TNFα]*[IFNγ]*[CXCL9]*[mCXCL10]*[IL1β], M1 score) divided by the multiplication of 4 M2 markers ([ARG1]*[IL10]*[V165a]*[IL1RA], M2 score), was chosen as the output of interest for all PRCC calculations (and also other analyses in this study). During the preliminary sensitivity analysis (as described in the Calibration/Validation section), when the stimulus itself is a marker, then in that particular run of sensitivity analysis this stimulus was removed from the calculation of M1/M2 score. For the results displayed in Fig.6 in main text, we performed sensitivity analysis first (as described above) and then removed the parameters that directly control the production/degradation of single markers that has no autocrine mechanisms in the model, since targeting these processes are less meaningful as they can only regulate one out of the many macrophages response markers; parameters that are Hill constants were also removed for similar reasons.

For uncertainty analysis, we selected the top-ranked free parameters from seven runs (10 parameters were selected from each run) of sensitivity analyses (under the 7 stimuli, one at a time) and this collective set contained 25 distinct parameters after removing the duplicates. The complete calibration datasets were resampled 100 times. For each datapoint in the calibration datasets, we assumed that its value during resampling would randomly fall within a normal distribution with the mean and standard deviation (or standard error, if applicable) values that we directly obtained from the corresponding literature study. And for datapoints with only mean values available, we assumed that their standard deviations equal to 10% of the mean values. Finally, the 100 resampled datasets were fed into the optimization algorithm (as described above) to obtain 100 sets of new parameter estimates; during bootstrapping, parameter values were allowed to vary from 0.1x to 10x (of their reference values). The final readout of the uncertainty analysis is the relative value distribution of these 25 parameters.
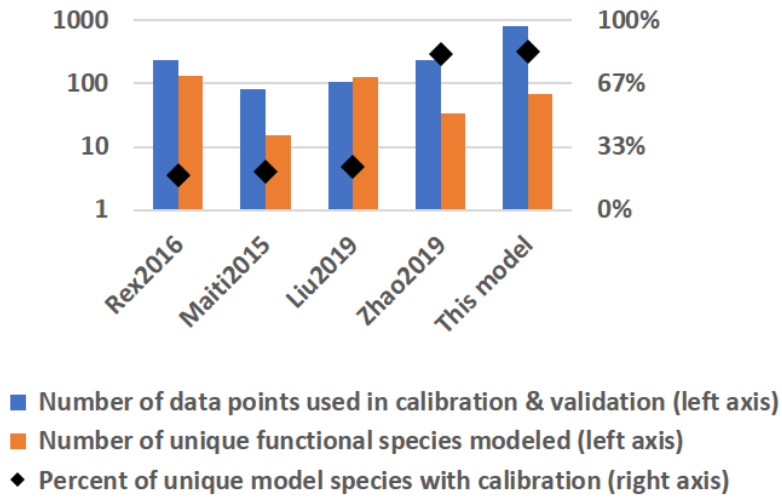
Figure S1

Figure S1. Model specifics compared to previous mathematical multi-pathway models of macrophage polarization; related to Figure 1. Compared to previous modeling studies on macrophage polarization (Rex et al., 2016; Maiti et al., 2015; Liu et al., 2019; Zhao et al., 2019), the current model was able to incorporate a significantly larger amount of quantitative experimental data (blue bars) for its calibration and validation, while it enables users to dynamically simulate a very high degree of mechanistic complexity in terms of pathway details, marker regulation and diverse application scenarios.
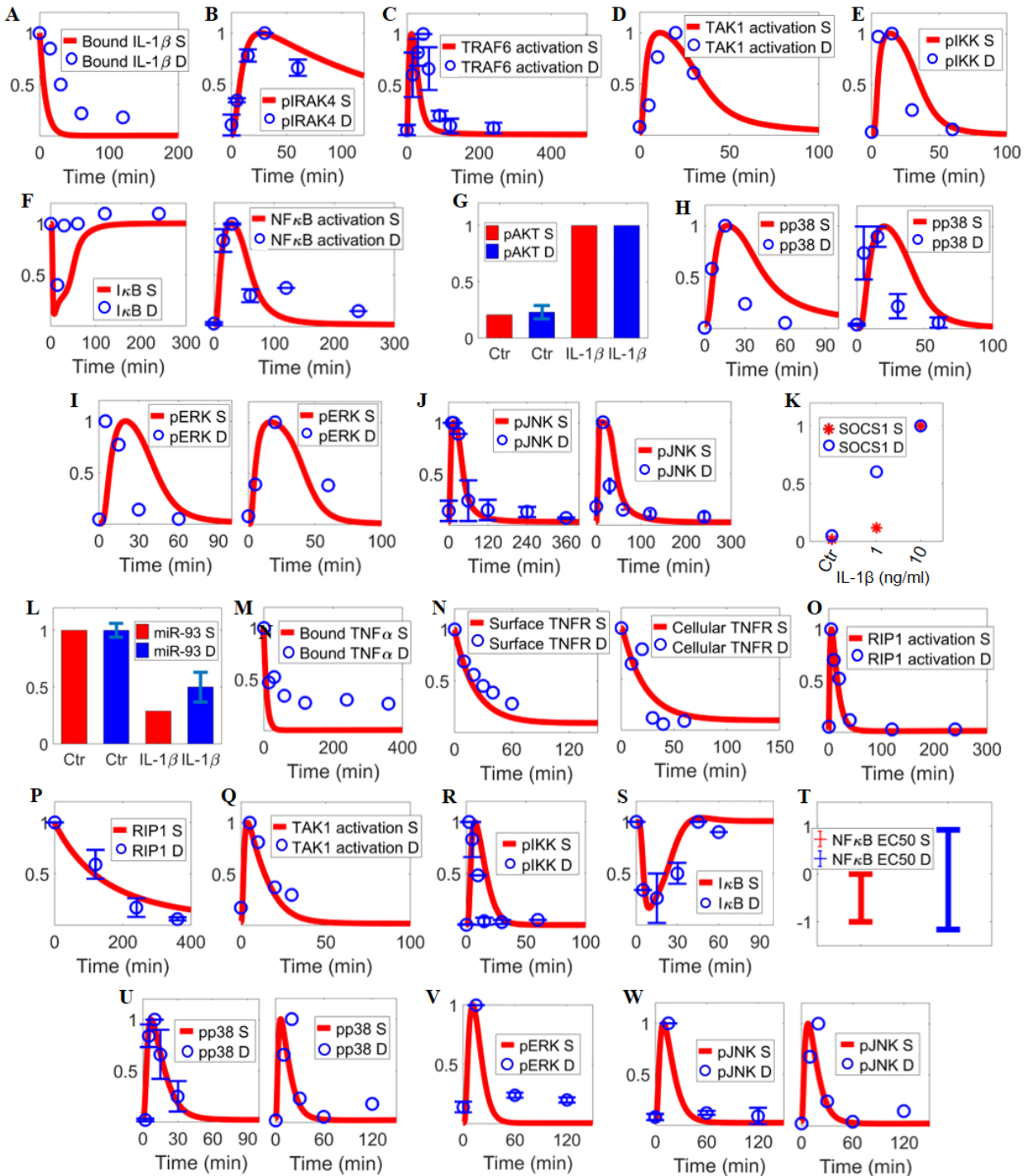
Figure S2

Figure S2. Additional quantitative model calibration of pathway signal transduction (part 2); related to Figure 2. Model simulations and corresponding experimental data are shown together (references are listed in the order of the data mentioned). (A) Cell surface receptor-bound IL-1β

undergoes internalization (Kilian et al., 1991). (B) IL-1β induces activation of IRAK4 (Vollmer et al., 2017), (C) TRAF6 (Shembade et al., 2010), (D) TAK1 (Cheung et al., 2003), (E) IKK (Funakoshi-Tago et al., 2009), (F) transient downregulation of IκB (Shembade et al., 2007) and subsequent NFκB activation (Funakoshi-Tago et al., 2009; Suzuki et al., 2002; Shembade et al., 2008), and (G) AKT activation (Neumann et al., 2002; Gulen et al., 2012). (H) IL-1β also induces activation of p38 (5 ng/ml (Vollmer et al., 2017) and 10 ng/ml (Suzuki et al., 2002; Funakoshi-Tago et al., 2009)), (I) ERK (10 ng/ml (Funakoshi-Tago et al., 2009) and 100 ng/ml (Hu et al., 2005)), (J) JNK (10 ng/ml (Suzuki et al., 2002; Shembade et al., 2008) and 20 ng/ml (Shembade et al., 2007)), and (K) upregulates SOCS1 (Choi et al., 2013); IL-1β can downregulate miR-93 expression (Xue et al., 2019). (M) Cell surface receptor-bound TNFα undergoes internalization (Imamura et al., 1987). (N) TNFα induces internalization (left) and degradation (right) of TNFR (Fischer et al., 2011). (O) TNFα induces activation of RIP1 (Shembade et al., 2010), (Q) TAK1 (Cheung et al., 2003), (R) IKK (Waterfield et al., 2004; Geng et al., 2017), (S) transient downregulation of IκB (Ermolaeva et al., 2008; Lo et al., 2011) and (T) dose-dependent activation of NFκB (simulated range of EC50 is within the experimental range EC50) (Trask, 2004). (P) Cellular expression of RIP1 is downregulated by A20 overexpression (simulated as 100x A20 initial condition) with cycloheximide treatment (simulated as 0x protein production rates) (Shembade et al., 2009). (U) TNFα also induces activation of p38 (40 ng/ml (Winston et al., 1997) and 100 ng/ml (Dzamko et al., 2012)), (V) ERK (Etemadi et al., 2015), and (W) JNK (20 ng/ml (Etemadi et al., 2015) and 100 ng/ml (Dzamko et al., 2012)). (A-W) All values are for protein levels unless noted otherwise and are normalized (y-axes are relative expression, except in T as described below). For normalization and display of results (simulation and data in A-W): A, IκB in F, L-N, P, S normalized to the respective t=0 values; G normalized to the maximum pAKT levels in response to IL-1β; y-axis in T is the log10 transformed TNFα concentrations in ng/ml; all others normalized to their respective maximum values. S–simulation, D–experimental data, Ctr–control/untreated condition.
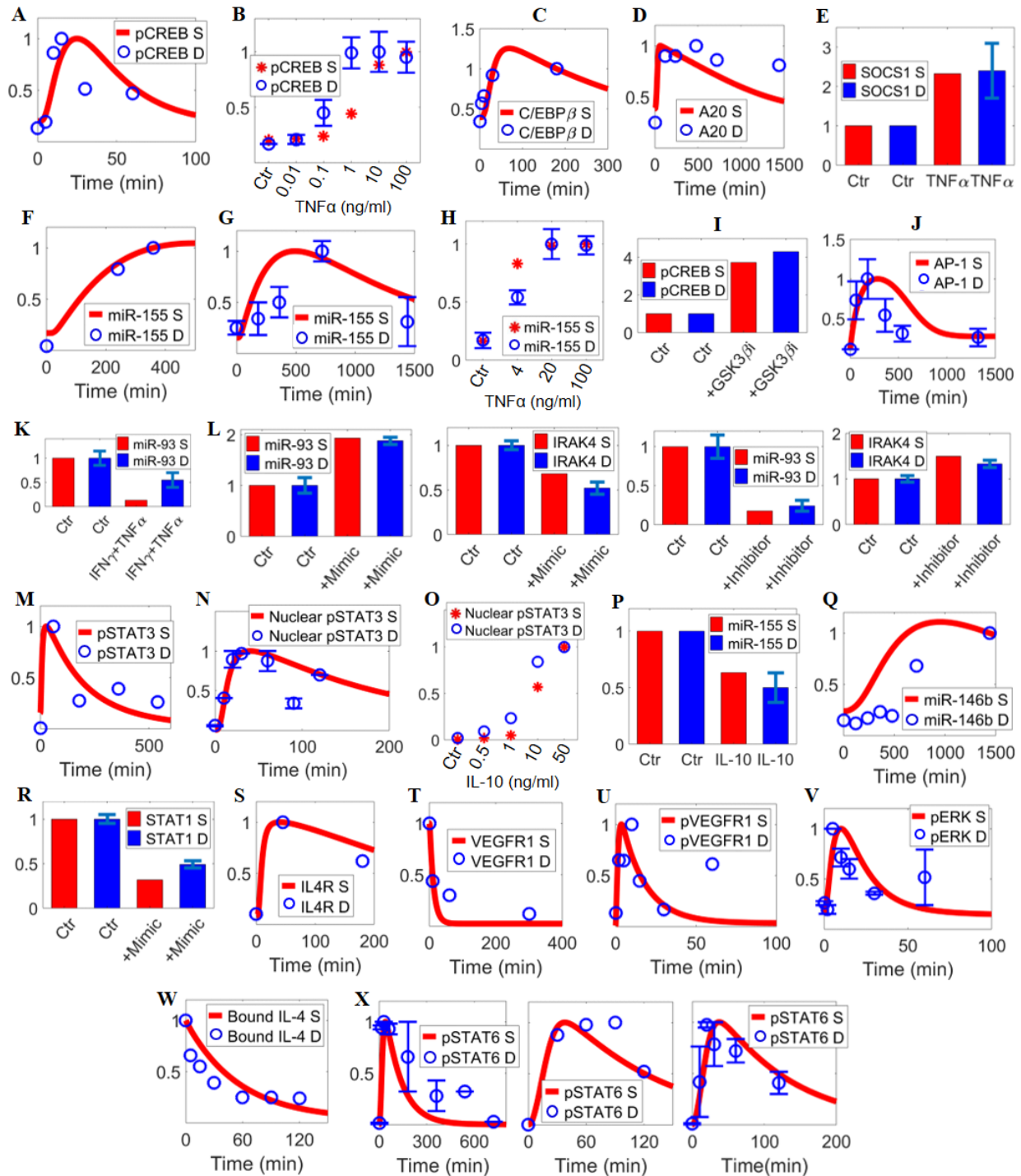
Figure S3

Figure S3. Additional quantitative model calibration of pathway signal transduction (part 3); related to Figure 2. Model simulations and corresponding experimental data are shown together (references are listed in the order of the data mentioned). (A-B) TNFα induces time-course (Koga et al.,

2016) and dose-dependent activation (Ono et al., 2006) of CREB. (C) TNFα induces expression of C/EBPβ (Yin et al., 1996), (D) A20 (Tran et al., 2009), (E) SOCS1 (simulated SOCS1 protein level is compared to SOCS1 mRNA data) (Ueki et al., 2004), (F-G) time-course (10 ng/ml (O'Connell et al., 2007) and 50 ng/ml (Migita et al., 2017)) and (H) dose-dependent expression of miR-155 (Migita et al., 2017). (I-J) Inhibition of GSK3β (simulated using the IC50 value from (Zhang et al., 2003)) results in activation of CREB and AP-1 (simulated AP-1 protein level is compared to c-Jun mRNA data) (Gotschel et al., 2008). (K) TNFα plus IFNγ treatments can downregulate miR-93 expression (Yee et al., 2017). (L) Overexpression ('mimic') of miR-93 inhibits IRAK4 and inhibition of miR-93 ('inhibitor') promotes IRAK4 expression (Tian et al., 2017). (M-N) IL-10 induces time-course (in whole-cell (Yasukawa et al., 2003) and nucleus (Niemand et al., 2003)) and (O) dose-dependent activation of STAT3 (Niemand et al., 2003). (P) IL-10 downregulates miR-155 (McCoy et al., 2010) and (Q) induces miR-146b (Curtale et al., 2013), and (R) miR-146b overexpression ('mimic') can inhibit STAT1 protein expression (He et al., 2016). (S) IL-10 also induces expression of IL4R (simulated IL4R protein production rate is compared to IL4R mRNA data) (Lang et al., 2002). (T) VEGF induces ligand-mediated VEGFR1 degradation (Kobayashi et al., 2004), (U) VEGFR1 phosphorylation and (V) ERK activation (Feliers et al., 2005). (W) Cell surface receptor-bound IL-4 undergoes internalization (Kawakami et al., 2002). (X) IL-4 (at 10 ng/ml (Covarrubias et al., 2016; Dickensheets et al., 2007; Yao et al., 2016), 20 ng/ml (Li et al., 2017) and 50 ng/ml (Rex et al., 2016; Kimura et al., 2016)) induces STAT6 activation. (A-X) All values are for protein levels unless noted otherwise and are normalized (y-axes are relative expression). For normalization and display of results (simulation and data in A-X): E, I, K, L, P, R, T, W normalized to the respective t=0 values; C, F, Q normalized to the respective values at the last experimental timepoints; all others normalized to their respective maximum values. S–simulation, D–experimental data, Ctr–control/untreated condition.
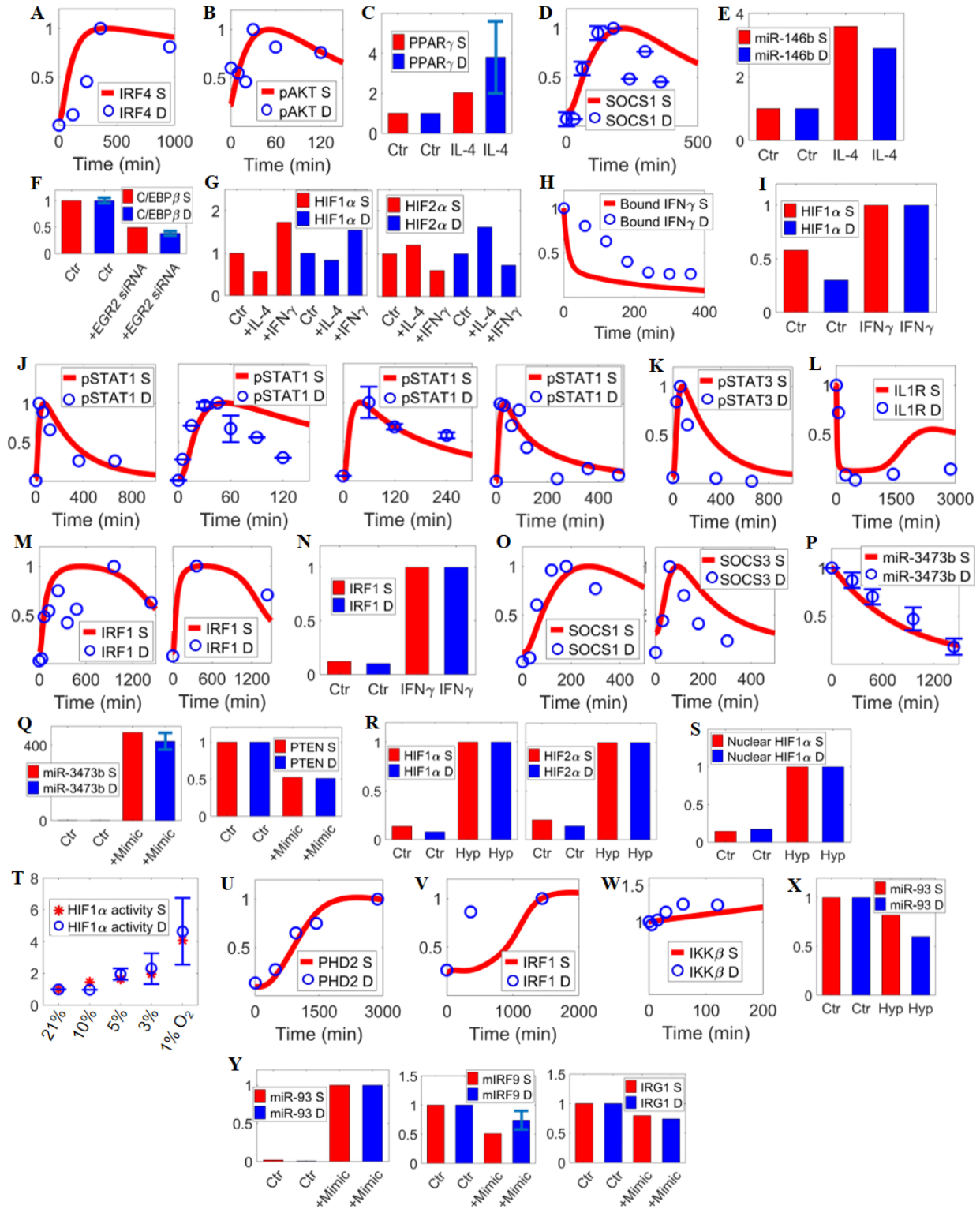
Figure S4

Figure S4. Additional quantitative model calibration of pathway signal transduction (part 4); related to Figure 2. Model simulations and corresponding experimental data are shown together (references are listed in the order of the data mentioned). (A) IL-4 induces IRF4 expression (Hsu et al., 2018), (B) AKT activation (Kimura et al., 2016), (C) expression of PPARγ (Kim et al., 2018; Date et al., 2014), (D) SOCS1 (simulated SOCS1 protein level is compared to SOCS1 mRNA data) (Dickensheets et al., 2007), and (E) miR-146b (Malik, 2016). (F) C/EBPβ is downregulated by EGR2 siRNA (implemented as 0.1x EGR2 production rate, simulated C/EBPβ protein level is compared to C/EBPβ mRNA data) (Veremeyko et al., 2018). (G) IL-4 and IFNγ selectively regulate HIF1α and HIF2α under hypoxia (Takeda et al., 2010). (H) Cell surface receptor-bound IFNγ undergoes internalization (Celada and Schreiber, 1987). (I) IFNγ induces HIF1α stabilization under normoxia (Takeda et al., 2010). (J) IFNγ (at 10 ng/ml (Kim et al., 2015), 20 ng/ml (Li et al., 2017), 50 ng/ml – original data as shown in Fig.S9A, 125 ng/ml (Wormald et al., 2006)) potently induces STAT1 activation. (K) IFNγ also induces STAT3 activation (Kim et al., 2015). (L) IFNγ represses production of IL1R (simulated IL1R protein production rate is compared to IL1R mRNA data) (Hu et al., 2005). (M-N) IFNγ (at 2.5 ng/ml (Vila-del Sol et al., 2008), 100 U/ml (Carta et al., 2001), 10 ng/ml (Liu et al., 2003)) induces IRF1 expression. (O) IFNγ upregulates SOCS1 and SOCS3 expression (simulated SOCS1/3 protein levels are compared to SOCS1/3 mRNA data) (Dickensheets et al., 2007). (P) IFNγ downregulates miR-3473b; (Q) overexpression ('mimic') of miR-3473b inhibits PTEN abundance (Wu et al., 2014). (R) Hypoxia stabilizes cellular HIF1α and HIF2α (Imtiyaz et al., 2010); (S) hypoxia promotes HIF1α activation in nucleus (Ramanathan et al., 2007) and (T) in dose-dependent manners (Cummins et al., 2006). (U) Hypoxia induces PHD2 expression (Berra et al., 2003), (V) IRF1 expression (Carta et al., 2001), and (W) IKKβ expression (Cummins et al., 2006). (X) Hypoxia downregulates miR-93; (Y) overexpression of miR-93 ('mimic') decreases IRF9 mRNA expression and IRG1 (simulated IRG1 protein level is compared to IRG1 mRNA data) (Ganta et al., 2017). (A-Y) All values are for protein levels unless noted otherwise and are normalized (y-axes are relative expression). For normalization and display of results (simulation and data in A-Y): C, E, F, H, L, P, Q, W, X, mIRF9 and IRG1 in Y normalized to the respective t=0 (Ctr condition) values; U-V normalized to the respective values at the last experimental timepoints; G normalized to the values at the Ctr (hypoxia-treated) condition; I normalized to the values at 48 h of IFNγ treatment; N normalized to the values at 16 h of IFNγ treatment; R normalized to the values at 24 h of hypoxia; S normalized to the values at 12 h of hypoxia; T normalized to the values at 21% O_2; miR-93 in Y normalized to the values at 24 h of mimic transfection; all others normalized to their respective maximum values. S–simulation, D–experimental data, Hyp–hypoxia; Ctr–control/untreated condition unless otherwise noted.
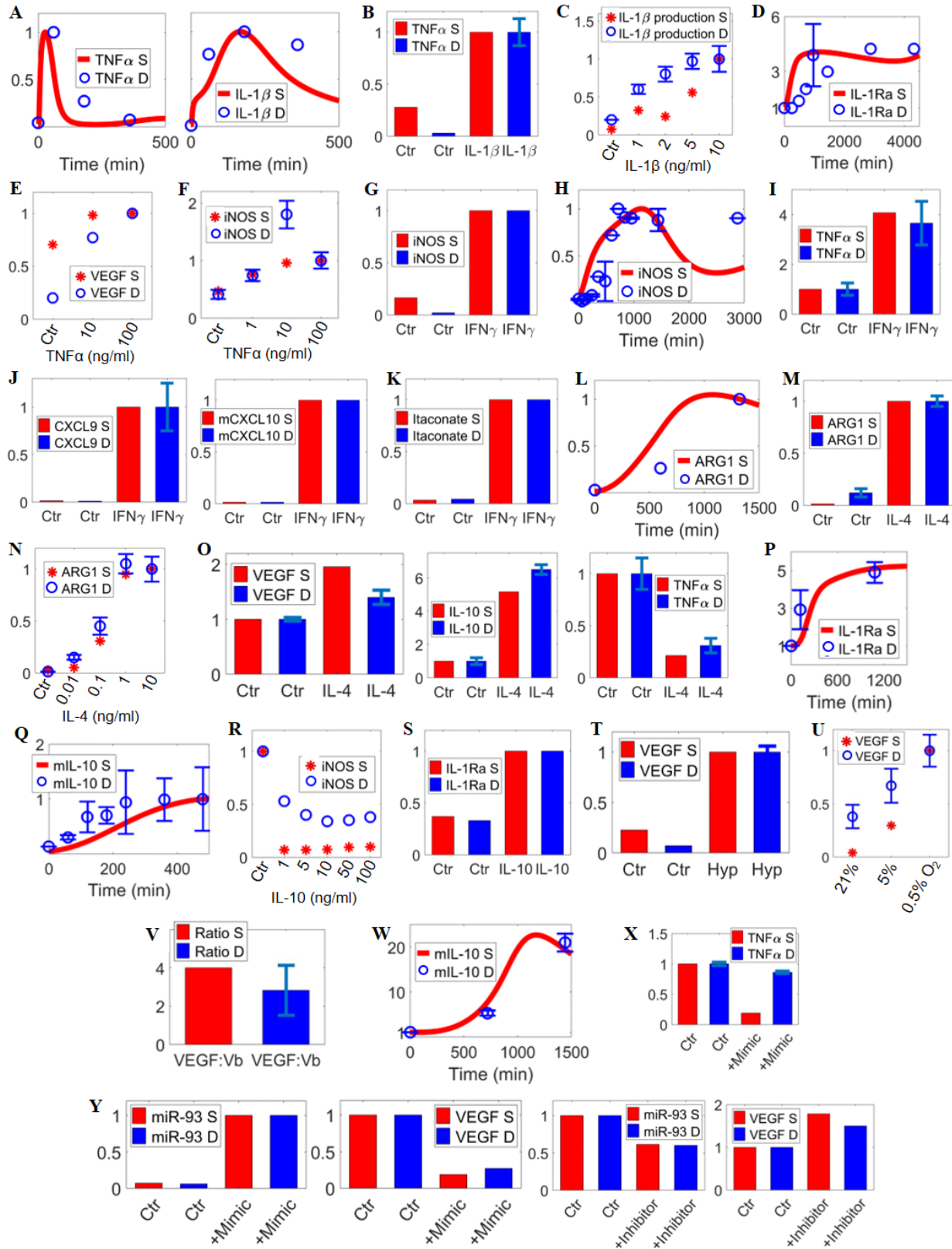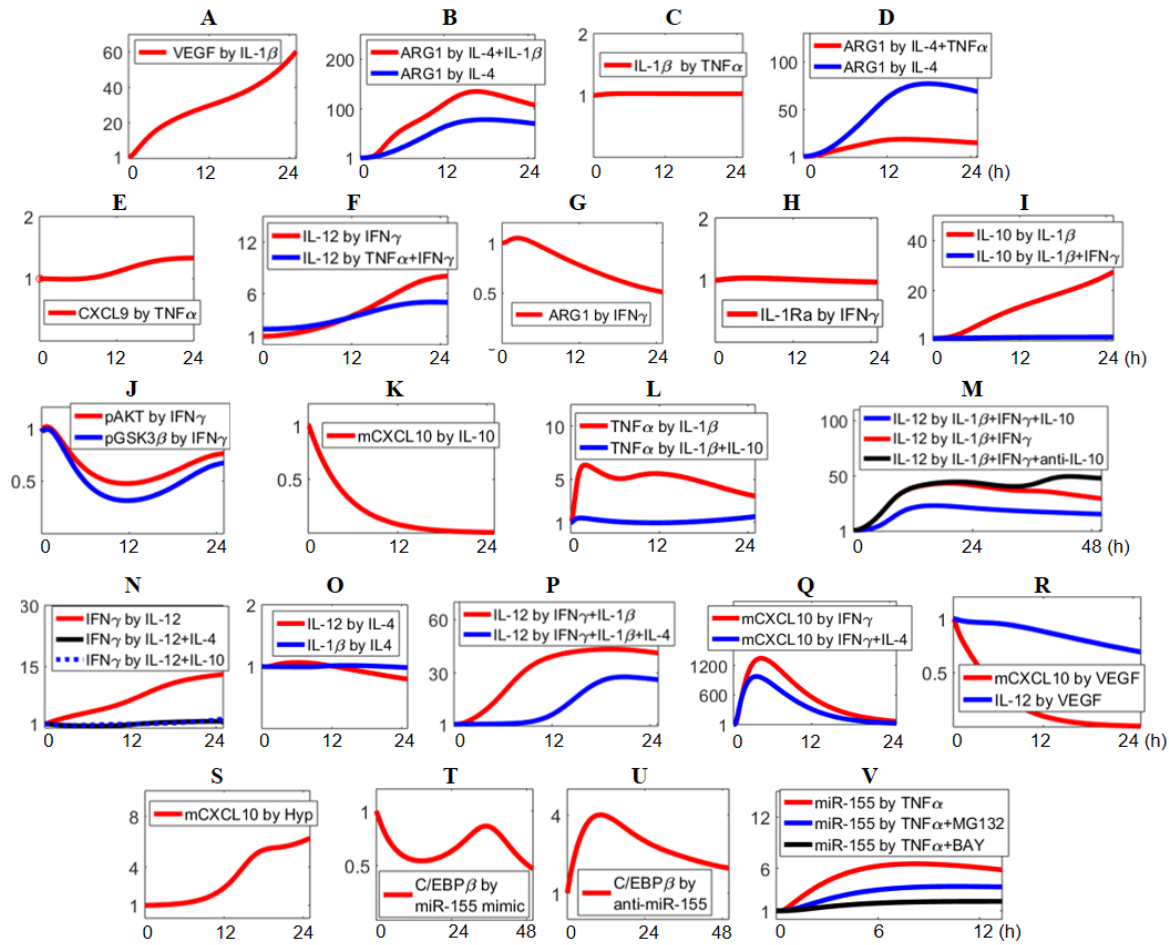
Figure S5

Figure S5. Additional quantitative model calibration of M1-M2 marker regulation (part 2); related to Figure 3. Model simulations and corresponding experimental data are shown together (references are listed in the order of the data mentioned). (A) IL-1β induces production of TNFα and IL-1β (simulated protein production rates are compared to the respective mRNA data) (Hu et al., 2005). (B) IL-1β induces TNFα secretion (Jayaraman et al., 2013), (C) IL-1β production in a dose-dependent manner (simulated IL-1β protein production rates are compared to data of IL-1β promoter activities) (Toda et al., 2002), and (D) secretion of IL-1Ra (Gabay et al., 1997; Kovalovsky et al., 1998). (E-F) TNFα dose-dependently induces VEGF secretion (Lu et al., 2012) and iNOS activity (simulated iNOS protein levels are compared to data of NO concentration) (Peiheng He, 2016). (G-H) IFNγ induces iNOS expression (Ohata et al., 1998; Vila-del Sol et al., 2007), (I) TNFα secretion (Davis et al., 2013), (J) CXCL9 secretion and CXCL10 mRNA expression (Mundra et al., 2016), and (K) itaconate production (Naujoks et al., 2016). (L-M) IL-4 induces ARG1 expression (Sheldon et al., 2013; Zanin et al., 2012) and (N) its dose-response relationship (Tachdjian et al., 2010); results in M and N compare simulated ARG1 protein levels to data of urea levels. (O) IL-4 induces VEGF secretion (Lim et al., 2017), IL-10 secretion, and downregulation of TNFα secretion (Zhang et al., 2011); combined IL-4 plus IL-13 treatments in data is simplified as IL-4 treatment only in simulations. (P) IL-4 induces IL-1Ra secretion over time (Liu et al., 1998; O'Connor et al., 2007). (Q) IL-10 induces IL-10 mRNA production (Staples et al., 2007), (R) inhibits iNOS production (Villalta et al., 2011), and (S) increases IL-1Ra secretion (Liu et al., 1998). (T-U) Hypoxia increases VEGF secretion (Mei et al., 2014) and its dose response (Eubank et al., 2011); (W) hypoxia increases IL-10 mRNA production (Meng et al., 2018). (V) Ratio of total VEGF to VEGF165b at control condition (Nowak et al., 2008). (X) Overexpression of miR-93 ('mimic') decreases hypoxia-induced TNFα secretion (Ganta et al., 2017). (Y) Overexpression of miR-93 decreases VEGF protein levels and inhibition of miR-93 ('inhibitor') increases VEGF protein levels (Lv et al., 2015). (A-Y) All values are for protein levels unless noted otherwise and are normalized (y-axes are relative expression, except for V as described above). For normalization and display of results (simulation and data in A-Y): D, I, O, P, R, W normalized to the respective t=0 (Ctr condition) values; C, E, F, N, U normalized to the values at the highest treatment concentration; L, Q normalized to the respective values at the last experimental timepoints; X normalized to the values at the Ctr (hypoxia-treated) condition; B normalized to the values at 24 h of IL-1β treatment; J normalized to the values at 24 h (for CXCL10) and 72 h (for CXCL9) of IFNγ treatment; K normalized to the values at 18 h of IFNγ treatment; M normalized to the values at 24 h of IL-4 treatment; S normalized to the values at 24 h of IL-10 treatment; T normalized to the values at 16 h of hypoxia; X normalized to the values at Ctr (hypoxia-treated) condition; miR-93 (mimic panel) in Y normalized to the values at 48 h of mimic transfection, the other 3 panels in Y normalized to the respective t=0 values; all others normalized to their respective maximum values. S–simulation, D–experimental data, Hyp–hypoxia; Ctr–control/untreated condition unless otherwise noted.

Figure S6

Figure S6. Constraining the model with additional qualitative experimental data; related to Figure 3. In addition to the quantitative datasets used in calibration, a number of qualitative macrophage data from literature was also incorporated into our model formulation and calibration. (A) IL-1β induces VEGF production (Lu et al., 2012). (B) IL-1β enhances IL-4-induced ARG1 expression (Sato et al., 2012). (C) TNFα does not significantly upregulate IL-1β secretion (Jayaraman et al., 2013; Lawlor et al., 2015). (D) TNFα inhibits IL-4-induced ARG1 expression. (Schleicher et al., 2016). (E) TNFα does not significantly upregulate CXCL9 secretion (Mundra et al., 2016). (F) TNFα can negatively regulate IL-12 secretion (Hodge-Dufour et al., 1998). (G) IFNγ inhibits ARG1 expression (Piccolo et al., 2017). (H) IFNγ does not significantly upregulate IL-1Ra (Liu et al., 1998). (I) IFNγ can negatively regulate IL-10 secretion (Hu et al., 2006). (J) IFNγ negatively regulates AKT activation and inhibitory phosphorylation of GSK3β (Hu et al., 2006). (K) IL-10 can downregulate CXCL10 expression (Cheeran et al., 2003). (L) IL-10 can negatively regulate TNFα secretion (Denys et al., 2002). (M) IL-10 can negatively regulate IL-12 secretion while inhibition of IL-10 signaling can promote IL-12 secretion (Rahim et al., 2005). (N) IL-

4 and IL-10 can decrease IFNγ secretion (Schindler et al., 2001). (O) IL-4 does not significantly upregulate secretion of IL-1β or IL-12 (Zhang et al., 2011). (P) IL-4 can inhibit IL-12 secretion (Bonder et al., 1999) and (Q) CXCL10 expression (Piccolo et al., 2017). (R) VEGF can reduce IL-12 secretion and CXCL10 expression (Wheeler et al., 2018). (S) Hypoxia increases CXCL10 expression (Danielsson et al., 2008). (T-U) Overexpression (mimic) of miR-155 reduces C/EBPβ expression and inhibition of miR-155 promotes C/EBPβ expression (Arranz et al., 2012). (V) Inhibition of NFκB signaling (through two types of inhibitors) can reduce miR-155 expression (Bala et al., 2011). (A-V) All results are normalized (y-axes, relative expression) to respective values at the t=0/control/untreated condition.
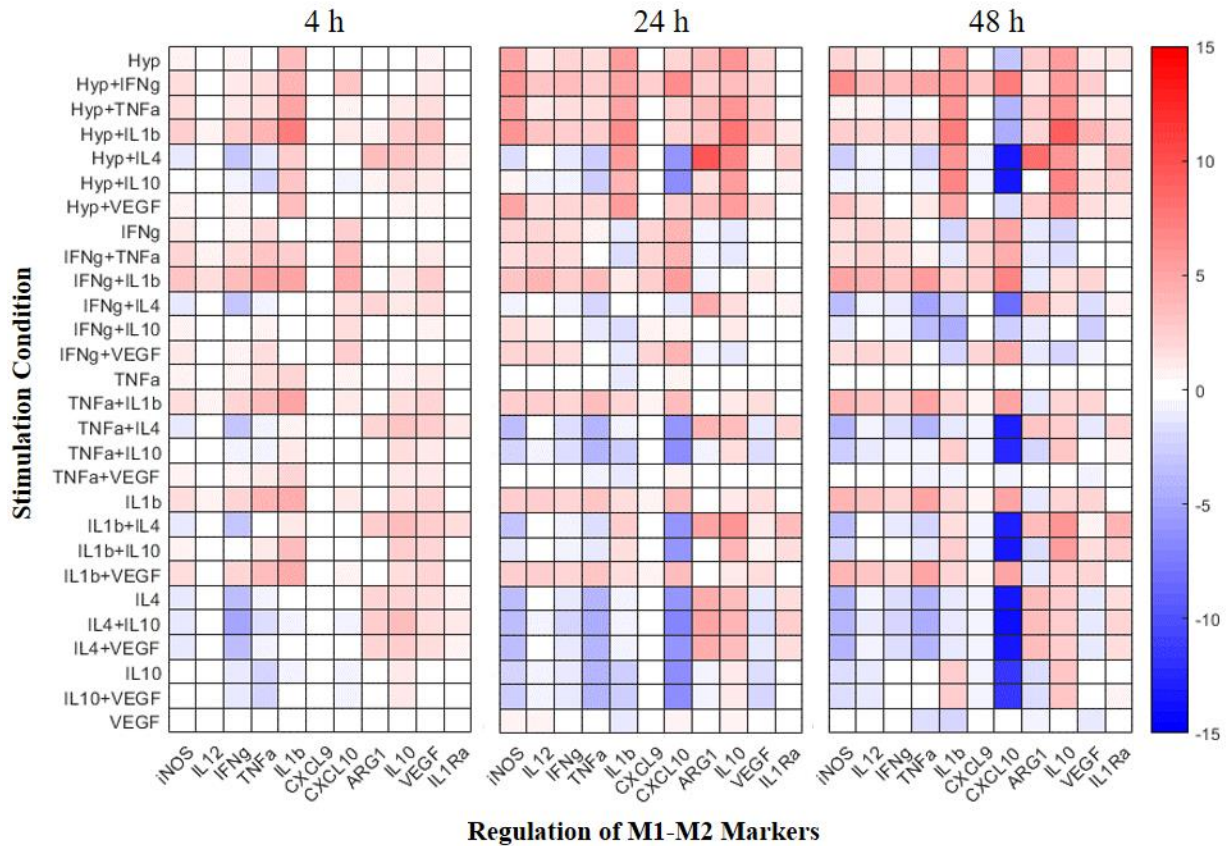
Figure S7

Figure S7. Macrophage polarization map under simulated *in vivo* stimulation conditions; related to Figure 5. A model-generated map of M1-M2 marker regulation (at 4, 24 and 48 h of stimulation) by macrophages under different stimulation conditions *in vivo* (7 cases of single stimulus, 21 cases of pairwise combined stimuli). For the 6 cytokines, their *in vivo* stimulation concentrations are assumed to be at 100 pg/ml; *in vivo* hypoxia is assumed to be 0.5% O2 (McKeown, 2014). Among the M1-M2 markers described, iNOS, ARG1, IL-12, IL-1Ra, CXCL9 are protein levels, CXCL10 is mRNA level, and the remaining ones are the respective protein production rates calculated by the model. All results are normalized to the untreated/t=0 values and then log2 transformed. Hyp–hypoxia.
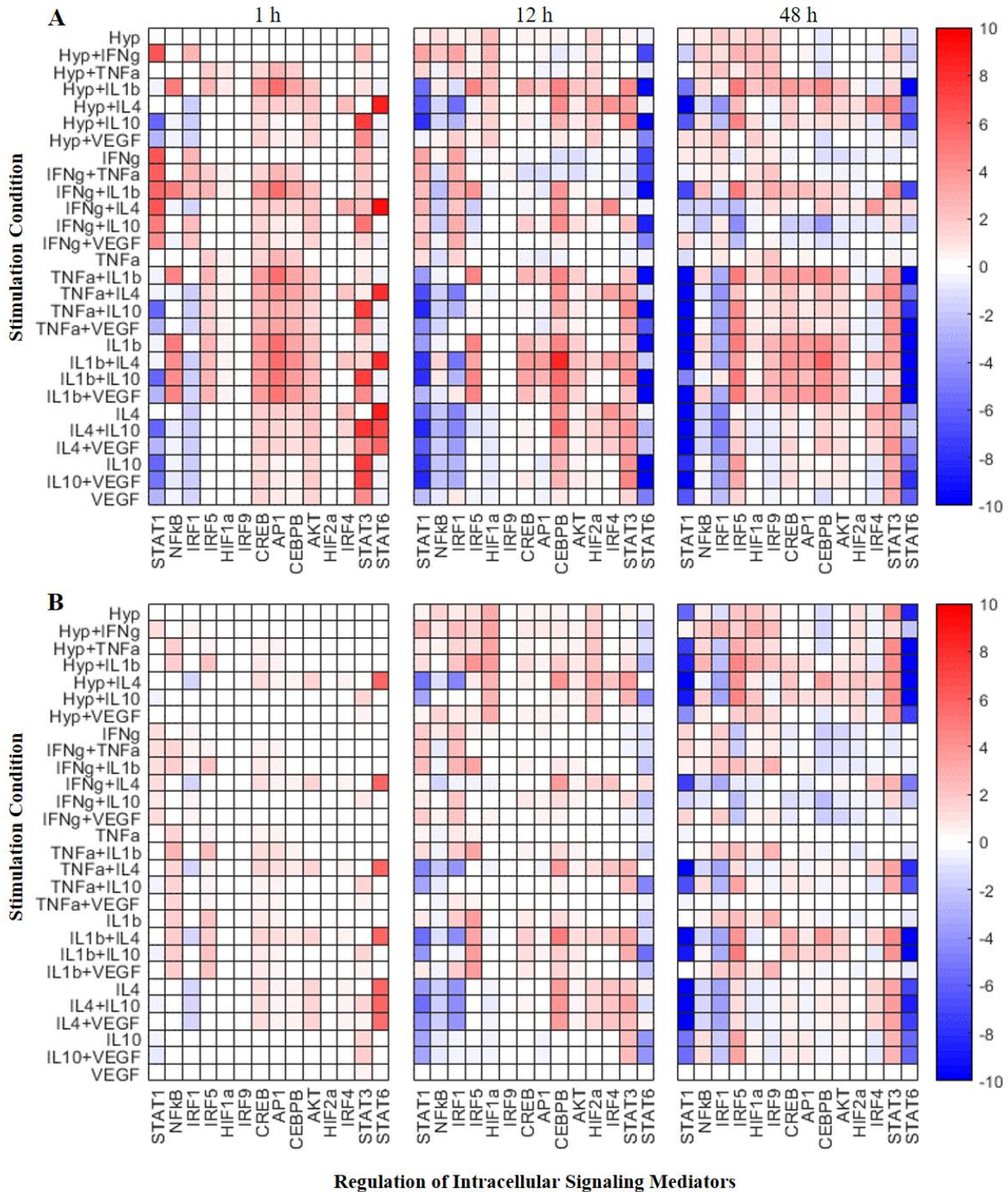
Figure S8

Figure S8. Macrophage transcriptional regulation map under simulated (A) *in vitro* **and (B)** *in vivo* **stimulation conditions; related to Figure 5.** A model-generated map of macrophage transcriptional regulation (at 1, 12 and 48 h of stimulation) under different stimulation conditions *in vitro and in vivo* (7

cases of single stimulus, 21 cases of pairwise combined stimuli, all conditions are the same as in Figs.5A and S7). For all the transcriptional mediators described, STAT1/3/6 refer to the respective activated dimers in nucleus, HIF1/2α refer to the respective HIFα/HIF1β heterodimers in nucleus, NFκB refer to free NFκB molecules in nucleus, CREB and AKT refer to respective phosphorylated forms, all others refer to respective protein expression levels in cell. All results are normalized to the untreated/t=0 values and then log2 transformed. Hyp–hypoxia.
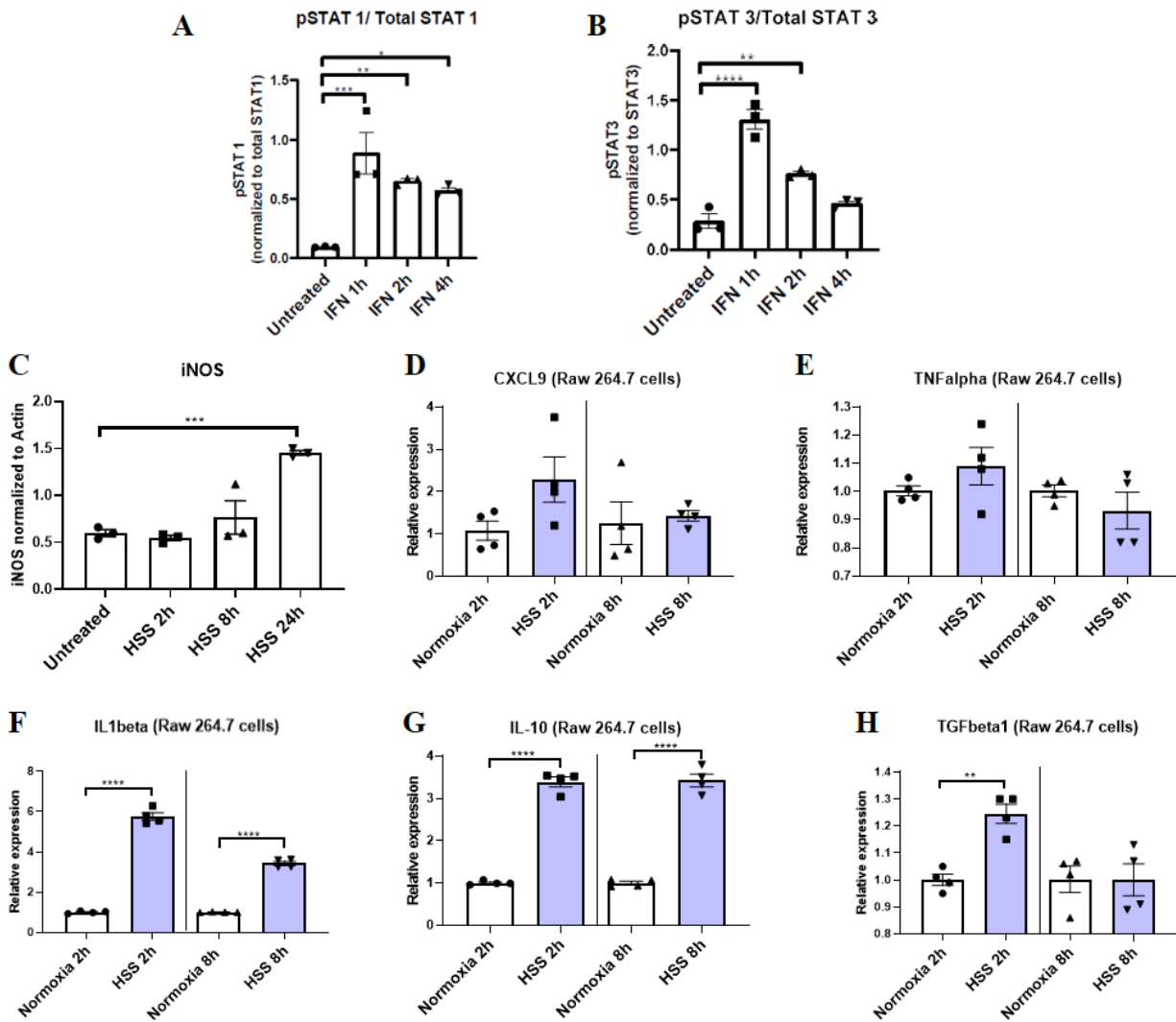
Figure S9

Figure S9. Experimental analysis of STAT signaling and HSS-induced M1-M2 marker regulation; related to Figures 2 and 6. Data shown here were used in model calibration (in Figs.2, S4) and analysis (in Fig.6). (A-B) Western Blotting analysis of pSTAT1 and pSTAT3 expression normalized to STAT1 and STAT3 respectively in macrophages treated with interferon gamma (IFN) for the times indicated. (C) Western Blotting analysis of iNOS expression normalized to actin in macrophages exposed to hypoxia serum starvation (HSS) for the times indicated. (D, F, G) qPCR analysis of CXCL9, IL-1β and IL-10 expression normalized to Rplp0 in macrophages under normoxia or HSS for the times indicated. (E and H) qPCR analysis of TNFα and TGFβ1 normalized to GAPDH in macrophages under normoxia or HSS for the times indicated. (A-H) Mean values, standard deviations and individual datapoints are displayed (A-C: n=3; D-H: n=4; * $p<0.05$; ** $p<0.01$; *** $p<0.001$; **** $p<0.0001$).
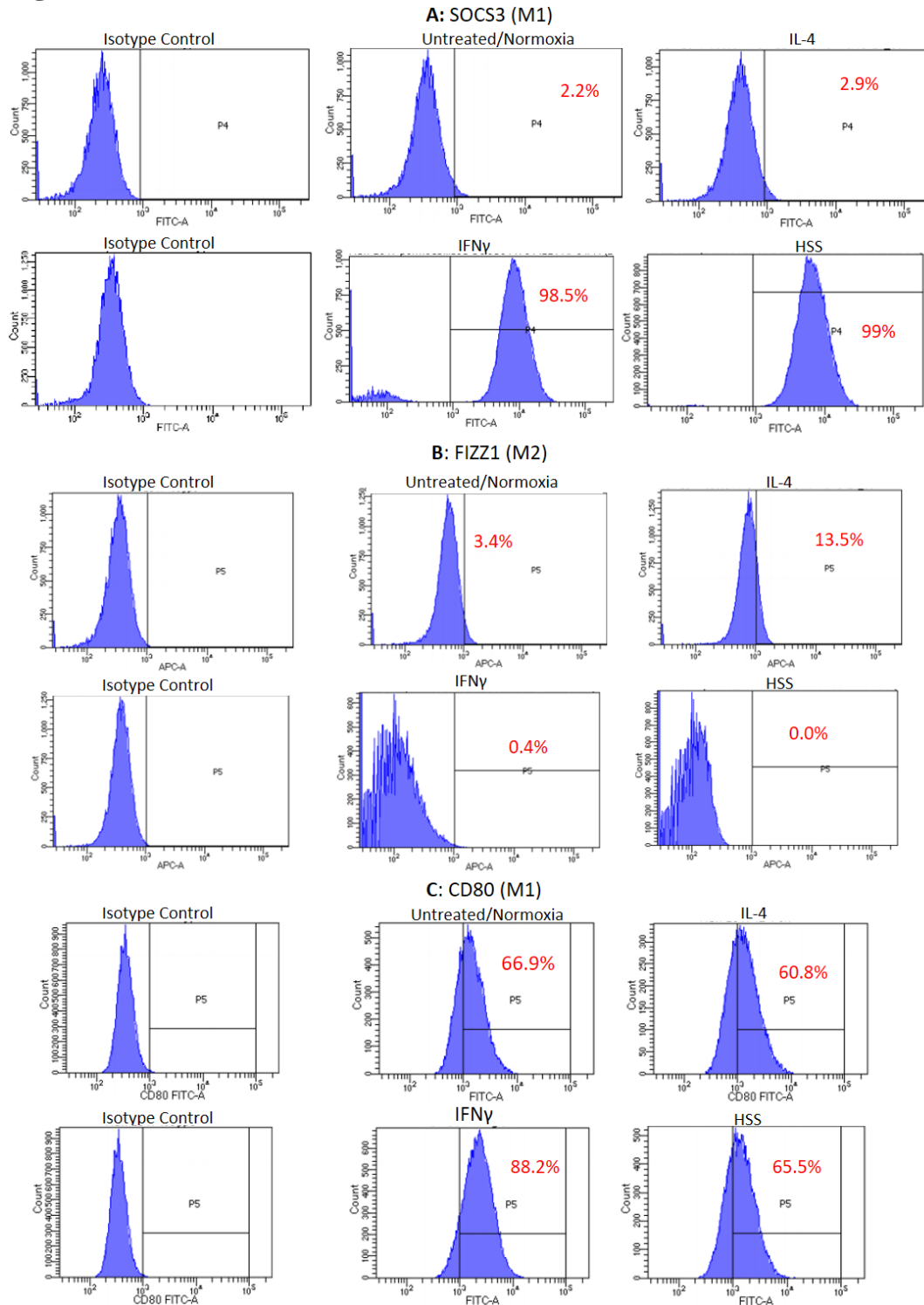
Figure S10

Figure S10. Flow cytometry analysis of macrophage markers; related to Figure 6. Data shown here were used in model analysis (in Fig.6). (A-C) Percentages of parent events sorting SOCS3, FIZZ1 or CD80 as M1-M2 markers in macrophages under normoxia, treated with 10 ng/ml of IL-4, treated with 50 ng/ml of IFNγ, and under hypoxia serum starvation (HSS) for 6 hours.

Figure S11

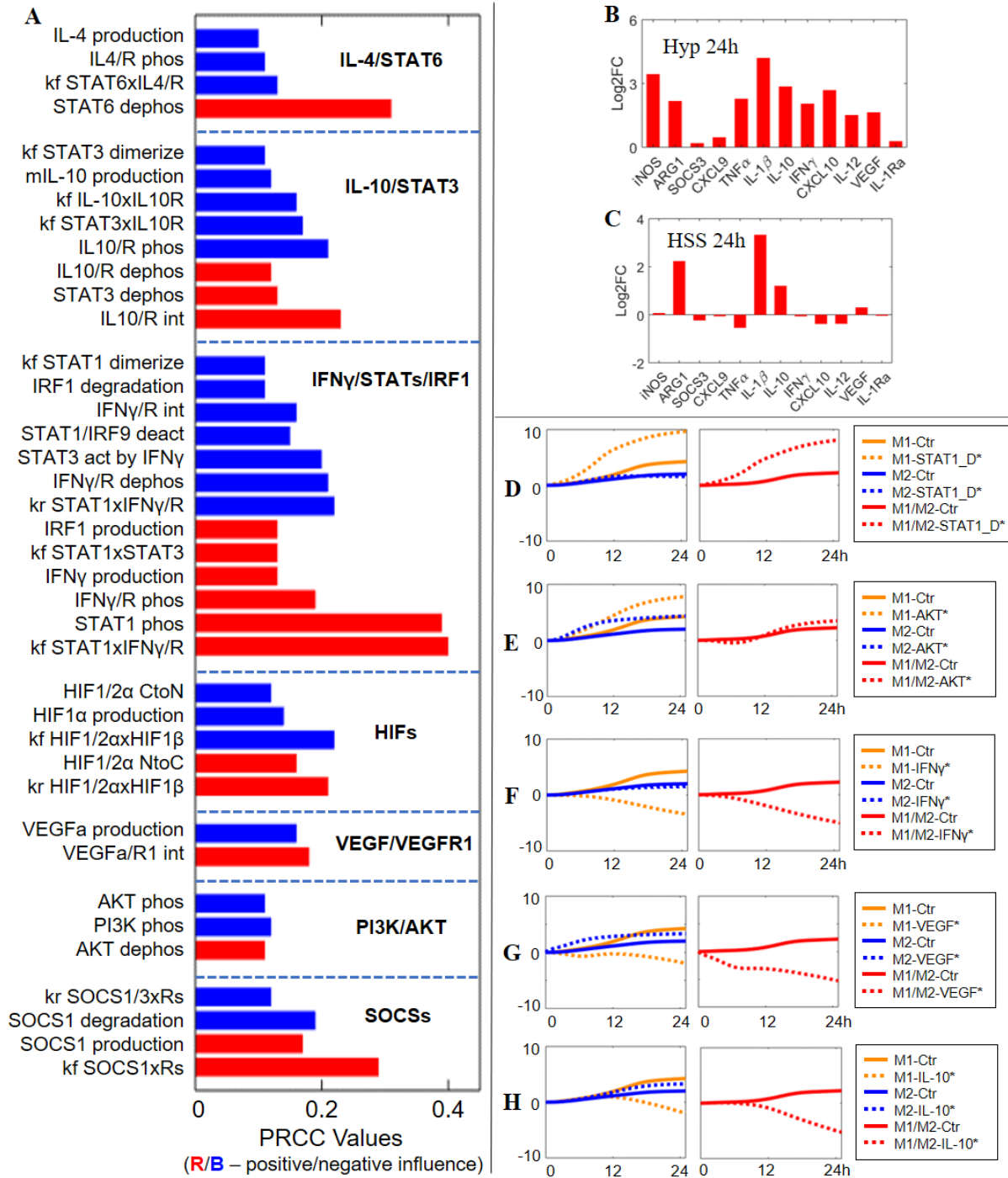**Figure S11. Macrophage response under HSS and *in silico* targeted interventions to promote M2-like phenotypes; related to Figure 6.** (A) Sensitivity indices (red – positive, blue – negative) of the most influential model parameters (e.g. absolute PRCC values greater than 0.1) that control M1 and M2 marker expression in terms of the 24h time-course integral of M1/M2 score in simulated HSS* (represented in

model as 2% O_2 plus global reduction in protein production rates). The identified parameters are categorized into 7 modules and their functions are briefly described. (B) Model-derived profile of macrophage M1-M2 marker expression at 24 h under HSS (simulated as hypoxia only). (C) Model-derived profile of macrophage M1-M2 marker expression at 24 h under simulated HSS*. (B-C) Expression levels are normalized to the t=0 (control condition) values and then log2 transformed. (D-H) Simulated M1 (orange), M2 (blue) profiles (e.g. M1 and M2 scores) and overall M1/M2 scores (red) over time under hypoxia (2% O_2) with various targeted interventions (label as 'species*') proposed by the sensitivity analysis. Results are normalized to the respective values at t=0 and then log10 transformed (y-axes). Implementation of targeted interventions: (D) inhibition of STAT1 dimerization – 0.01x kf5; (E) increased AKT activation – 10x k138; (F) Inhibition of IFNγ production – 0.1x k73; (G) Increased VEGF (pro-angiogenic form) production – 10x k72; (H) Increased IL-10 production – 10x k44. (A) More details about the listed parameters are described in Table S1 (parameter labels from top to bottom are k104, kf102, kf24, k26; kf125, k44, kf144, kf146, kf145, kr145, k127, k148; kf5, k85, k12, k117, k134, kr2, kr3, k52, kf131, k73, kf2, k4, kf3; kf58, k54, kf60, kr58, kr60; k72, k201; k138, k136, k140; kr11, k101, k135, kf11).

Figure S12
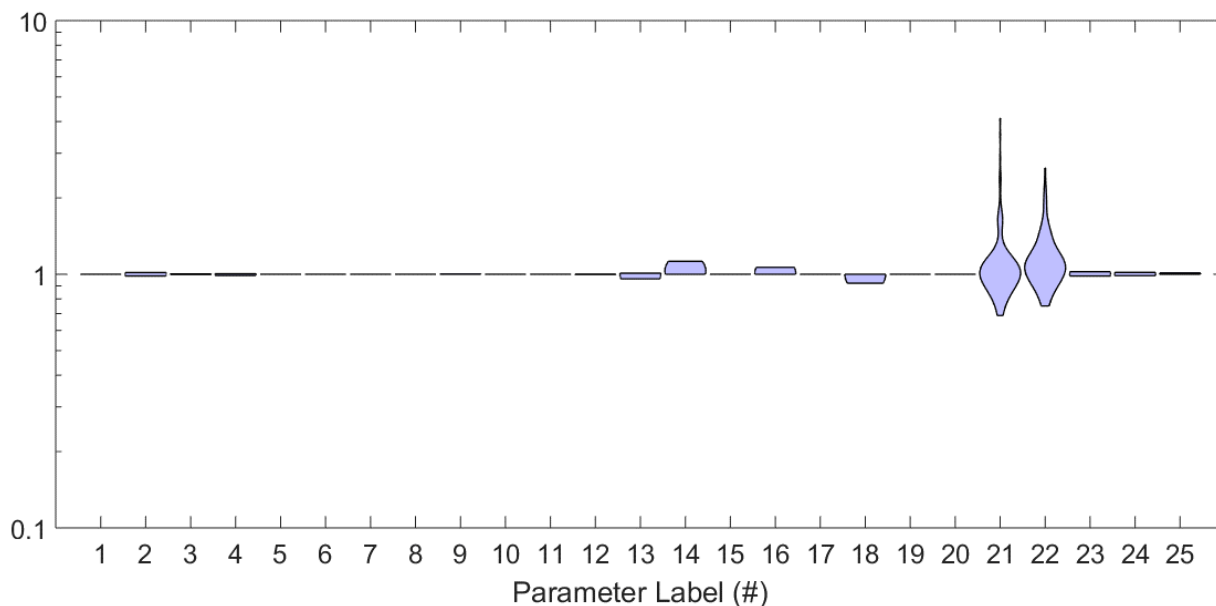
Figure S12. Parameter estimate distributions after bootstrapping; related to Figure 6. Parameter estimate distributions (represented by violin plots) of the top 25 most influential parameters. All parameter values were allowed to vary from 0.1x to 10x during bootstrapping and are here normalized to their respective reference values for display (y-axis in log scale). The parameters labeled #1-25 are kf3, kr2, k4, kr3, kf2, kf146, k117, kf11, k148, k12, k134, kf131, k52, k201, kf207, k209, k202, k203, k127, k135, k150, k82, kf145, k73, kf73 (see Table S1 for more details of these parameters).

Figure S13
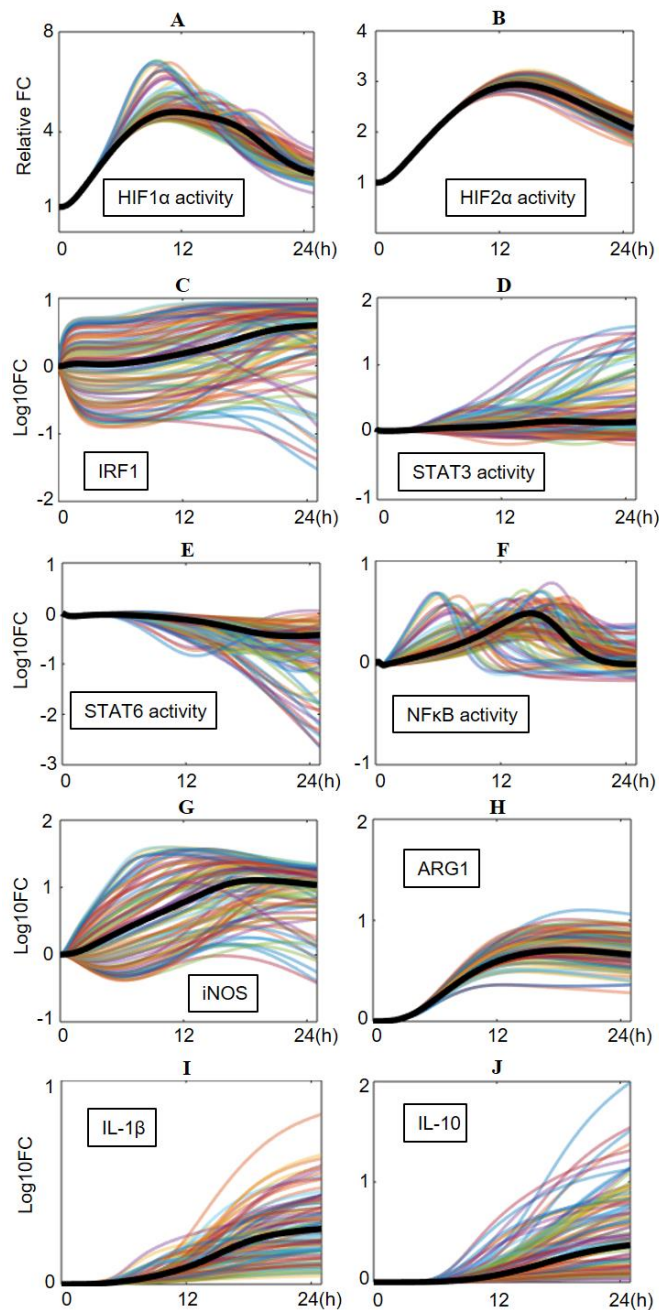
Figure S13. In silico analysis of hypoxia-driven transcriptional and marker regulation at the single-cell level; related to Figure 7. Simulated time-course responses (under hypoxia, 2% O_2) of 100 model-generated virtual macrophages in terms of their transcriptional activities of (A) HIF1α, (B) HIF2α, (C) IRF1, (D) STAT3, (E) STAT6, (F) NFκB, and M1-M2 marker regulation of (G-H) cellular iNOS and ARG1 expression, and (I-J) IL-1β and IL-10 secretion. (A-J) Results are normalized to the respective values at t=0 for A-B and then log10 transformed for C-J (y-axes). Black bolded lines are the trajectories of the reference model.

Figure S14
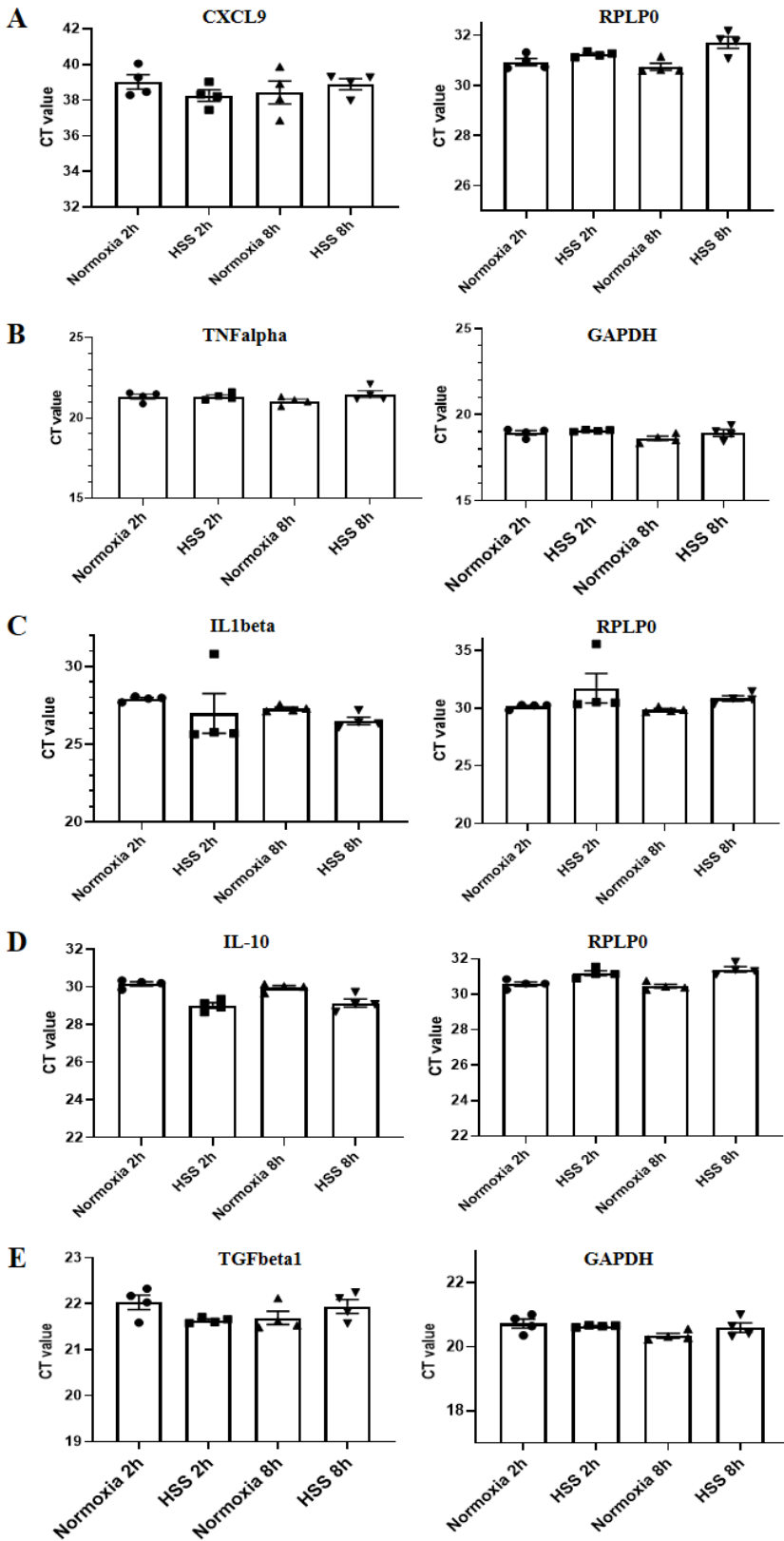
Figure S14. Raw data for the qPCR analysis presented in Fig.S9; related to Figure 6. (A, C, D) qPCR CT values under normoxia and hypoxia serum starvation (HSS), for the times indicated, for CXCL9, IL-1β, IL-10 and Rplp0. (B, E) qPCR CT values under normoxia and HSS, for the times indicated, for TNFα, TGFβ1 and GAPDH. (A-E) Mean levels, standard deviations and individual datapoints are displayed (n=4).

Figure S15
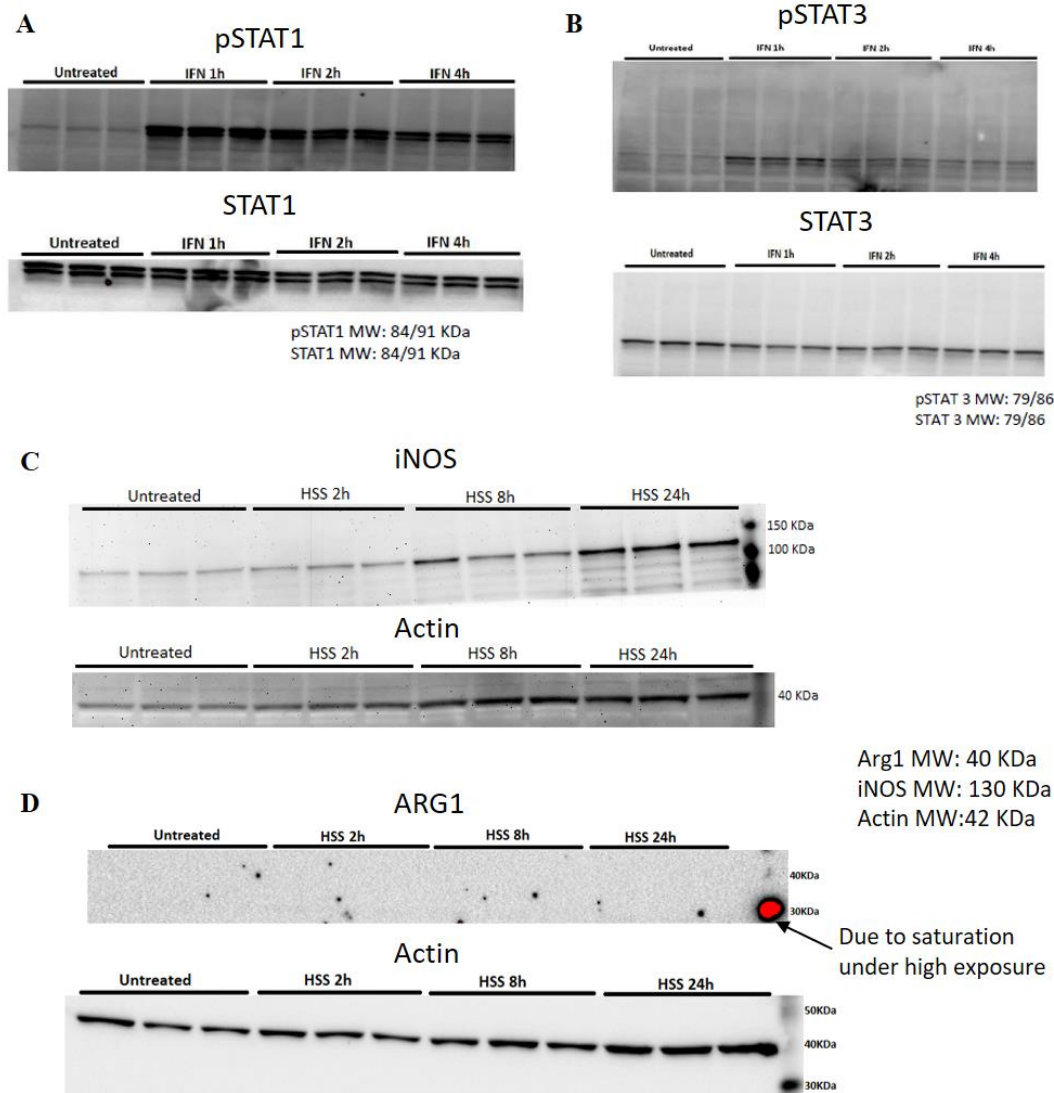
Figure S15. Raw data for the Western Blot analysis presented in Fig.S9; related to Figures 2 and 6. (A-B) Western Blots (n=3) of pSTAT1/pSTAT3 and total STAT1/STAT3 expression in macrophages treated with interferon gamma (IFN) for the times indicated. (C-D) Western Blots (n=3) of iNOS, ARG1 (below detection limit) and Actin expression in macrophages exposed to hypoxia serum starvation (HSS) for the times indicated.
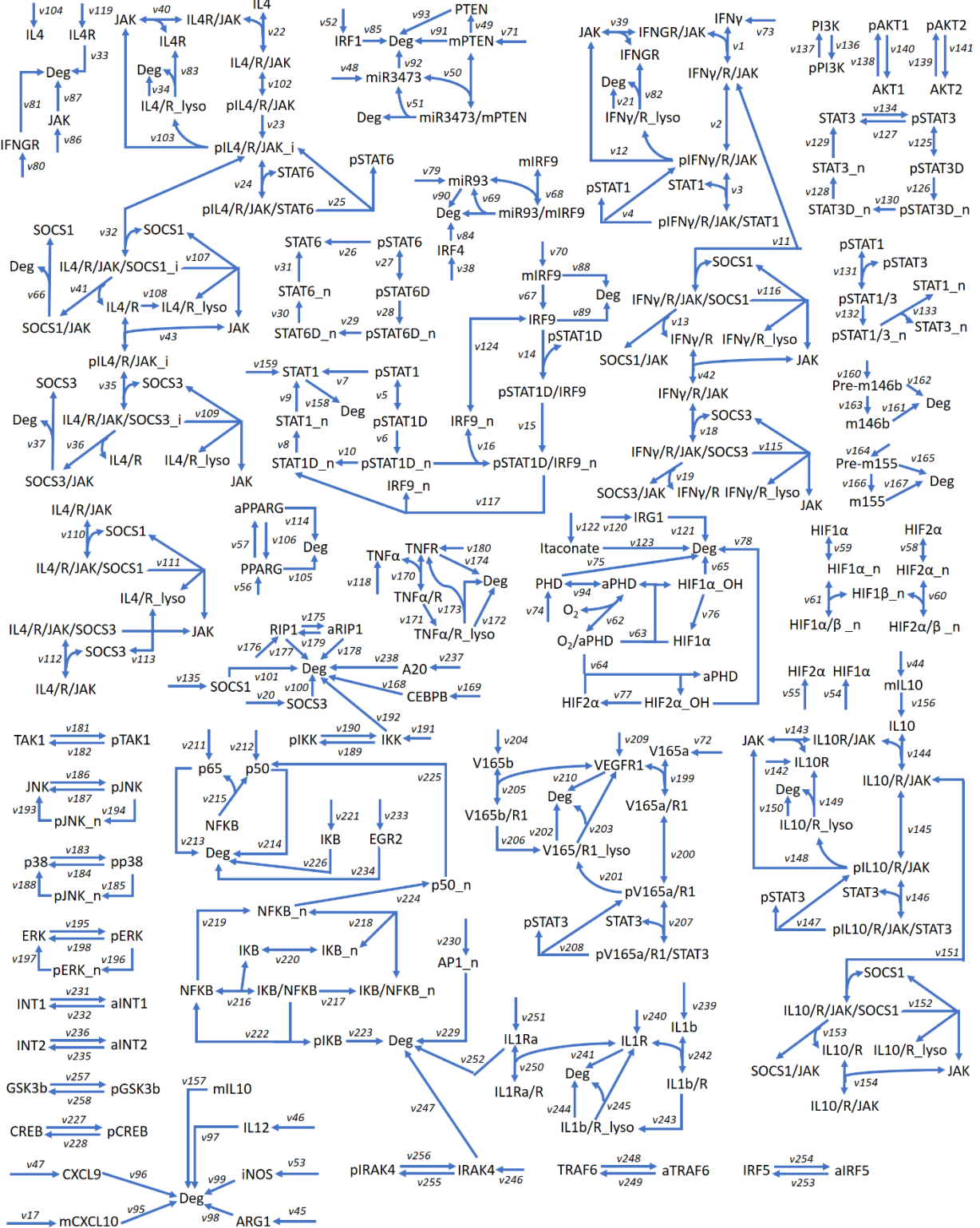
Figure S16. Detailed model diagram; related to Figure 1. A more detailed model diagram with all model species and reaction fluxes (labeled). Note that not all regulatory mechanisms were depicted here due to the size limit of the figure (e.g. transcriptional regulations were not explicitly drawn here); please refer to Table S1 for a full mechanistic description of the model.

References for Supplemental Information

ARRANZ, A., DOXAKI, C., VERGADI, E., MARTINEZ DE LA TORRE, Y., VAPORIDI, K., LAGOUDAKI, E. D., IERONYMAKI, E., ANDROULIDAKI, A., VENIHAKI, M., MARGIORIS, A. N., STATHOPOULOS, E. N., TSICHLIS, P. N. & TSATSANIS, C. 2012. Akt1 and Akt2 protein kinases differentially contribute to macrophage polarization. *Proc Natl Acad Sci U S A,* 109**,** 9517-22.

BALA, S., MARCOS, M., KODYS, K., CSAK, T., CATALANO, D., MANDREKAR, P. & SZABO, G. 2011. Up-regulation of microRNA-155 in macrophages contributes to increased tumor necrosis factor {alpha} (TNF{alpha}) production via increased mRNA half-life in alcoholic liver disease. *J Biol Chem,* 286**,** 1436-44.

BERRA, E., BENIZRI, E., GINOUVES, A., VOLMAT, V., ROUX, D. & POUYSSEGUR, J. 2003. HIF prolyl-hydroxylase 2 is the key oxygen sensor setting low steady-state levels of HIF-1alpha in normoxia. *EMBO J,* 22**,** 4082-90.

BLOUIN, C. M. & LAMAZE, C. 2013. Interferon gamma receptor: the beginning of the journey. *Front Immunol,* 4**,** 267.

BONDER, C. S., FINLAY-JONES, J. J. & HART, P. H. 1999. Interleukin-4 regulation of human monocyte and macrophage interleukin-10 and interleukin-12 production. Role of a functional interleukin-2 receptor gamma-chain. *Immunology,* 96**,** 529-36.

BOUCHER, J. M., CLARK, R. P., CHONG, D. C., CITRIN, K. M., WYLIE, L. A. & BAUTCH, V. L. 2017. Dynamic alterations in decoy VEGF receptor-1 stability regulate angiogenesis. *Nat Commun,* 8**,** 15699.

CARTA, L., PASTORINO, S., MELILLO, G., BOSCO, M. C., MASSAZZA, S. & VARESIO, L. 2001. Engineering of macrophages to produce IFN-gamma in response to hypoxia. *J Immunol,* 166**,** 5374-80.

CASALETTO, J. B. & MCCLATCHEY, A. I. 2012. Spatial regulation of receptor tyrosine kinases in development and cancer. *Nat Rev Cancer,* 12**,** 387-400.

CELADA, A. & SCHREIBER, R. D. 1987. Internalization and degradation of receptor-bound interferon-gamma by murine macrophages. Demonstration of receptor recycling. *J Immunol,* 139**,** 147-53.

CENDROWSKI, J., MAMINSKA, A. & MIACZYNSKA, M. 2016. Endocytic regulation of cytokine receptor signaling. *Cytokine Growth Factor Rev,* 32**,** 63-73.

CHEERAN, M. C., HU, S., SHENG, W. S., PETERSON, P. K. & LOKENSGARD, J. R. 2003. CXCL10 production from cytomegalovirus-stimulated microglia is regulated by both human and viral interleukin-10. *J Virol,* 77**,** 4502-15.

CHEUNG, P. C., CAMPBELL, D. G., NEBREDA, A. R. & COHEN, P. 2003. Feedback control of the protein kinase TAK1 by SAPK2a/p38alpha. *EMBO J,* 22**,** 5793-805.

CHOI, Y. S., PARK, J. K., KANG, E. H., LEE, Y. K., KIM, T. K., CHUNG, J. H., ZIMMERER, J. M., CARSON, W. E., SONG, Y. W. & LEE, Y. J. 2013. Cytokine signaling-1 suppressor is inducible by IL-1beta and inhibits the catabolic effects of IL-1beta in chondrocytes: its implication in the paradoxical joint-protective role of IL-1beta. *Arthritis Res Ther,* 15**,** R191.

COVARRUBIAS, A. J., AKSOYLAR, H. I., YU, J., SNYDER, N. W., WORTH, A. J., IYER, S. S., WANG, J., BEN-SAHRA, I., BYLES, V., POLYNNE-STAPORNKUL, T., ESPINOSA, E. C., LAMMING, D., MANNING, B. D., ZHANG, Y., BLAIR, I. A. & HORNG, T. 2016. Akt-mTORC1 signaling regulates Acly to integrate metabolic input to control of macrophage activation. *Elife,* 5.

CROKER, B. A., KIU, H. & NICHOLSON, S. E. 2008. SOCS regulation of the JAK/STAT signalling pathway. *Semin Cell Dev Biol,* 19**,** 414-22.

CUMMINS, E. P., BERRA, E., COMERFORD, K. M., GINOUVES, A., FITZGERALD, K. T., SEEBALLUCK, F., GODSON, C., NIELSEN, J. E., MOYNAGH, P., POUYSSEGUR, J. & TAYLOR, C. T. 2006. Prolyl hydroxylase-1 negatively regulates IkappaB kinase-beta, giving insight into hypoxia-induced NFkappaB activity. *Proc Natl Acad Sci U S A,* 103**,** 18154-9.

CURTALE, G., MIROLO, M., RENZI, T. A., ROSSATO, M., BAZZONI, F. & LOCATI, M. 2013. Negative regulation of Toll-like receptor 4 signaling by IL-10-dependent microRNA-146b. *Proc Natl Acad Sci U S A,* 110**,** 11499-504.

DANIELSSON, K. N., RYDBERG, E. K., INGELSTEN, M., AKYUREK, L. M., JIRHOLT, P., ULLSTROM, C., FORSBERG, G. B., BOREN, J., WIKLUND, O. & HULTEN, L. M. 2008. 15-Lipoxygenase-2 expression in human macrophages induces chemokine secretion and T cell migration. *Atherosclerosis,* 199**,** 34-40.

DATE, D., DAS, R., NARLA, G., SIMON, D. I., JAIN, M. K. & MAHABELESHWAR, G. H. 2014. Kruppel-like transcription factor 6 regulates inflammatory macrophage polarization. *J Biol Chem,* 289**,** 10318-29.

DAVIS, M. J., TSANG, T. M., QIU, Y., DAYRIT, J. K., FREIJ, J. B., HUFFNAGLE, G. B. & OLSZEWSKI, M. A. 2013. Macrophage M1/M2 polarization dynamically adapts to changes in cytokine microenvironments in Cryptococcus neoformans infection. *mBio,* 4**,** e00264-13.

DELGOFFE, G. M. & VIGNALI, D. A. 2013. STAT heterodimers in immunity: A mixed message or a unique signal? *JAKSTAT,* 2**,** e23060.

DENYS, A., UDALOVA, I. A., SMITH, C., WILLIAMS, L. M., CIESIELSKI, C. J., CAMPBELL, J., ANDREWS, C., KWAITKOWSKI, D. & FOXWELL, B. M. 2002. Evidence for a dual mechanism for IL-10 suppression of TNF-alpha production that does not involve inhibition of p38 mitogen-activated protein kinase or NF-kappa B in primary human macrophages. *J Immunol,* 168**,** 4837-45.

DICKENSHEETS, H., VAZQUEZ, N., SHEIKH, F., GINGRAS, S., MURRAY, P. J., RYAN, J. J. & DONNELLY, R. P. 2007. Suppressor of cytokine signaling-1 is an IL-4-inducible gene in macrophages and feedback inhibits IL-4 signaling. *Genes Immun,* 8**,** 21-7.

DRIPPS, D. J., BRANDHUBER, B. J., THOMPSON, R. C. & EISENBERG, S. P. 1991. Interleukin-1 (IL-1) receptor antagonist binds to the 80-kDa IL-1 receptor but does not initiate IL-1 signal transduction. *J Biol Chem,* 266**,** 10331-6.

DZAMKO, N., INESTA-VAQUERA, F., ZHANG, J., XIE, C., CAI, H., ARTHUR, S., TAN, L., CHOI, H., GRAY, N., COHEN, P., PEDRIOLI, P., CLARK, K. & ALESSI, D. R. 2012. The IkappaB kinase family phosphorylates the Parkinson's disease kinase LRRK2 at Ser935 and Ser910 during Toll-like receptor signaling. *PLoS One,* 7**,** e39132.

ENDO, Y., BLINOVA, K., ROMANTSEVA, T., GOLDING, H. & ZAITSEVA, M. 2014. Differences in PGE2 production between primary human monocytes and differentiated macrophages: role of IL-1beta and TRIF/IRF3. *PLoS One,* 9**,** e98517.

ERMOLAEVA, M. A., MICHALLET, M. C., PAPADOPOULOU, N., UTERMOHLEN, O., KRANIDIOTI, K., KOLLIAS, G., TSCHOPP, J. & PASPARAKIS, M. 2008. Function of TRADD in tumor necrosis factor receptor 1 signaling and in TRIF-dependent inflammatory responses. *Nat Immunol,* 9**,** 1037-46.

ETEMADI, N., CHOPIN, M., ANDERTON, H., TANZER, M. C., RICKARD, J. A., ABEYSEKERA, W., HALL, C., SPALL, S. K., WANG, B., XIONG, Y., HLA, T., PITSON, S. M., BONDER, C. S., WONG, W. W., ERNST, M., SMYTH, G. K., VAUX, D. L., NUTT, S. L., NACHBUR, U. & SILKE, J. 2015. TRAF2 regulates TNF and NF-kappaB signalling to suppress apoptosis and skin inflammation independently of Sphingosine kinase 1. *Elife,* 4.

EUBANK, T. D., RODA, J. M., LIU, H., O'NEIL, T. & MARSH, C. B. 2011. Opposing roles for HIF-1alpha and HIF-2alpha in the regulation of angiogenesis by mononuclear phagocytes. *Blood,* 117**,** 323-32.

FELIERS, D., CHEN, X., AKIS, N., CHOUDHURY, G. G., MADAIO, M. & KASINATH, B. S. 2005. VEGF regulation of endothelial nitric oxide synthase in glomerular endothelial cells. *Kidney Int,* 68**,** 1648-59.

FISCHER, R., MAIER, O., NAUMER, M., KRIPPNER-HEIDENREICH, A., SCHEURICH, P. & PFIZENMAIER, K. 2011. Ligand-induced internalization of TNF receptor 2 mediated by a di-leucin motif is dispensable for activation of the NFkappaB pathway. *Cell Signal,* 23**,** 161-70.

FUNAKOSHI-TAGO, M., KAMADA, N., SHIMIZU, T., HASHIGUCHI, Y., TAGO, K., SONODA, Y. & KASAHARA, T. 2009. TRAF6 negatively regulates TNFalpha-induced NF-kappaB activation. *Cytokine,* 45**,** 72-9.

GABAY, C., SMITH, M. F., EIDLEN, D. & AREND, W. P. 1997. Interleukin 1 receptor antagonist (IL-1Ra) is an acute-phase protein. *J Clin Invest,* 99**,** 2930-40.

GANTA, V. C., CHOI, M. H., KUTATELADZE, A., FOX, T. E., FARBER, C. R. & ANNEX, B. H. 2017. A MicroRNA93-Interferon Regulatory Factor-9-Immunoresponsive Gene-1-Itaconic Acid Pathway Modulates M2-Like Macrophage Polarization to Revascularize Ischemic Muscle. *Circulation,* 135**,** 2403-2425.

GENG, J., ITO, Y., SHI, L., AMIN, P., CHU, J., OUCHIDA, A. T., MOOKHTIAR, A. K., ZHAO, H., XU, D., SHAN, B., NAJAFOV, A., GAO, G., AKIRA, S. & YUAN, J. 2017. Regulation of RIPK1 activation by TAK1-mediated phosphorylation dictates apoptosis and necroptosis. *Nat Commun,* 8**,** 359.

GOTSCHEL, F., KERN, C., LANG, S., SPARNA, T., MARKMANN, C., SCHWAGER, J., MCNELLY, S., VON WEIZSACKER, F., LAUFER, S., HECHT, A. & MERFORT, I. 2008. Inhibition of GSK3 differentially modulates NF-kappaB, CREB, AP-1 and beta-catenin signaling in hepatocytes, but fails to promote TNF-alpha-induced apoptosis. *Exp Cell Res,* 314**,** 1351-66.

GREEN, D. S., YOUNG, H. A. & VALENCIA, J. C. 2017. Current prospects of type II interferon gamma signaling and autoimmunity. *J Biol Chem,* 292**,** 13925-13933.

GULEN, M. F., BULEK, K., XIAO, H., YU, M., GAO, J., SUN, L., BEUREL, E., KAIDANOVICH-BEILIN, O., FOX, P. L., DICORLETO, P. E., WANG, J. A., QIN, J., WALD, D. N., WOODGETT, J. R., JOPE, R. S., CARMAN, J., DONGRE, A. & LI, X. 2012. Inactivation of the enzyme GSK3alpha by the kinase IKKi promotes AKT-mTOR signaling pathway that mediates interleukin-1-induced Th17 cell maintenance. *Immunity,* 37**,** 800-12.

HANSEN, B., DITTRICH-BREIHOLZ, O., KRACHT, M. & WINDHEIM, M. 2013. Regulation of NF-kappaB-dependent gene expression by ligand-induced endocytosis of the interleukin-1 receptor. *Cell Signal,* 25**,** 214-28.

HE, X., TANG, R., SUN, Y., WANG, Y. G., ZHEN, K. Y., ZHANG, D. M. & PAN, W. Q. 2016. MicroR-146 blocks the activation of M1 macrophage by targeting signal transducer and activator of transcription 1 in hepatic schistosomiasis. *EBioMedicine,* 13**,** 339-347.

HO, H. H. & IVASHKIV, L. B. 2006. Role of STAT3 in type I interferon responses. Negative regulation of STAT1-dependent inflammatory gene activation. *J Biol Chem,* 281**,** 14111-8.

HODGE-DUFOUR, J., MARINO, M. W., HORTON, M. R., JUNGBLUTH, A., BURDICK, M. D., STRIETER, R. M., NOBLE, P. W., HUNTER, C. A. & PURE, E. 1998. Inhibition of interferon gamma induced interleukin 12 production: a potential mechanism for the anti-inflammatory activities of tumor necrosis factor. *Proc Natl Acad Sci U S A,* 95**,** 13806-11.

HSU, A. T., LUPANCU, T. J., LEE, M. C., FLEETWOOD, A. J., COOK, A. D., HAMILTON, J. A. & ACHUTHAN, A. 2018. Epigenetic and transcriptional regulation of IL4-induced CCL17 production in human monocytes and murine macrophages. *J Biol Chem,* 293**,** 11415-11423.

HU, X., HO, H. H., LOU, O., HIDAKA, C. & IVASHKIV, L. B. 2005. Homeostatic role of interferons conferred by inhibition of IL-1-mediated inflammation and tissue destruction. *J Immunol,* 175**,** 131-8.

HU, X., PAIK, P. K., CHEN, J., YARILINA, A., KOCKERITZ, L., LU, T. T., WOODGETT, J. R. & IVASHKIV, L. B. 2006. IFN-gamma suppresses IL-10 production and synergizes with TLR2 by regulating GSK3 and CREB/AP-1 proteins. *Immunity,* 24**,** 563-74.

IMAMURA, K., SPRIGGS, D. & KUFE, D. 1987. Expression of tumor necrosis factor receptors on human monocytes and internalization of receptor bound ligand. *J Immunol,* 139**,** 2989-92.

IMTIYAZ, H. Z., WILLIAMS, E. P., HICKEY, M. M., PATEL, S. A., DURHAM, A. C., YUAN, L. J., HAMMOND, R., GIMOTTY, P. A., KEITH, B. & SIMON, M. C. 2010. Hypoxia-inducible factor 2alpha regulates macrophage function in mouse models of acute and tumor inflammation. *J Clin Invest,* 120**,** 2699-714.

JAYARAMAN, P., SADA-OVALLE, I., NISHIMURA, T., ANDERSON, A. C., KUCHROO, V. K., REMOLD, H. G. & BEHAR, S. M. 2013. IL-1beta promotes antimicrobial immunity in macrophages by regulating TNFR signaling and caspase-3 activation. *J Immunol,* 190**,** 4196-204.

KAWAKAMI, K., KAWAKAMI, M., LELAND, P. & PURI, R. K. 2002. Internalization property of interleukin-4 receptor alpha chain increases cytotoxic effect of interleukin-4 receptor-targeted cytotoxin in cancer cells. *Clin Cancer Res,* 8**,** 258-66.

KILIAN, P. L., KAFFKA, K. L., BIONDI, D. A., LIPMAN, J. M., BENJAMIN, W. R., FELDMAN, D. & CAMPEN, C. A. 1991. Antiproliferative effect of interleukin-1 on human ovarian carcinoma cell line (NIH:OVCAR-3). *Cancer Res,* 51**,** 1823-8.

KIM, G. D., DAS, R., RAO, X., ZHONG, J., DEIULIIS, J. A., RAMIREZ-BERGERON, D. L., RAJAGOPALAN, S. & MAHABELESHWAR, G. H. 2018. CITED2 Restrains Proinflammatory Macrophage Activation and Response. *Mol Cell Biol,* 38.

KIM, H. S., KIM, D. C., KIM, H. M., KWON, H. J., KWON, S. J., KANG, S. J., KIM, S. C. & CHOI, G. E. 2015. STAT1 deficiency redirects IFN signalling toward suppression of TLR response through a feedback activation of STAT3. *Sci Rep,* 5**,** 13414.

KIMURA, T., NADA, S., TAKEGAHARA, N., OKUNO, T., NOJIMA, S., KANG, S., ITO, D., MORIMOTO, K., HOSOKAWA, T., HAYAMA, Y., MITSUI, Y., SAKURAI, N., SARASHINA-KIDA, H., NISHIDE, M., MAEDA, Y., TAKAMATSU, H., OKUZAKI, D., YAMADA, M., OKADA, M. & KUMANOGOH, A. 2016. Polarization of M2 macrophages requires Lamtor1 that integrates cytokine and amino-acid signals. *Nat Commun,* 7**,** 13130.

KOBAYASHI, S., SAWANO, A., NOJIMA, Y., SHIBUYA, M. & MARU, Y. 2004. The c-Cbl/CD2AP complex regulates VEGF-induced endocytosis and degradation of Flt-1 (VEGFR-1). *FASEB J,* 18**,** 929-31.

KOGA, Y., HISADA, T., ISHIZUKA, T., UTSUGI, M., ONO, A., YATOMI, M., KAMIDE, Y., AOKI-SAITO, H., TSURUMAKI, H., DOBASHI, K. & YAMADA, M. 2016. CREB regulates TNF-alpha-induced GM-CSF secretion via p38 MAPK in human lung fibroblasts. *Allergol Int,* 65**,** 406-413.

KOVALOVSKY, D., PAEZ PEREDA, M., SAUER, J., PEREZ CASTRO, C., NAHMOD, V. E., STALLA, G. K., HOLSBOER, F. & ARZT, E. 1998. The Th1 and Th2 cytokines IFN-gamma and IL-4 antagonize the inhibition of monocyte IL-1 receptor antagonist by glucocorticoids: involvement of IL-1. *Eur J Immunol,* 28**,** 2075-85.

KURGONAITE, K., GANDHI, H., KURTH, T., PAUTOT, S., SCHWILLE, P., WEIDEMANN, T. & BOKEL, C. 2015. Essential role of endocytosis for interleukin-4-receptor-mediated JAK/STAT signalling. *J Cell Sci,* 128**,** 3781-95.

LANG, R., PATEL, D., MORRIS, J. J., RUTSCHMAN, R. L. & MURRAY, P. J. 2002. Shaping gene expression in activated and resting primary macrophages by IL-10. *J Immunol,* 169**,** 2253-63.

LAWLOR, K. E., KHAN, N., MILDENHALL, A., GERLIC, M., CROKER, B. A., D'CRUZ, A. A., HALL, C., KAUR SPALL, S., ANDERTON, H., MASTERS, S. L., RASHIDI, M., WICKS, I. P., ALEXANDER, W. S., MITSUUCHI, Y., BENETATOS, C. A., CONDON, S. M., WONG, W. W., SILKE, J., VAUX, D. L. & VINCE, J. E. 2015. RIPK3 promotes cell death and NLRP3 inflammasome activation in the absence of MLKL. *Nat Commun,* 6**,** 6282.

LI, X., ZHANG, Z., LI, L., GONG, W., LAZENBY, A. J., SWANSON, B. J., HERRING, L. E., ASARA, J. M., SINGER, J. D. & WEN, H. 2017. Myeloid-derived cullin 3 promotes STAT3 phosphorylation by inhibiting OGT expression and protects against intestinal inflammation. *J Exp Med,* 214**,** 1093-1109.

LIM, J. E., CHUNG, E. & SON, Y. 2017. A neuropeptide, Substance-P, directly induces tissue-repairing M2 like macrophages by activating the PI3K/Akt/mTOR pathway even in the presence of IFNgamma. *Sci Rep,* 7**,** 9417.

LIU, J., CAO, S., HERMAN, L. M. & MA, X. 2003. Differential regulation of interleukin (IL)-12 p35 and p40 gene expression and interferon (IFN)-gamma-primed IL-12 production by IFN regulatory factor 1. *J Exp Med,* 198**,** 1265-76.

LIU, J. S., AMARAL, T. D., BROSNAN, C. F. & LEE, S. C. 1998. IFNs are critical regulators of IL-1 receptor antagonist and IL-1 expression in human microglia. *J Immunol,* 161**,** 1989-96.

LIU, X., ZHANG, J., ZEIGLER, A. C., NELSON, A. R., LINDSEY, M. L. & SAUCERMAN, J. J. 2019. Network analysis reveals a distinct axis of macrophage activation in response to conflicting inflammatory cues. *bioRxiv***,** 844464.

LO, S. Z., STEER, J. H. & JOYCE, D. A. 2011. Tumor necrosis factor-alpha promotes survival in methotrexate-exposed macrophages by an NF-kappaB-dependent pathway. *Arthritis Res Ther,* 13**,** R24.

LOPEZ-BERGAMI, P., LAU, E. & RONAI, Z. 2010. Emerging roles of ATF2 and the dynamic AP1 network in cancer. *Nat Rev Cancer,* 10**,** 65-76.

LU, P., LI, L., LIU, G., BABA, T., ISHIDA, Y., NOSAKA, M., KONDO, T., ZHANG, X. & MUKAIDA, N. 2012. Critical role of TNF-alpha-induced macrophage VEGF and iNOS production in the experimental corneal neovascularization. *Invest Ophthalmol Vis Sci,* 53**,** 3516-26.

LV, X., CHEN, P. & LIU, W. 2015. Down regulation of MiR-93 contributes to endometriosis through targeting MMP3 and VEGFA. *Am J Cancer Res,* 5**,** 1706-17.

MAITI, S., DAI, W., ALANIZ, R. C., HAHN, J. & JAYARAMAN, A. 2015. Mathematical Modeling of Pro- and Anti-Inflammatory Signaling in Macrophages. *Processes,* 3**,** 1-18.

MALIK, D. 2016. *MicroRNAs in the regulation of alternatively activated macrophages.* the University of Edinburgh.

MARCHETTI, M., MONIER, M. N., FRADAGRADA, A., MITCHELL, K., BAYCHELIER, F., EID, P., JOHANNES, L. & LAMAZE, C. 2006. Stat-mediated signaling induced by type I and type II interferons (IFNs) is differentially controlled through lipid microdomain association and clathrin-dependent endocytosis of IFN receptors. *Mol Biol Cell,* 17**,** 2896-909.

MARINO, S., HOGUE, I. B., RAY, C. J. & KIRSCHNER, D. E. 2008. A methodology for performing global uncertainty and sensitivity analysis in systems biology. *J Theor Biol,* 254**,** 178-96.

MCCOY, C. E., SHEEDY, F. J., QUALLS, J. E., DOYLE, S. L., QUINN, S. R., MURRAY, P. J. & O'NEILL, L. A. 2010. IL-10 inhibits miR-155 induction by toll-like receptors. *J Biol Chem,* 285**,** 20492-8.

MCKEOWN, S. R. 2014. Defining normoxia, physoxia and hypoxia in tumours-implications for treatment response. *Br J Radiol,* 87**,** 20130676.

MEI, Y., THOMPSON, M. D., SHIRAISHI, Y., COHEN, R. A. & TONG, X. 2014. Sarcoplasmic/endoplasmic reticulum Ca2+ ATPase C674 promotes ischemia- and hypoxia-induced angiogenesis via coordinated endothelial cell and macrophage function. *J Mol Cell Cardiol,* 76**,** 275-82.

MENG, X., GROTSCH, B., LUO, Y., KNAUP, K. X., WIESENER, M. S., CHEN, X. X., JANTSCH, J., FILLATREAU, S., SCHETT, G. & BOZEC, A. 2018. Hypoxia-inducible factor-1alpha is a critical transcription factor for IL-10-producing B cells in autoimmune disease. *Nat Commun,* 9**,** 251.

MIGITA, K., IWANAGA, N., IZUMI, Y., KAWAHARA, C., KUMAGAI, K., NAKAMURA, T., KOGA, T. & KAWAKAMI, A. 2017. TNF-alpha-induced miR-155 regulates IL-6 signaling in rheumatoid synovial fibroblasts. *BMC Res Notes,* 10**,** 403.

MITCHELL, T. J. & JOHN, S. 2005. Signal transducer and activator of transcription (STAT) signalling and T-cell lymphomas. *Immunology,* 114**,** 301-12.

MUNDER, M., MALLO, M., EICHMANN, K. & MODOLELL, M. 1998. Murine macrophages secrete interferon gamma upon combined stimulation with interleukin (IL)-12 and IL-18: A novel pathway of autocrine macrophage activation. *J Exp Med,* 187**,** 2103-8.

MUNDRA, J. J., JIAN, J., BHAGAT, P. & LIU, C. J. 2016. Progranulin inhibits expression and release of chemokines CXCL9 and CXCL10 in a TNFR1 dependent manner. *Sci Rep,* 6**,** 21115.

NAUJOKS, J., TABELING, C., DILL, B. D., HOFFMANN, C., BROWN, A. S., KUNZE, M., KEMPA, S., PETER, A., MOLLENKOPF, H. J., DORHOI, A., KERSHAW, O., GRUBER, A. D., SANDER, L. E., WITZENRATH, M., HEROLD, S., NERLICH, A., HOCKE, A. C., VAN DRIEL, I., SUTTORP, N., BEDOUI, S., HILBI, H., TROST,

M. & OPITZ, B. 2016. IFNs Modify the Proteome of Legionella-Containing Vacuoles and Restrict Infection Via IRG1-Derived Itaconic Acid. *PLoS Pathog,* 12**,** e1005408.

NEGISHI, H., OHBA, Y., YANAI, H., TAKAOKA, A., HONMA, K., YUI, K., MATSUYAMA, T., TANIGUCHI, T. & HONDA, K. 2005. Negative regulation of Toll-like-receptor signaling by IRF-4. *Proc Natl Acad Sci U S A,* 102**,** 15989-94.

NEUMANN, D., LIENENKLAUS, S., ROSATI, O. & MARTIN, M. U. 2002. IL-1beta-induced phosphorylation of PKB/Akt depends on the presence of IRAK-1. *Eur J Immunol,* 32**,** 3689-98.

NIEMAND, C., NIMMESGERN, A., HAAN, S., FISCHER, P., SCHAPER, F., ROSSAINT, R., HEINRICH, P. C. & MULLER-NEWEN, G. 2003. Activation of STAT3 by IL-6 and IL-10 in primary human macrophages is differentially modulated by suppressor of cytokine signaling 3. *J Immunol,* 170**,** 3263-72.

NOWAK, D. G., WOOLARD, J., AMIN, E. M., KONOPATSKAYA, O., SALEEM, M. A., CHURCHILL, A. J., LADOMERY, M. R., HARPER, S. J. & BATES, D. O. 2008. Expression of pro- and anti-angiogenic isoforms of VEGF is differentially regulated by splicing and growth factors. *J Cell Sci,* 121**,** 3487-95.

O'CONNELL, R. M., TAGANOV, K. D., BOLDIN, M. P., CHENG, G. & BALTIMORE, D. 2007. MicroRNA-155 is induced during the macrophage inflammatory response. *Proc Natl Acad Sci U S A,* 104**,** 1604-9.

O'CONNOR, J. C., SHERRY, C. L., GUEST, C. B. & FREUND, G. G. 2007. Type 2 diabetes impairs insulin receptor substrate-2-mediated phosphatidylinositol 3-kinase activity in primary macrophages to induce a state of cytokine resistance to IL-4 in association with overexpression of suppressor of cytokine signaling-3. *J Immunol,* 178**,** 6886-93.

O'SHEA, J. J., SCHWARTZ, D. M., VILLARINO, A. V., GADINA, M., MCINNES, I. B. & LAURENCE, A. 2015. The JAK-STAT pathway: impact on human disease and therapeutic intervention. *Annu Rev Med,* 66**,** 311-28.

OHATA, T., FUKUDA, K., MURAKAMI, A., OHIGASHI, H., SUGIMURA, T. & WAKABAYASHI, K. 1998. Inhibition by 1'-acetoxychavicol acetate of lipopolysaccharide- and interferon-gamma-induced nitric oxide production through suppression of inducible nitric oxide synthase gene expression in RAW264 cells. *Carcinogenesis,* 19**,** 1007-12.

ONO, H., ICHIKI, T., OHTSUBO, H., FUKUYAMA, K., IMAYAMA, I., IINO, N., MASUDA, S., HASHIGUCHI, Y., TAKESHITA, A. & SUNAGAWA, K. 2006. CAMP-response element-binding protein mediates tumor necrosis factor-alpha-induced vascular cell adhesion molecule-1 expression in endothelial cells. *Hypertens Res,* 29**,** 39-47.

PEIHENG HE, F. Y., SHUAI HUANG, YUANQING GUO, HUA WANG, YUTIAN WU 2016. Anti-inflammatory effect of pristimerin on TNFα-induced inflammatory responses in murine macrophages. *Int J Clin Exp Pathol,* 9**,** 1186-1194.

PICCOLO, V., CURINA, A., GENUA, M., GHISLETTI, S., SIMONATTO, M., SABO, A., AMATI, B., OSTUNI, R. & NATOLI, G. 2017. Opposing macrophage polarization programs show extensive epigenomic and transcriptional cross-talk. *Nat Immunol,* 18**,** 530-540.

PLOTNIKOV, A., ZEHORAI, E., PROCACCIA, S. & SEGER, R. 2011. The MAPK cascades: signaling components, nuclear roles and mechanisms of nuclear translocation. *Biochim Biophys Acta,* 1813**,** 1619-33.

RAHIM, S. S., KHAN, N., BODDUPALLI, C. S., HASNAIN, S. E. & MUKHOPADHYAY, S. 2005. Interleukin-10 (IL-10) mediated suppression of IL-12 production in RAW 264.7 cells also involves c-rel transcription factor. *Immunology,* 114**,** 313-21.

RAMANATHAN, M., PINHAL-ENFIELD, G., HAO, I. & LEIBOVICH, S. J. 2007. Synergistic up-regulation of vascular endothelial growth factor (VEGF) expression in macrophages by adenosine A2A receptor agonists and endotoxin involves transcriptional regulation via the hypoxia response element in the VEGF promoter. *Mol Biol Cell,* 18**,** 14-23.

REN, J., CHEN, X. & CHEN, Z. J. 2014. IKKbeta is an IRF5 kinase that instigates inflammation. *Proc Natl Acad Sci U S A,* 111**,** 17438-43.

REX, J., ALBRECHT, U., EHLTING, C., THOMAS, M., ZANGER, U. M., SAWODNY, O., HAUSSINGER, D., EDERER, M., FEUER, R. & BODE, J. G. 2016. Model-Based Characterization of Inflammatory Gene Expression Patterns of Activated Macrophages. *PLoS Comput Biol,* 12**,** e1005018.

SATO, A., OHTAKI, H., TSUMURAYA, T., SONG, D., OHARA, K., ASANO, M., IWAKURA, Y., ATSUMI, T. & SHIODA, S. 2012. Interleukin-1 participates in the classical and alternative activation of microglia/macrophages after spinal cord injury. *J Neuroinflammation,* 9**,** 65.

SCHINDLER, H., LUTZ, M. B., ROLLINGHOFF, M. & BOGDAN, C. 2001. The production of IFN-gamma by IL-12/IL-18-activated macrophages requires STAT4 signaling and is inhibited by IL-4. *J Immunol,* 166**,** 3075-82.

SCHLEICHER, U., PADUCH, K., DEBUS, A., OBERMEYER, S., KONIG, T., KLING, J. C., RIBECHINI, E., DUDZIAK, D., MOUGIAKAKOS, D., MURRAY, P. J., OSTUNI, R., KORNER, H. & BOGDAN, C. 2016. TNF-Mediated Restriction of Arginase 1 Expression in Myeloid Cells Triggers Type 2 NO Synthase Activity at the Site of Infection. *Cell Rep,* 15**,** 1062-1075.

SHELDON, K. E., SHANDILYA, H., KEPKA-LENHART, D., POLJAKOVIC, M., GHOSH, A. & MORRIS, S. M., JR. 2013. Shaping the murine macrophage phenotype: IL-4 and cyclic AMP synergistically activate the arginase I promoter. *J Immunol,* 191**,** 2290-8.

SHEMBADE, N., HARHAJ, N. S., LIEBL, D. J. & HARHAJ, E. W. 2007. Essential role for TAX1BP1 in the termination of TNF-alpha-, IL-1- and LPS-mediated NF-kappaB and JNK signaling. *EMBO J,* 26**,** 3910-22.

SHEMBADE, N., HARHAJ, N. S., PARVATIYAR, K., COPELAND, N. G., JENKINS, N. A., MATESIC, L. E. & HARHAJ, E. W. 2008. The E3 ligase Itch negatively regulates inflammatory signaling pathways by controlling the function of the ubiquitin-editing enzyme A20. *Nat Immunol,* 9**,** 254-62.

SHEMBADE, N., MA, A. & HARHAJ, E. W. 2010. Inhibition of NF-kappaB signaling by A20 through disruption of ubiquitin enzyme complexes. *Science,* 327**,** 1135-9.

SHEMBADE, N., PARVATIYAR, K., HARHAJ, N. S. & HARHAJ, E. W. 2009. The ubiquitin-editing enzyme A20 requires RNF11 to downregulate NF-kappaB signalling. *EMBO J,* 28**,** 513-22.

STAPLES, K. J., SMALLIE, T., WILLIAMS, L. M., FOEY, A., BURKE, B., FOXWELL, B. M. & ZIEGLER-HEITBROCK, L. 2007. IL-10 induces IL-10 in primary human monocyte-derived macrophages via the transcription factor Stat3. *J Immunol,* 178**,** 4779-85.

SUPRUNENKO, T. & HOFER, M. J. 2016. The emerging role of interferon regulatory factor 9 in the antiviral host response and beyond. *Cytokine Growth Factor Rev,* 29**,** 35-43.

SUZUKI, N., SUZUKI, S., DUNCAN, G. S., MILLAR, D. G., WADA, T., MIRTSOS, C., TAKADA, H., WAKEHAM, A., ITIE, A., LI, S., PENNINGER, J. M., WESCHE, H., OHASHI, P. S., MAK, T. W. & YEH, W. C. 2002. Severe impairment of interleukin-1 and Toll-like receptor signalling in mice lacking IRAK-4. *Nature,* 416**,** 750-6.

TACHDJIAN, R., AL KHATIB, S., SCHWINGLSHACKL, A., KIM, H. S., CHEN, A., BLASIOLI, J., MATHIAS, C., KIM, H. Y., UMETSU, D. T., OETTGEN, H. C. & CHATILA, T. A. 2010. In vivo regulation of the allergic response by the IL-4 receptor alpha chain immunoreceptor tyrosine-based inhibitory motif. *J Allergy Clin Immunol,* 125**,** 1128-1136 e8.

TAKEDA, N., O'DEA, E. L., DOEDENS, A., KIM, J. W., WEIDEMANN, A., STOCKMANN, C., ASAGIRI, M., SIMON, M. C., HOFFMANN, A. & JOHNSON, R. S. 2010. Differential activation and antagonistic function of HIF-{alpha} isoforms in macrophages are essential for NO homeostasis. *Genes Dev,* 24**,** 491-501.

TIAN, F., YUAN, C., HU, L. & SHAN, S. 2017. MicroRNA-93 inhibits inflammatory responses and cell apoptosis after cerebral ischemia reperfusion by targeting interleukin-1 receptor-associated kinase 4. *Exp Ther Med,* 14**,** 2903-2910.

TODA, Y., TSUKADA, J., MISAGO, M., KOMINATO, Y., AURON, P. E. & TANAKA, Y. 2002. Autocrine induction of the human pro-IL-1beta gene promoter by IL-1beta in monocytes. *J Immunol,* 168**,** 1984-91.

TRAN, T. M., TEMKIN, V., SHI, B., PAGLIARI, L., DANIEL, S., FERRAN, C. & POPE, R. M. 2009. TNFalpha-induced macrophage death via caspase-dependent and independent pathways. *Apoptosis,* 14**,** 320-32.

TRASK, O. J., JR. 2004. Nuclear Factor Kappa B (NF-kappaB) Translocation Assay Development and Validation for High Content Screening. *In:* SITTAMPALAM, G. S., GROSSMAN, A., BRIMACOMBE, K., ARKIN, M., AULD, D., AUSTIN, C. P., BAELL, J., BEJCEK, B., CAAVEIRO, J. M. M., CHUNG, T. D. Y., COUSSENS, N. P., DAHLIN, J. L., DEVANARYAN, V., FOLEY, T. L., GLICKSMAN, M., HALL, M. D., HAAS, J. V., HOARE, S. R. J., INGLESE, J., IVERSEN, P. W., KAHL, S. D., KALES, S. C., KIRSHNER, S., LAL-NAG, M., LI, Z., MCGEE, J., MCMANUS, O., RISS, T., SARADJIAN, P., TRASK, O. J., JR., WEIDNER, J. R., WILDEY, M. J., XIA, M. & XU, X. (eds.) *Assay Guidance Manual.* Bethesda (MD).

TUCKERMAN, J. R., ZHAO, Y., HEWITSON, K. S., TIAN, Y. M., PUGH, C. W., RATCLIFFE, P. J. & MOLE, D. R. 2004. Determination and comparison of specific activity of the HIF-prolyl hydroxylases. *FEBS Lett,* 576**,** 145-50.

UEKI, K., KONDO, T. & KAHN, C. R. 2004. Suppressor of cytokine signaling 1 (SOCS-1) and SOCS-3 cause insulin resistance through inhibition of tyrosine phosphorylation of insulin receptor substrate proteins by discrete mechanisms. *Mol Cell Biol,* 24**,** 5434-46.

VAREY, A. H., RENNEL, E. S., QIU, Y., BEVAN, H. S., PERRIN, R. M., RAFFY, S., DIXON, A. R., PARASKEVA, C., ZACCHEO, O., HASSAN, A. B., HARPER, S. J. & BATES, D. O. 2008. VEGF 165 b, an antiangiogenic VEGF-A isoform, binds and inhibits bevacizumab treatment in experimental colorectal carcinoma: balance of pro- and antiangiogenic VEGF-A isoforms has implications for therapy. *Br J Cancer,* 98**,** 1366-79.

VEREMEYKO, T., YUNG, A. W. Y., ANTHONY, D. C., STREKALOVA, T. & PONOMAREV, E. D. 2018. Early Growth Response Gene-2 Is Essential for M1 and M2 Macrophage Activation and Plasticity by Modulation of the Transcription Factor CEBPbeta. *Front Immunol,* 9**,** 2515.

VILA-DEL SOL, V., DIAZ-MUNOZ, M. D. & FRESNO, M. 2007. Requirement of tumor necrosis factor alpha and nuclear factor-kappaB in the induction by IFN-gamma of inducible nitric oxide synthase in macrophages. *J Leukoc Biol,* 81**,** 272-83.

VILA-DEL SOL, V., PUNZON, C. & FRESNO, M. 2008. IFN-gamma-induced TNF-alpha expression is regulated by interferon regulatory factors 1 and 8 in mouse macrophages. *J Immunol,* 181**,** 4461-70.

VILLALTA, S. A., RINALDI, C., DENG, B., LIU, G., FEDOR, B. & TIDBALL, J. G. 2011. Interleukin-10 reduces the pathology of mdx muscular dystrophy by deactivating M1 macrophages and modulating macrophage phenotype. *Hum Mol Genet,* 20**,** 790-805.

VOLLMER, S., STRICKSON, S., ZHANG, T., GRAY, N., LEE, K. L., RAO, V. R. & COHEN, P. 2017. The mechanism of activation of IRAK1 and IRAK4 by interleukin-1 and Toll-like receptor agonists. *Biochem J,* 474**,** 2027-2038.

WANG, Z., JI, J., PENG, D., MA, F., CHENG, G. & QIN, F. X. 2016. Complex Regulation Pattern of IRF3 Activation Revealed by a Novel Dimerization Reporter System. *J Immunol,* 196**,** 4322-30.

WATERFIELD, M., JIN, W., REILEY, W., ZHANG, M. & SUN, S. C. 2004. IkappaB kinase is an essential component of the Tpl2 signaling pathway. *Mol Cell Biol,* 24**,** 6040-8.

WEI, S. H., MING-LUM, A., LIU, Y., WALLACH, D., ONG, C. J., CHUNG, S. W., MOORE, K. W. & MUI, A. L. 2006. Proteasome-mediated proteolysis of the interleukin-10 receptor is important for signal downregulation. *J Interferon Cytokine Res,* 26**,** 281-90.

WHEELER, K. C., JENA, M. K., PRADHAN, B. S., NAYAK, N., DAS, S., HSU, C. D., WHEELER, D. S., CHEN, K. & NAYAK, N. R. 2018. VEGF may contribute to macrophage recruitment and M2 polarization in the decidua. *PLoS One,* 13**,** e0191040.

WINSTON, B. W., CHAN, E. D., JOHNSON, G. L. & RICHES, D. W. 1997. Activation of p38mapk, MKK3, and MKK4 by TNF-alpha in mouse bone marrow-derived macrophages. *J Immunol,* 159**,** 4491-7.

WORMALD, S., ZHANG, J. G., KREBS, D. L., MIELKE, L. A., SILVER, J., ALEXANDER, W. S., SPEED, T. P., NICOLA, N. A. & HILTON, D. J. 2006. The comparative roles of suppressor of cytokine signaling-1 and -3 in the inhibition and desensitization of cytokine signaling. *J Biol Chem,* 281**,** 11135-43.

WU, C., XUE, Y., WANG, P., LIN, L., LIU, Q., LI, N., XU, J. & CAO, X. 2014. IFN-gamma primes macrophage activation by increasing phosphatase and tensin homolog via downregulation of miR-3473b. *J Immunol,* 193**,** 3036-44.

XUE, H., TU, Y., MA, T., WEN, T., YANG, T., XUE, L., CAI, M., WANG, F. & GUAN, M. 2019. miR-93-5p attenuates IL-1beta-induced chondrocyte apoptosis and cartilage degradation in osteoarthritis partially by targeting TCF4. *Bone,* 123**,** 129-136.

YAO, Y., WANG, Y., ZHANG, Z., HE, L., ZHU, J., ZHANG, M., HE, X., CHENG, Z., AO, Q., CAO, Y., YANG, P., SU, Y., ZHAO, J., ZHANG, S., YU, Q., NING, Q., XIANG, X., XIONG, W., WANG, C. Y. & XU, Y. 2016. Chop Deficiency Protects Mice Against Bleomycin-induced Pulmonary Fibrosis by Attenuating M2 Macrophage Production. *Mol Ther,* 24**,** 915-25.

YASUKAWA, H., OHISHI, M., MORI, H., MURAKAMI, M., CHINEN, T., AKI, D., HANADA, T., TAKEDA, K., AKIRA, S., HOSHIJIMA, M., HIRANO, T., CHIEN, K. R. & YOSHIMURA, A. 2003. IL-6 induces an anti-inflammatory response in the absence of SOCS3 in macrophages. *Nat Immunol,* 4**,** 551-6.

YEE, D., SHAH, K. M., COLES, M. C., SHARP, T. V. & LAGOS, D. 2017. MicroRNA-155 induction via TNF-alpha and IFN-gamma suppresses expression of programmed death ligand-1 (PD-L1) in human primary cells. *J Biol Chem,* 292**,** 20683-20693.

YIN, M., YANG, S. Q., LIN, H. Z., LANE, M. D., CHATTERJEE, S. & DIEHL, A. M. 1996. Tumor necrosis factor alpha promotes nuclear localization of cytokine-inducible CCAAT/enhancer binding protein isoforms in hepatocytes. *J Biol Chem,* 271**,** 17974-8.

ZANIN, R. F., BRAGANHOL, E., BERGAMIN, L. S., CAMPESATO, L. F., FILHO, A. Z., MOREIRA, J. C., MORRONE, F. B., SEVIGNY, J., SCHETINGER, M. R., DE SOUZA WYSE, A. T. & BATTASTINI, A. M. 2012. Differential macrophage activation alters the expression profile of NTPDase and ecto-5'-nucleotidase. *PLoS One,* 7**,** e31205.

ZETTERBERG, A. & SKOLD, O. 1969. The effect of serum starvation on DNA, RNA and protein synthesis during interphase in L-cells. *Exp Cell Res,* 57**,** 114-8.

ZHANG, H. C., WHITE, K. B., YE, H., MCCOMSEY, D. F., DERIAN, C. K., ADDO, M. F., ANDRADE-GORDON, P., ECKARDT, A. J., CONWAY, B. R., WESTOVER, L., XU, J. Z., LOOK, R., DEMAREST, K. T., EMANUEL, S. & MARYANOFF, B. E. 2003. Macrocyclic bisindolylmaleimides as inhibitors of protein kinase C and glycogen synthase kinase-3. *Bioorg Med Chem Lett,* 13**,** 3049-53.

ZHANG, W., XU, W. & XIONG, S. 2011. Macrophage differentiation and polarization via phosphatidylinositol 3-kinase/Akt-ERK signaling pathway conferred by serum amyloid P component. *J Immunol,* 187**,** 1764-77.

ZHAO, C., MIRANDO, A. C., SOVE, R. J., MEDEIROS, T. X., ANNEX, B. H. & POPEL, A. S. 2019. A mechanistic integrative computational model of macrophage polarization: Implications in human pathophysiology. *PLoS Comput Biol,* 15**,** e1007468.